Small molecule screen identifies inducers of mammalian cardiomyocyte proliferation

Inaugural Dissertation
submitted to the
Faculty of Medicine
in partial fulfillment of the requirements
for the PhD-Degree
of the Faculties of Medicine
of the Justus Liebig University Giessen

by
Magadum, Ajit
of
Kunnur, India

Giessen (2013)

From the Max Planck Institute for Heart and Lung Research
Director / Chairman: Prof. Dr. Dr. Thomas Braun, Max Planck Institute for Heart and Lung Research, Bad Nauheim, Germany

First Supervisor: Prof. Dr. Heinrich Sauer

Committee Member:

Date of Doctoral Defense: 12/02/2014

SUPERVISED BY

Prof. Dr. Heinrich Sauer,
Physiologisches Institut Fachbereich Medizin der
Justus-Liebig-Universität,
Aulweg 35392 Giessen, Germany.

DEDICATED TO MY PARENTS, GRANDPARENTS AND WIFE

DECLARATION

"I declare that I have completed this dissertation single-handedly without the unauthorized help of a second party and only with the assistance acknowledged therein. I have appropriately acknowledged and referenced all text passages that are derived literally from or are based on the content of published or unpublished work of others, and all information that relates to verbal communications. I have abided by the principles of good scientific conduct laid down in the charter of the Justus Liebig University of Giessen in carrying out the investigations described in the dissertation."

Ajit Magadum

Contents

Abbreviations

AMP	Adenosine monophosphate
AMPK	5’ adenosine monophosphate-activated protein kinase
ANF	Atrial natriuretic factor
ATP	Adenosine 5’triphosphate
BMP	Bone morphogenic protein
BrdU	5-bromo-2'-deoxyuridine
BSA	Bovine serum albumin
CAD	Coronory heart disease
cAMP	Cycline adenosine monophosphate
cDNA	Complementary DNA
CDK	Cyclin-dependent kinase
CHD	Congenital heart disease
CIP/KIP	Cdk interacting protein/kinase inhibitory protein
CKI	Cyclin-dependent kinase inhibitor
DAPI	4,6-diamino-2-phenylindole
DCM	Dilated cardiomyopathy
dH_2O	Distilled water
DMEM	Dulbeco’s modified eagle medium
DMSO	Dimethyl sulfoxide
DNA	Deoxyribonucleic acid
dNTP	Deoxyribonucleotide triphosphate
DTT	Dithiothreitol
E	Embryonic day
EC_{50}	Effector concentration for half–maximum response
ECL	Enhanced chemiluminiscence
E.coli	*Escherichia coli*
EDTA	Ethylene diamine tetra acetic acid
ERK	Extracellular receptor kinase
ESC	Embryonic stem cells
EtBr	Ethidium bromide
FCS	Fetal Calf Serum

FGF	Fibroblast growth factor
Fucci	Fluorescent Ubiquitination-based Cell Cycle Indicator
g	Acceleration of gravity
g	Gram
GAPDH	Glyceraldehyde-3-phosphate dehydrogenase
GFP	Green fluorescent protein
GSK3B	Glycogen synthase kinase 3 beta
h	Hour
H&E	Hematoxylin and eosin stain
HSC	Hematopoietic stem cell
HEPES	4-(2-hydroxyethyl)-1-piperazine ethane sulfonic acid
HCl	Hydrochloric acid
HRP	Horseradish peroxidase
ICC	Immunocytochemistry
IGF	Insulin-like growth factor
IHC	Immunohistochemistry
INCENP	Inner centromere protein
INK4	Inhibitor of kinase 4
IPTG	Isopropyl-D-1-thiogalactopyranoside
I/R	Ischemia-reperfusion
kDa	Kilo dalton
KCl	Potassium chloride
KH_2PO_4	Potassium dihydrogen phosphate
KLP3A	kinesin-like protein 3A
l	Liter
M	Molar
mAG1	Monomeric azami-green 1
mg	Milligram
$MgCl_2$	Magnesium chloride
MHC	Myosin heavy chain
MI	Myocardial infarction
min	Minute
mKO2	Monomeric kusabira-orange 2
MKLP1	Mitotic kinesin-like protein

ml	Milliliter
mM	Millimolar
mmol	Millimol
MMLV	Moloney murine leukemia virus
M.O.I.	Multiplicity of infection
MOPS	3-[N-morpholino] propane sulfonic acid
mRNA	Messenger RNA
MSC	Mesenchymal stem cells
NaCl	Sodium chloride
Na_2HPO_4	Disodium hydrogen phosphate
NaN_3	Sodium azide
NaOH	Sodium hydroxide
ng	Nanogram
NP40	Nonidet P40
OD	Optical density
P	Postnatal day
p38	MAP (mitogen activated protein) kinase
PBS	Phosphate buffered saline
PCNA	Proliferating cell nuclear antigen
PCR	Polymerase chain reaction
Pdk1	Phosphoinositide-dependent kinase-1
pH	Negative logarithm of hydrogen ion concentration
PLK1	polo-like kinase 1
PKA	Protein kinase A
PKC	Protein kinase C
PMSF	Phenyl methane sulfonyl fluoride
PPAR	Peroxisome proliferator-activated receptor
RNA	Ribonucleic acid
RNase	Ribonuclease
rpm	Revolutions per minute
RT	Room temperature
RT-PCR	Reverse transcription followed by polymerase chain reaction
SDS	Sodium dodecyl sulfate
s	Second

SHARP	SMRT and histone deacetylase-associated repressor protein
SMRT	Silencing mediator for retinoid or thyroid-harmone receptors
T_a	Annealing temperature
TAC	Transverse aortic constriction
Taq	*Thermus aquaticus*
TAE	Tris-acetate-EDTA
TBE	Tris-borate-EDTA
TBS	Tris buffered saline
TE	Tris-EDTA
TMCM	Tamoxifen-inducible MerCreMer
TMVPD	Tamoxifen-inducible VP16-PPAR delta
TTNPB	4-[(*E*)-2-(5,6,7,8-Tetrahydro-5,5,8,8-tetramethyl-2-naphthalenyl) -1-propenyl]benzoic acid
TWEAK	TNF-related WEAK inducer of apoptosis
U	Unit
UV	Ultraviolet
V	Volt
W	Watt
WB	Western blot
w/v	Weight/volume
v/v	Volume/volume

1. Introduction

1.1 The heart

The heart is a hollow muscle that pumps blood throughout the blood vessels by repeated, rhythmic contractions. The body requires oxygen and nutrients to carry on the process of life. A network of arteries and veins transports oxygen-rich blood to the body and carries oxygen-poor blood back to the lungs. At the center of this continuous process is the heart, a beating muscle about the size of the fist in adult humans. The heart pumps approximately 5 liters of blood every minute, beating at 72 beats per minute and each heart beat circulates blood to both the lungs and the body. This is possible because of the heart's complex internal structure.

1.2 Heart development

The heart is the first functional organ in the developing embryo and arises from cardiac progenitor cells derived from the embryonic mesoderm in the so-called heart field region[1].The heart field initially forms as a crescent shaped structure in the anterior part of the embryo that later develops into a linear tube[2, 3] (Figure 1.1).

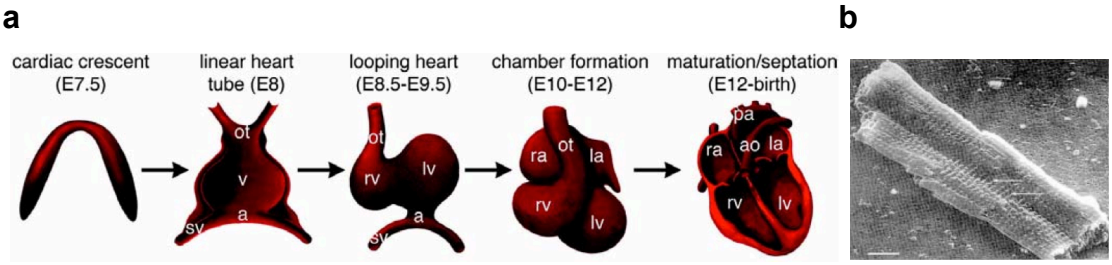

Figure 1.1. Summary of mouse heart development. (a) Five major stages of heart development are shown: (1) cardiac crescent formation at embryonic day (E) 7.5; (2) formation of the linear heart tube at E8; (3) looping and the initiation of chamber morphogenesis at E8.5 to E9.5; (4) chamber formation; and (5) chamber maturation and septation and valve formation. ao indicates aorta; a, atrium; la, left atrium; lv, left ventricle; ra, right atrium; rv, right ventricle; ot, outflow tract; sv, sinus venosa; and pa, pulmonary artery (adapted from Bruneau, 2002[4]). **(b)** Scanning electron micrograph of an isolated adult cardiomyocyte (adapted from McDermott, 2007[5]).

The tubular heart undergoes segmentation along the anterior-posterior axis, followed by rightward looping. This process results in the formation of the

right and left ventricles, the atrioventricular canal, the sinoatrial, and the outflow tract segments[6, 7]. Subsequently, the ventral side of the heart tube rotates and forms the outer curvature of the heart, with the dorsal side becoming the inner curvature[8]. The individual chambers balloon out from the outer curvature due to the rapid proliferation of resident myocardial cells. The developmental process is characterised by several transcription factors that are required for proper heart development like Nkx2.5, GATA4, MEF2, eHAND, Tbx5 and HRT [9-13]. Recent studies have shown that mutations in the genes encoding these transcription factors can cause congenital heart anomalies.

The contractile tissue of the heart is composed of individual cells, the cardiomyocytes (Figure 1.1 b). The cardiomyocyte is approximately 25 µm in diameter and about 100 µm in length. These cells contract constantly about 3 billion times and pump around 7000 liters of blood per day along 100.000 miles of blood vessels[14]. The cardiomyocyte is composed of bundles of myofibrils that contain myofilaments. The myofibrils have distinct, repeating microanatomical units, termed sarcomeres, which represent the basic contractile units of the cardiomyocyte.

1.3 Loss of cardiomyocytes during heart disease

Cardiomyopathies, also called "heart muscle disease", are the measurable deterioration of the function of the myocardium. Heart disease is the predominant cause of disability and death in industrialized nations accounting for about 40% of all postnatal deaths[15, 16]. There are different types of cardiomyopathies like ischemic cardiomyopathy, nonischemic cardiomyopathy, dilated cardiomyopathy and hypertrophic cardiomyopathy.

Ischemic cardiomyopathy/ myocardial infarction is a chronic disorder caused by either recurrent heart attacks or coronary artery disease (CAD). CAD is a disease in which there is hardening of the arteries on the surface of the heart (the coronary vessels) due to atherosclerotic plaques, which can result in occlusion (blockage) of a coronary artery following the rupture of a vulnerable atherosclerotic plaque. The resulting ischemia, in which the heart muscle does not receive enough oxygen-rich blood and energy metabolism gets exhausted, causes death or damage of cardiomyocytes. Myocardial infarction (MI) diminishes dramatically the number of cardiomyocytes, which

cannot be compensated by cardiac hypertrophy (increase in cardiomyocyte size). MI leads to a casscade of events including local hypoxia, infiltration of neutrofills, strong inflamatory response, developement of fibrous tissue, which collectively form a scar[17]. This leads to a decrease in the overall functionality of the heart. In addition, these events cause a local environment where cardiomyocytes near the scar are under different hemodynamic and metabolic pressure resulting in continous loss of cardiomyocytes. As cardiomyocytes are unable to undergo proliferation, it is very important to prevent cardiomyocyte loss or to reverse cardiac disease by adding new cardiomyocytes. There are different approches under consideration such as induction of cardiomyocyte proliferation, stem cell and progenitor based cell therapy approaches and tissue engineering[18]. Inhibition of cardiomyocyte apoptosis or improvement in survival of existing cardiomyocytes are some alternative stratergies to avoid major loss of cardiomyocytes in cardiac diseases[19, 20].

Cardiomyocyte generation may help to improve heart function also in other cardiac diseases like dilated cardiomyopathy (DCM) (involves dilation or enlargement of the heart's ventricles together with the thinning of the chamber walls) and arrhythmias (irregular heartbeats, conditions in which there is abnormal electrical activity in the heart).

a **b**

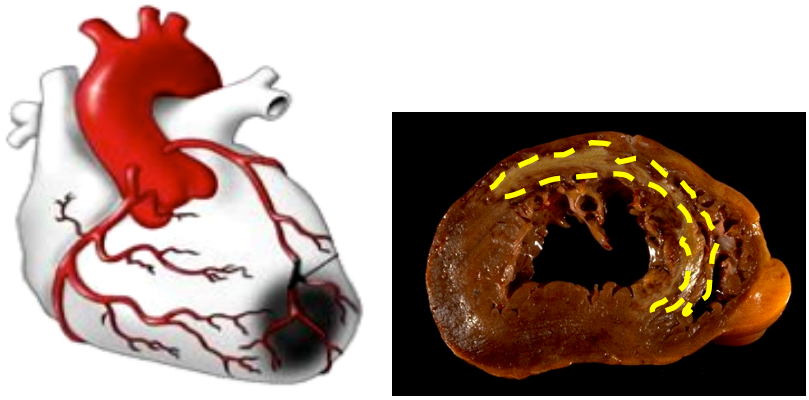

Figure 1.2: Cardiomyopathies (a) Myocardial infarction as result of a blocked left anterior descending coronary artery (adopted from pyroenergen.com). **(b)** Cross section of a human heart after myocardial infarction (scar: yellow dotted line) (adopted from http://library.med.utah.edu/WebPath/CVHTML/CV021.html)

1.4 Newt and zebrafish heart regeneration

Oberpriller showed in 1974 that adult newts can regenerate their hearts. In 2002, Ken Poss demonstrated that also adult zebrafish can regenerate their heart after removal of the apical region of the ventricle (Figure 1.3). The injury seals by a quick clotting mechanism, and the heart keeps sufficient contractile force to continue to drive circulation. First, within several days the clot seals the apex matures into a complex, fibrin clot. The fibrin clot in zebrafish is not typically replaced by scar tissue like in mammalian hearts. The injured heart apex was regenerated by generating new muscle in the next 30 days[21-23]. Higher indices of cardiomyocyte DNA synthesis and mitosis were detectable one week post injury and were observable for a few more weeks[21]. Both newt and zebrafish adult cardiomyocytes re-enter the cell cycle after injury[24 25]. These data suggested that cardiac regeneration is accomplished by re-induction of cardiomyocyte proliferation.

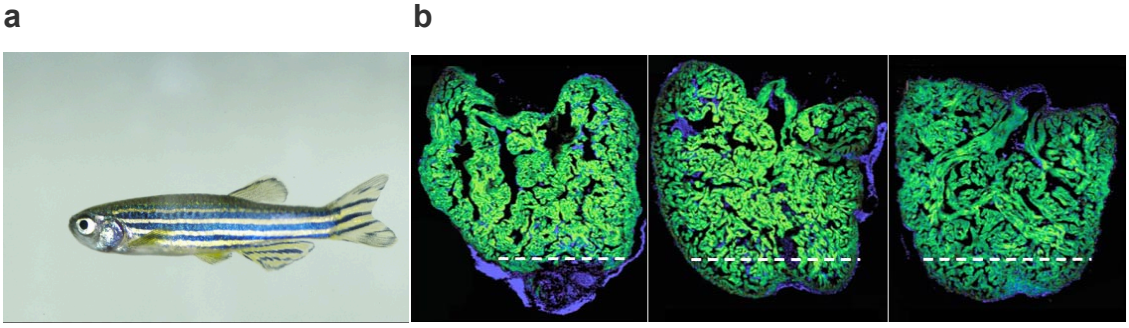

Figure 1.3: Regenerating adult zebrafish heart. (a) Zebrafish. (**b)** Following surgical removal of a portion of the zebrafish ventricle, cardiomyocytes (green cells) adjacent to the wound site (dotted line) undergo proliferation and regenerate the heart (adopted from Jopling c. *et.al* 2010).

In the absence of lineage tracing technology the cellular origins of newly regenerated cardiomyocytes after resection of the ventricular apex had been unclear. Recently new genetic fate-mapping approaches based on the Cre/Lox system revealed that regenerated cardiomyocytes are derived from the proliferation of differentiated pre-existing cardiomyocytes[22, 23]. This was further supported by induction of the expression of positive cell cycle regulators and the decrease of the expression of cell cycle inhibitors. Specifically, it has been shown that the polo-like kinase 1 [23] and a fibroblast growth factor (FGF) receptor[22] are essential components of cardiomyocyte proliferation during zebrafish heart regeneration. In addition, they determined by optical voltage

mapping of surface myocardium in whole ventricles that electrical conduction is re-established between existing and regenerated cardiomyocytes between 2 and 4 weeks post-injury. This indicates that newly formed myocardium is functionally incorporated into existing tissue.

1.5 Basic events of the mammalian cell cycle

Observations in zebrafish and newts suggest that induction of cardiomyocyte proliferation is a possible strategy to regenerate the human heart. Cell proliferation is a process where a single cell undergoes well-orchestrated events to form two daughter cells. The two most important events that occur during the passage through the cell cycle are the S phase (DNA-synthesis) and the M (mitosis) phase (Figure 1.3)[26]. To ensure proper progression through each phase, cells have developed a series of well controlled events that are governed by various molecular regulators such as cyclins, cyclin-dependent kinases (CDKs), CDK activators, CDK inhibitors (CDKIs) and members of the retinoblastoma protein family[27, 28]. Different cyclin-CDK complexes are required for distinct cell cycle events and their activities are regulated by cyclinH/CDK7 and CKIs ($p21^{CIP1}$, $p27^{KIP1}$, $p57^{KIP2}$) in both positive as well as negative manners, respectively. Cell cycle exit in most cell types is primarily mediated by the CIP/KIP (*i.e.* $p21^{CIP1}$, $p27^{KIP1}$, $p57^{KIP2}$) and INK4 (i.e. p16INK4a, p15INK4b, p18INK4c and p19INK4d) family of CDKI proteins[29]. CDKIs regulate the cell cycle by inhibiting CDK activation either by binding to monomeric CDKs or disrupting Cyclin-CDK complexes.

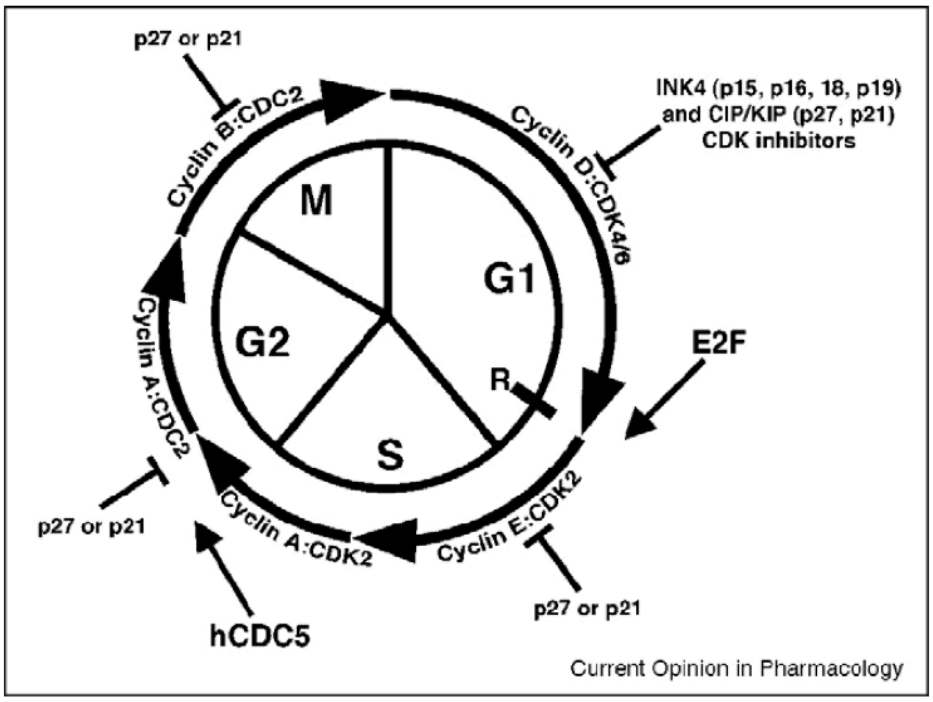

Figure 1.4: Mammalian cell cycle. The cell cycle is divided into 4 major phases. DNA replication is confined to the part of cell cycle known as S phase. Cell division occurs during M phase. G1 phase is the gap between M phase and S phase; G2 is the gap between S phase and M phase (Alberts, 1994).

The S phase is the part of the cell cycle in which DNA is replicated. It occurs between G_1 phase and G_2 phase and results in duplication of nuclear material. The M phase comprises karyokinesis (nuclear division) and cytokinesis (cytoplasmic division). The main purpose of mitosis is to segregate sister chromatids into two daughter cells, such that each daughter cell inherits one complete set of chromosomes. Mitosis is divided into five distinct stages: prophase, prometaphase, metaphase, anaphase and telophase. During mitosis the pairs of chromatids condense and attach to fibers that pull the sister chromatids to opposite sides of the cell.

Cytokinesis is the final step of cell division. It is responsible for equal partitioning and separation of the cytoplasm, the nuclei, organelles and the cell membrane between daughter cells to complete mitosis. There are four major events contributing to cytokinesis (Figure 1.5) which include (a) determination of the division site, (b) cleavage furrow formation followed by membrane ingression, (c) midbody formation, and (d) cell separation[30].

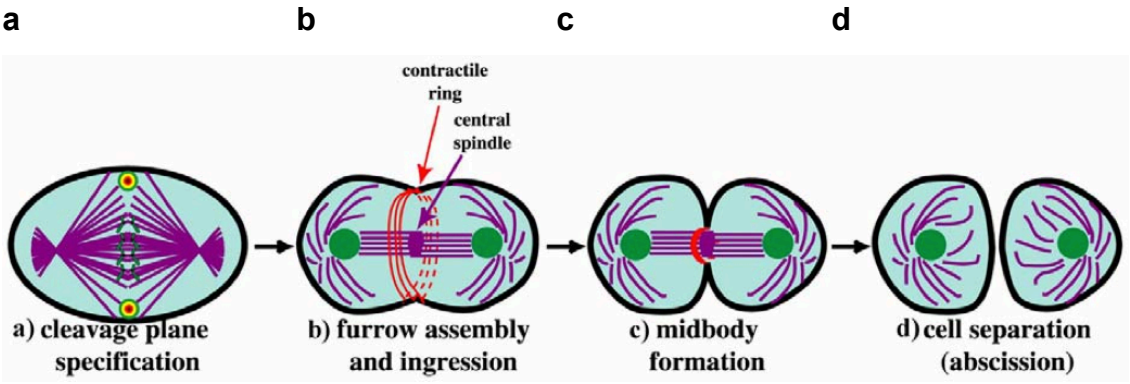

Figure 1.5: The subprocesses and the structures that mediate cytokinesis[30]. Four major events contributing to cytokinesis which include **(a)** determination of the cell division site, **(b)** cleavage furrow formation followed by ingression of membrane, **(c)** midbody formation and finally **(d)** cell separation (from Glotzer *et al*., 2005).

Two major classes of proteins are important for cytokinesis: 1) chromosomal passenger proteins, which localize initially to chromosomes and centromeres and subsequently to the midzone and furrow (*e.g.* INCENP, Aurora-B/Ip11 kinase, anillin and Bir1/Survivin)[31-34]. The mis-localization of any of these proteins affects cytokinesis. Previously, mis-localization of anillin after 10% serum stimulation has been associated to failure of cytokinesis in cardiomyocytes resulting in binucleation rather than proliferation. 2) Microtubule motor proteins like MKLP1, KLP3A and the polo kinase family[35]. These proteins provide structural support to localize and build the cleavage furrow[36]. The furrow contains actin, myosin and other proteins that are organized into a contractile ring called the actomyosin ring. This ring ingresses generating a membrane barrier [36, 37] and the ingressing furrow constricts components of the spindle midzone into a well focused structure called the midbody (Figure 1.5 (c)). In the final cytokinetic event, called abscission, the furrow seals, generating two daughter cells[30, 38-40](Figure 1.5 d).

To achieve sucessful cytokinesis, many components of the cytokinesis machinery are highly regulated to ensure that they are able to perform a particular function at only a particular stage of the cell cycle.

1.6 Cardiomyocyte cell cycle activity during heart development

1.6.1 Cardiomyocyte proliferation

Cell cycle activity is an intrinsic component of cardiac differentiation and morphogenesis. An exceedingly high level of DNA synthesis (around 70%) is seen in the precardiac mesoderm of the myoepicardial plate in E8 mouse embryos[41, 42]. The onset of cardiomyogenic differentiation is accompanied by transient reduction in DNA synthesis (45%) at embryonic day (E) 11. This high rate of cell cycle activity contributes to the "ballooning" of ventricular cardiomyocytes from the tubular heart[8]. At later stages, the DNA synthesis rate is approximately 2-fold greater in cardiomyocytes of the compact layer of the myocardium as compared to the trabeculae. Subsequently, cardiomyocyte proliferation gradually declines and shortly after birth cardiomyocytes stop to proliferate[43, 44].

Fetal cardiomyocytes express high levels of cyclins and cyclin-dependent kinases involved in G1, S, G2 and M-phase like cyclin D, A, B, E, Cdc2, Cdk2, Cdk4 and Cdk6 at both mRNA and protein levels[45-48]. Their associated kinase activities are also highly present. The protein levels of cyclins and their associated kinases become progressively and significantly downregulated in postnatal cardiomyocytes compared to fetal cardiomyocytes. The protein levels of cyclins A, B, D, E and Cdc2 become even undetectable in adult cardiomyocytes at protein level. Kinases like Plk1, Aurora B and other midbody proteins, which are involved particularly in late mitosis and cytokinesis, were demonstrated to be downregulated on both mRNA and protein level during heart development[49]. The downregulation in the expression of positive cell cycle regulators during normal development of cardiomyocytes have been shown to be concomitant with the specific upregulation of the CDKI molecules $p21^{cip1}$ and $p27^{kip1}$ [50, 51]. A review of the expression patterns of cell cycle proteins is provided in Table 1.1.

Table 1. Expression of cell cycle-related proteins in cardiomyocytes during development

Gene	Cell Cycle Activity	Expression Level		
		EMB	NEO	AD
Cyc D1	Cdk cofactor, positive regulator of restriction point transit	++	+	-
Cyc D2	Cdk cofactor, positive regulator of restriction point transit	++	+	-
Cyc D3	Cdk cofactor, positive regulator of restriction point transit	++	+	-
CDK4	Phosphorylates RB, promotes restriction point transit	++	+	-
p16	Inhibits Cdk 4 and 6; blocks restriction point and G1/S transit	ND	-	ND
p18	Inhibits Cdk 4 and 6; blocks restriction point and G1/S transit	++	++	-
p21	Inhibits Cdk 2, 4, and 6; blocks restriction point and G1/S transit	+	+	++
p27	Inhibits Cdk 2, 4, and 6; blocks restriction point and G1/S transit	+	+	+
p57	Inhibits Cdk 2, 4, and 6; blocks restriction point and G1/S transit	++	+	+
Cyc E	Cdk cofactor, positive regulator of G1/S transit	++	+	-
Cyc A	Cdk cofactor, positive regulator of S and G2/M transit	++	+	-
CDK2	Promotes G1/S transit when complexed with Cyc E	++	+	-
RB	Regulates G1/S transit by inhibiting E2F family member activity	+	+	+
p107	Regulates G1/S transit by inhibiting E2F family member activity	++	+	+/-
p130	Regulates G1/S transit by inhibiting E2F family member activity	+	++	ND
E2F1	Transcription factor for cell cycle genes, inhibited by RB family	ND	+	-
p53	Tumor suppressor that promotes cell cycle arrest or apoptosis	ND	ND	-
p193	BH3-only proapoptosis protein induces apoptosis at G1/S	++	+	-
PCNA	Required for DNA synthesis during S-phase and repair	++	+	-
Cyc B	Cdk cofactor, positive regulator of G2/M transit	++	+	-
cdc2	Promotes G2/M transit when complexed with Cyc B	++	+	-

Table 1.1: Expression of cell cycle-related proteins in cardiomyocytes during heart development as determined by western blot (adapted from Pasumarthi *et al*., 2002). For expression level, the relative level of expression refers to values within an individual study only; - refers to not detected and ND, not determined.

1.6.2. Cardiomyocyte hypertrophy and binucleation

After Birth mammalian cardiomyocytes stop to proliferate and the increase in heart size is mediated by hypertrophy. This transition from hyperplasia to hypertrophy is marked by an increase in cell size and binucleation as cardiomyocytes lose their ability to complete cytokinesis[52]. Cardiomyocytes grow in cell size and volume and exhibit enhanced protein synthesis as well as a higher organization of the sarcomere to adapt to the demand for an increased workload and the greater hemodynamic challenge [53] [54] (Figure 1.6). For example, the heart weight of a rat increases from 33.1 mg at postnatal day 1 to 134.3 mg at postnatal day 12. Similarly the cardiomyocyte cell volume increased from 1503 μm^3 to 3533 μm^3. The cardiomyocyte number was increased from 13.6 x 10^6 to 21.9 x 10^6 [44]. The numbers of binucleated

cardiomyocytes were increased from 2.3% on day 1 to around 90.3% on day 12.

In rodents, the accumulation of binucleated cardiomyocytes starts around postnatal day four and by the third postnatal week 90% of the cardiomyocytes are binucleated[43]. In pigs the nuclei number can even go up to 32 [55]. In humans, the withdrawal of cardiomyocytes from the cell cycle occurs within the first few weeks of life[56] and the nuclei of cardiomyocytes in man attain an increase in ploidy. In contrast, adult cardiomyocytes from lower vertebrates like zebrafish are capable to divide and even regenerate their heart after injury [25, 57 21]. This might be due to the fact that adult zebrafish contain mono-nucleated cardiomyocytes. The difference in binucleated cardiomyocytes in different species may be due to the species-specific hemodynamic demand[58]. The emergence of binucleation/polyploidy in mammals after birth may be due to the downregulation of proteins involved in cytokinesis. Recent immunofluorescence studies indicated that incorrect furrow ingression fails to promote abscission[59] resulting in asymmetric furrow ingression (due to diffused localization of Anillin, a scaffold protein to stabilize RhoA and CD2AP) causing binucleation[60].

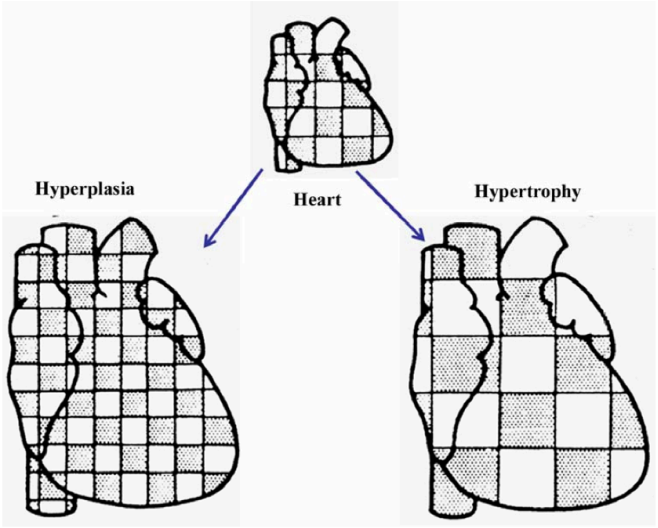

Figure 1.6: Schematic representation of heart development at the cellular level. Before birth heart growth is due to hyperplasia with a switch shortly after birth to the hypertrophic phase, where heart growth is due to increase in cell size and binucleation (adapted from Preeti Ahuja PhD thesis 2006).

The accurate balance of polyploidization in different species suggests that polyploidization is controlled by a specific cellular program that has evolved

to avoid the tetraploidy checkpoint, acquisition of multiple centromers, aberrant mitosis, and chromosomal instability[61]. All mammalian species studied so far seem to own a program that allows generation of cardiomyocytes with different degrees of polyploidy after birth but the exact reason and the regulatory mechanisms which drive physiological polyploidization remain unknown[62].

During cardiac disease cardiomyocytes increase their polyploidy/ binucleation levels possibly due to response of cardiomyocytes to strong mitotic stimuli and lack of the cell division machinery adopting an abortive cell cycle[63]. Instead of cell division cardiomyocytes undergo under pathological conditions hypertrophy. Although this is initially compensatory for an increased workload, prolongation of this process leads to congestive heart failure, arrhythmia, and sudden death.

1.7 Cardiomyocyte cell cycle exit

Cellular differentiation describes the process by which a less specialized (unspecialized) cell becomes more specialized. Exit from the cell cycle is often essential for cell differentiation[64]. However, fetal cardiomyocytes proliferate during development even though they already contain a contractile apparatus and actively contract[65].

Mammalian cardiomyocyte cell cycle exit during neonatal phases correlates with the up-regulation of both $p21^{CIP1}$ and $p27^{KIP1}$ that persists in the adult heart[50, 66]. The deletion of $p27^{KIP1}$ abrogates cell cycle withdrawal after birth. (ii) Overexpression of $p21^{CIP1}$ prevents serum-induced protein synthesis and fetal gene expression in cultured neonatal cardiomyocytes[67]. (iii) Down-regulation of $p27^{KIP1}$ and $p21^{CIP1}$ in varied pathological states indicate that these CDKIs contribute to cardiomyocyte cell cycle withdrawal. In contrast to $p21^{CIP1}$ and $p27^{KIP1}$, $p57^{KIP2}$ is expressed exclusively in the fetal mammalian heart and is more known regarding differentiation and anti-apoptosis. The INK4 family members do not appear to be significantly expressed in fetal or neonatal mammalian hearts and thus are unlikely to regulate cardiomyocyte cell cycle exit during development[67, 68].

Besides changes in cell cycle activity there are other important changes occurring during the switch from hyperplastic to hypertrophic growth including: (i) Isoform switching from beta-MHC to alpha-MHC. (ii) Isoform

switching of genes required for metabolism (*e.g.* GLUT1 to GLUT4)[69] and sarcomere proteins (*e.g.* slow skeletal Troponin I to cardiac Troponin I)[70]. (iii) Decreased expression of atrial natriuretic factor (ANF)[71]. Collectively, these changes are referred as re-expression of the "fetal gene program".

1.8 Regeneration of the fetal and neonatal heart

The mammalian fetal heart exhibits significant regenerative capacity. Cardiomyocyte-specific inducible deletion of a chromosome X-linked gene encoding holocytochrome c synthase, which is required for cell viability, ablates 50% of fetal cardiomyocytes in male E13 mouse embryos[72]. By late-gestation the injured hearts exhibited almost complete recovery in morphology and size. There was an increase in DNA synthesis and mitosis observed in cardiomyocytes of injured compared to non-injured hearts. This suggested that proliferation of pre-existing cardiomyocytes contributed to the regeneration in fetal hearts, although contribution of stem cells and/or cardiac progenitor cells could not be ruled out in the regenerative response[73]. Similar observations were found in the early gestational sheep after MI. Regeneration was completed and heart function was recovered four weeks after MI [74]. Collectively, these observations indicate that the fetal heart has significant regenerative capacities and that cardiomyocyte proliferation contributes to this process.

More recently, Porrollo *et al*. had applied a resection injury model to the neonatal mouse heart[75]. In this study, approximately 15% of the muscle was removed from the left ventricular apex of one day-old mice (Figure 1.7). A large blood clot quickly sealed the wound after injury, and in a three-week period the ventricles fully healed without major scarring. Cardiomyocyte proliferation were boosted both near to and away from the resection plane to levels even higher than those normally seen in growing hearts. Genetic fate-mapping approaches identified that regenerated heart muscle cells are derived from the proliferation of differentiated pre-existing cardiomyocytes. By contrast, resection injuries performed in mice P7 led to the formation of a fibrotic scar and no regeneration. Thus, the capacity for myocardial regeneration is only transiently present in the neonatal mouse heart but is quickly lost by seven days after birth.

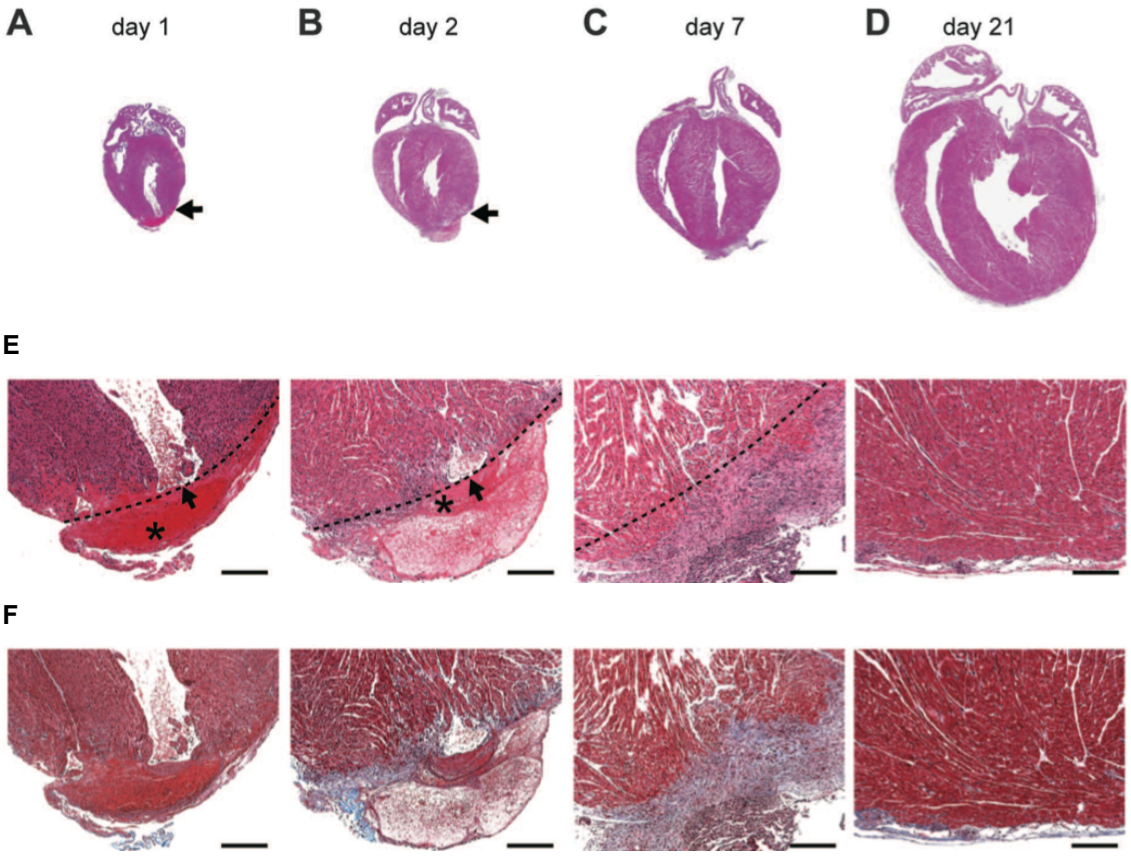

Figure 1.7: Heart regeneration in 1 day-old mice. 15% of the left ventricular apex of 1 day-old mice was removed. A large blood clot quickly sealed the wound after injury and in a three-week period the ventricles fully healed without major scarring. **(a** to **d),** Hematoxylin and eosin (H&E) staining of the mouse heart at 1, 2, 7, and 21 days post-resection. **(e)** H&E-stained sections at higher magnification. Dashed line indicates the resection plane. **(f)** Trichrome-stained serial sections showing decrease in cardiac fibrosis by day 21. (adapted from Porrollo 2011[75])

1.9 Loss of regeneration capacity of the heart after birth

As shown by Porrollo *et al*. P7 mice have lost the ability to regenerate the resected heart and instead form a fibrotic scar [75]. Cardiomyocytes in fetal and day 1 neonatal mammalian hearts are mono-nucleated (<97%) and proliferative like adult zebrafish cardiomyocytes. However, mammalian cardiomyocytes lose the ability to divide but still undergo DNA replication without cytokinesis or karyokinesis. Thus, most cardiomyocytes are binucleated with diploid nuclei in the adult mouse heart and mono-nucleated with polyploid nuclei in the adult human heart (Figure 1.8)[76]. Consequently, the mammalian heart is unable to regenerate after the postnatal switch from hyperplasia to hypertrophy.

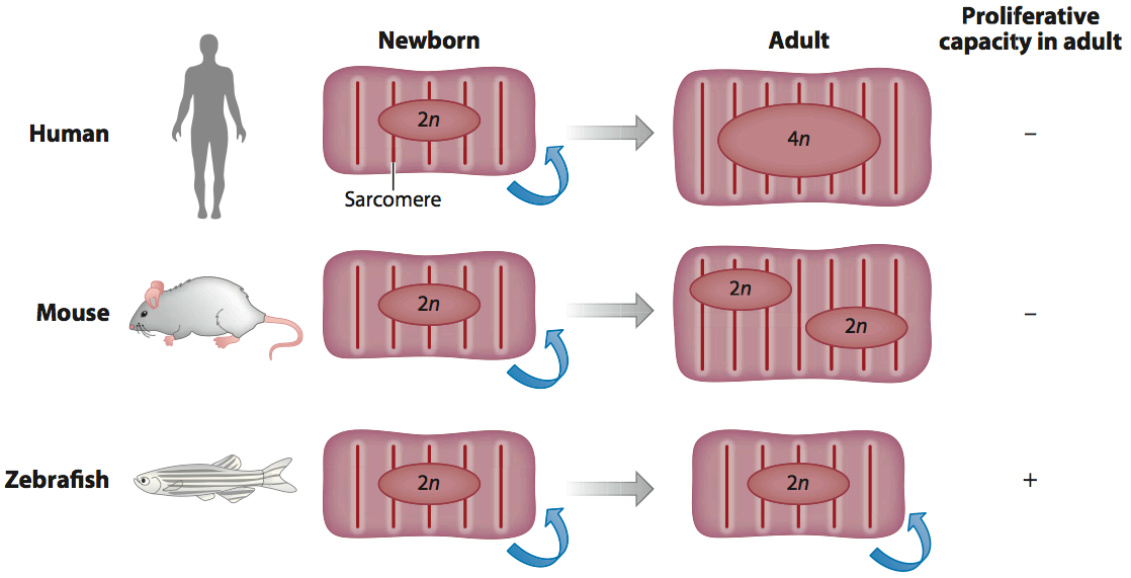

Figure 1.8: DNA content and proliferation capacity of cardiomyocytes during development and regeneration. Cardiomyocytes in fetal humans and mice are typically mono-nucleated with a diploid genome (2n) and increase in mass through cell division (blue arrows). Human cardiomyocytes after birth lose this capacity and typically undergo rounds of DNA replication without karyokinesis or cytokinesis, which results largely in mono-nucleated cardiomyocytes with tetraploid (4n) nuclei. Murine cardiomyocytes can a few days after birth only undergo DNA replication with karyokinesis but not cytokinesis, which results in binucleated cardiomyocytes (2n x 2n). By contrast, most cardiomyocytes in zebrafish hearts are mono-nucleated with a diploid genome (2n) throughout life maintaining significant proliferative and regeneration capacity (adapted from Kikuchi 2012[22]).

In addition, it has been shown that fibroblasts affect the proliferative behavior of cardiomyocytes. Cardiac embryonic fibroblasts stimulate proliferation of neonatal cardiomyocytes while adult fibroblast stimulate hypertrophy[77]. Considering that only around 30% of all cells in the adult heart are cardiomyocytes, age-related changes in fibroblast behavior might contribute to the developmental changes in mammalian cardiac regenerative capacity.

Mouse regenerative capacity is lost by postnatal day 7 and the mechanisms of cardiomyocyte cell cycle arrest remain unclear. However, recently Ahmed *et al* showed that Meis1 deletion in mouse cardiomyocytes was sufficient for extension of the postnatal proliferative window of cardiomyocytes from day 1 to day 7 and for re-activation of cardiomyocyte mitosis in the adult heart[78]. In contrast, overexpression of Meis1 in cardiomyocytes decreased neonatal myocyte proliferation and inhibited neonatal heart regeneration. Meis1

is required for transcriptional activation of CDK inhibitors $p15^{ink4b}$, $p16^{ink4a}$ and $p21^{CIP1}$. In addition, loss of Meis1 is known to regulate metabolism by switching energy metabolism from glycolysis to oxidative phosphorylation in HSC [79]. These results indicate that reversal of adult cardiomyocyte cell cycle arrest may be achievable through careful analysis of early postnatal events.

1.10 C14 carbon dating

In 2009, Bergmann *et. al*. showed that DNA synthesis occurs in human cardiomyocytes on the basis of C14 level in DNA. After the Limited Nuclear Test Ban Treaty in 1963, the C14 concentrations dropped exponentially by diffusion from the atmosphere. The C14 is incorporated in the human body through plants and animals. At any given time the C14 concentration in the human body mirrors that in the atmosphere[80, 81]. As DNA is stable after a cell has gone through its cell division, the concentration of C14 in DNA serves as a date mark for when a cell was born and can be used to retrospectivel birth date cells in humans[82, 83]. They used accelerator mass spectrometry to determine the extent of postnatal DNA synthesis in the human heart. They claimed that cardiomyocyte turnover involves at most 1% of cells annually in individuals at 25 years of age; by 75 years of age, it decreases to 0.45%[84]. This indicated annual turnover rates of cardiomyocytes of 0.2 to 2%. However, there was a clear negative correlation to age establishing that the turnover rate declines with age. By this premise ~50% of myocytes are replaced once during the course of life in humans, while an equal number lives as long as the organ and organism. They considered the involvement of polyploidization and estimated polyploidization-independent C14 values. However, this study did not exclude the differentiation of stem or progenitor cells into cardiomyocytes.

Recently similar low-level DNA synthesis data were shown by Senyo *et. al.* in mouse[85]. By combining two different pulse chase approaches, genetic fate-mapping with stable isotope labelling and multi-isotope imaging mass spectrometry, they showed that DNA synthesis of cardiomyocytes occurs at a low rate within newborn mice at 1%, in young adult at 0.015% and old adult mice at 0.007% per day. Interestingly, the rates were increased adjacent to areas of myocardial injury[85]. These values are similar to that of the Bergmann study. Genetic fate mapping showed that new cardiomyocytes were formed by

the division of pre-existing cardiomyocytes during normal ageing. Collectively, these study suggest that it might be possible to promote the regeneration of the mammalian heart through enhancing the endogenous cardiomyocyte turnover by cardiomyocyte proliferation.

1.11 Induction of postnatal cardiomyocyte proliferation

For many years the dogma is that adult cardiomyocytes are terminally differentiated [86]. However, recently, a number of reports in addition to the C14 dating have challenged this dogma. For example, the treatment with the mitogen FGF1 and pharmacological inhibition of the stress kinase p38 induces robust neonatal and adult cardiomyocyte mitosis *in vitro* as well i*n vivo*[87]. In addition, FGF1 stimulation together with p38 inhibition (FGF1+p38i) reduced scarring and rescued cardiac function after MI. This study further supported the idea that mammalian cardiac regeneration can be achieved through promotion of cardiomyocyte proliferation. During the last two decades many molecules have been found that induce fetal and postnatal cardiomyocyte proliferation. These include overexpression of cell cycle regulators[88-91] (*e.g.* cyclin D, cyclin A, cyclin B, Cdk2), overexpression of transcription factors[92] (e.g. c-Myc, E2F2) or viral proteins[93] (*e.g.* adenovirus E1A, SV40), knockout of cell cycle inhibitors[66, 94-96] (*e.g.* $p27^{KIP1}$, Retinoblastoma Protein) and external application of growth factors[97-99] (*e.g.* IGF-1, FGF2, TWEAK) or kinase inhibitors (*e.g.* BIO, a pharmacological inhibitor of GSK3B)[87]. Although many of these growth/ mitogenic factors are capable of inducing cell cycle activation in cardiomyocytes, they exhibit different abilities to promote proliferation in neonatal cardiomycoytes and in adult cardiomyocytes. These studies suggested that a subpopulation of cardiomyocytes may be capable of proliferation.

Factors promoting robust proliferation in adult cardiomyocytes have yet to be elucidated. To date, only the activation of TWEAK/FN14 signaling has demonstrated a significant induction of DNA synthesis in adult rat cardiomyocytes (around 40%)[99]. However, it did not induce significant mitosis and cytokinesis *in vitro*. Recently the human whole genome miRNA library was screened for neonatal cardiomyocyte proliferation using EdU (DNA analogue) in a 96-well format and found some positive hits[100]. Two of these positive hits,

hsa-miR-590 and hsa-miR-199a, were shown to promote cell cycle re-entry of neonatal and adult cardiomyocytes *in vitro* and *in vivo*. After MI in mice, these miRNAs stimulated marked cardiac regeneration and improved cardiac functional parameters. Thus, it appears promising to develop a mammalian cardiomyocyte high throughput-screening assay for inducers of cardiomyocyte proliferation to find new molecules with the potential to regenerate the mammalian heart[101].

1.12 Does heart regeneration occur from a subset of elite cardiomyocytes?

Cardiomyocytes are a heterogeneous population containing cells that may be better suited for cell division after injury with a specific gene expression signature. For example, a study reported recently that Neuregulin1 promotes proliferation of differentiated mono-nucleated adult mouse cardiomyocytes in cell culture as well as *in vivo*[102] consistent with the idea that some cardiomyocytes are more receptive to regeneration signals. A strong positive correlation exists between the percentage of mono-nucleated/diploid cardiomyocytes and the regenerative capacity of the heart. This positive correlation has led to the speculation that the adult human heart, where ~70 % of cardiomyocytes are mono-nucleated but polyploid, may maintain some margin of regenerative capacity[103 104].

During development P3 neonatal rat cardiomyocytes binucleate, unlike adult cardiomyocytes from hearts with regenerative capacity. Importantly, also 50% of neuregulin-treated mono-nucleated adult rodent cardiomyocytes become binucleated instead of undergoing cell division[102]. While adult cardiomyocytes in rodents are mainly binucleated and very few are mono-nucleated. In contrast, in humans the number of mono-nucleated cardiomyocytes is significantly larger. One hypothesis is that at least a subpopulation of mono-nucleated cardiomyocytes in humans maintained a differentiation level similar to P3 neonatal rodent cardiomyocytes. Then, identifying factors that promote P3 cardiomyocytes to divide rather than binucleate may provide a better approach to identifying regenerative factors for the adult human heart. FGF1+p38i treatment has been shown to efficiently promote P3 cardiomyocyte proliferation. However, its efficacy to induce

cardiomyocyte proliferation in adult rodent heart injury models is modest[87] and it is unlikely that the observed restoration of physiological parameters was solely due to cardiomyocyte proliferation. But FGF1+p38i treatment may have a more robust regenerative impact in human hearts.

1.13 Fucci (Fluorescent Ubiquitination-based Cell Cycle Indicator)

Recently Sawano *et al*. developed the so-called Fucci system[105]. This system has been used for the visualization of the progress in the cell cycle in the living cell. The principle of the system is based on Cdt1 and Geminin, the replication licensing factors, that are only present at a particular phase of the cell cycle [106]. The APCCdh1 and SCFSkp2 complexes are E3 ligase activities that mark a variety of proteins with Ubiquitinization in a cell cycle-dependent manner[107]. The SCFSkp2 complex is a direct substrate of the APCCdh1 complex but also functions as a feedback inhibitor of APCCdh1[108] [109] and these two ligase activities oscillate reciprocally during the cell cycle. The APCCdh1 complex is active in the late M and G1 phases, while the SCFSkp2 complex is active in the S and G2 phases (Figure 1.9 a).

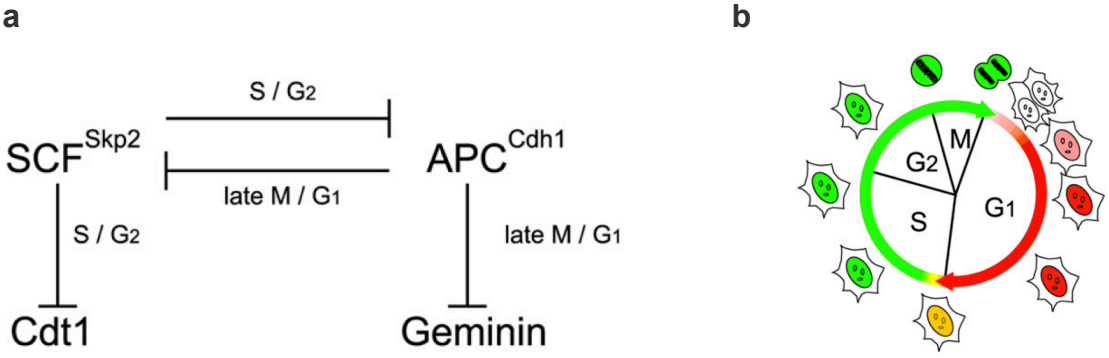

Figure 1.9: Fluorescent Indicator for Cell-Cycle Progression, Fucci. (a) Cell-cycle regulation by SCFSkp2 and APCCdh1 maintains bistability between G1 and S/G2/M phases. **(b)** A fluorescent probe that labels individual G1 phase nuclei in red and S/G2/M phase nuclei green. (adapted from Asako Sakaue-Sawano *et.al.* 2008)

Due to cell cycle-dependent proteolysis, protein levels of Geminin and Cdt1 oscillate inversely (Figure 1.9 b). Two fluorescent protein indicators such as monomeric Kusabira-Orange 2 (mKO2), fused to a fragment of Cdt1 (amino acids 30- 120), acts as an indicator for the G1 phase of the cell cycle. Similarly for visualizing S, G2 and M phases a fusion protein of a fragment of Geminin

(1-120) has a fluorescent protein monomeric Azami-Green1 (mAG1). These cell cycle indicators work by an ubiquitin-proteosome system via a rapid and highly selective degradation of these factors. Therefore, it can be used as an tool for investigating processes involving cell proliferation, growth and differentiation[105]. Although Fucci is composed of mKO2-hCdt1 (30/120) and mAG-hGem (1/110), single transfection of mAG-hGem (1/110) would be enough in conferring the information about proliferation.

1.14 Screening of chemical libraries

High-throughput screening of a molecule library is an important tool in modern research enabling to probe the diversity of chemical and biological space adding to published knowledge and to identify new biologically active small molecules creating data interesting to biologists and chemical biologists[110, 111].

To perform a high-throughput screening, the first task is to choose the right chemical library. There are diverse chemical libraries containing a variety of chemical compounds including natural, synthetic and semisynthetic compounds[111]. Each library includes a unique collection of small molecules including inhibitors, activators, and inducers, FDA-approved compounds, natural products, compounds for receptor de-orphaning, for chemical genomics, and for pathway targeting. To target a specific cellular phenomenon, organelle, pathway is of great interest. Therefore it is important to choose the library dependent on the addressed question and experimental setup.

Aim of the study

Newt, zebrafish and newborn mice can regenerate their heart after injury through cardiomyocyte proliferation. In contrast, adult cardiomyocytes have stopped to proliferate, exited the cell cycle and fail to reenter the cell cycle after injury. Consequently, the adult mammalian heart does not regenerate. Importantly, significant evidence has been accumulated over the last years suggesting that adult mammalian cardiomyocyte proliferation can be induced. Thus, it is important to identify novel inducer that efficiently induces mammalian cardiomyocyte proliferation in order to regenerate or repair the injured heart. One way to achieve this is the establishment of a screening platform.

The aim of this thesis is to develop a robust live fluorescence image-based cardiomyocyte proliferation screening system utilizing chemical molecule libraries to identify novel inducers of postnatal cardiomyocyte proliferation. The system should be applicable to large molecule screens and easy to handle. In addition, it should eliminate the need of laborious and expensive techniques like immunofluorescence staining, incorporation of nucleotide analogues or cell count assays.

The specific aims of this study were:

Aim 1: Development and validation of a Fluorescent Ubiquitination-based Cell Cycle Indicator (**Fucci***)* system for postnatal cardiomyocyte proliferation.

Aim 2: Screening of modulators of nuclear receptors and of an epigenetics chemical library and validation of positive hits.

Aim 3: Elucidation of downstream molecular signaling pathways for positive hits.

Aim 4: Determining the potentcy of positive hits to induce adult cardiomyocytes proliferation *in vitro*.

Aim 5: Assessing the relevance of the identified pathway for adult cardiomyocyte proliferation *in vivo.*

2. Materials

2.1 Equipment

2.1.1 Miscellaneous equipment

The equipment listed in Table 2 was used in this work.

Table 2.1: Name, model and supplier of used equipment.

Equipment	Model	Supplier
Agarose gel electrophoresis chamber	B2 Separationssystem	OWI
Aliqouting pipette	Repeater Plus	Eppendorf
Bacterial incubator	InnOva 4200	New Brunswick Scientific
Balance	ALC 3100.2	Acculab
Belly dancer	The belly dancer	Stovall
Chemical hood	Vinitex Air	Vinitex
CO_2 incubator	Galaxy R	New Brunswick Scientific
CO_2 incubator	Innova co-170	New Brunswick Scientific
Heating block	Digital Heatblock	VWR
Laminar flow	Herasafe KS	Heraeus
Luminescent image	LAS-4000	FujiFilm
Magnetic heating plate	Combimag RCT	IKA Werke
Magnetic stirrer	Stirrer	VWR
PCR cycler	Gene Amp PCR System 9700	Applied Biosystems
pH Meter	pH 221 Microprocessor pH Meter	HANNA Instruments
Pipettes 2,5 µl; 10 µl; 100µl; 200 µl 1000 µl	Research	Eppendorf
Plate reader	NanoQuant	Tecan
Power supply	EV243; EV231	Consort
Real-time PCR cycler	CFX96 Real-Time System C1000 Thermal Cycler	BioRad
Roller mixer	SRT6	Stuart

Equipment	Model	Supplier
Rotator	SB3	Stuart
SDS-PAGE electrophoresis chamber	X Cell Sure Lock	Invitrogen
Shaker	MHL20	HLC
Spectrophotometer	NanoDrop 2000c	PeqLab
Thermo-block	Digital heat block	VWR
Transfer chamber	X Cell II Blot Module	Invitrogen
Trans illuminator	Gel ix DNA and Protein imager	Itas
Vacuum pump	Diaphragma Vacuum pump	Vacuubrand
Vortex	VV3	VWR
Waterbath	U3	Sulabo

2.1.2 Microscopes

The microscopes used in this study are listed in Table 2.2.

Table 2.2: Microscope type, model and supplier of used centrifuges.

Microscopes	Model	Supplier
Confocal microscope	Axio Imager Z.1	Zeiss
Fluorescence	Leica DMI 3000 B	Leica
Fluorescence	Leica DM 6000 B	Leica

2.1.3 Centrifuges

The centrifuges used in this study are listed in Table 2.3.

Table 2.3: Centrifuge type, model and supplier of used centrifuges.

Centrifuge	Model	Supplier
Cooling centrifuge	Universal 320R	Hettich Zentrifugen
Cooling table centrifuge	Heraeus Fresco 17	Heraeus
Tabel top centrifuge	Centrifuge 5415C	Eppendorf

2.2 Miscellaneous materials

2.2.1 Disposables

The disposable materials listed in Table 2.4 were used in this work.

Table 2.4: Product, type and supplier of used disposable materials.

Materials	Type	Supplier
Aliquoting pipette tips	Combitips	Greiner bio-one
Bacterial culture tubes	14 ml PP Tube	Greiner bio-one
Cell culture dishes	10 cm	Greiner bio-one
Cell culture plates	24, 6, 96 Well Plates	Greiner bio-one
Cell scraper	Cell Scraper	Greiner bio-one
Coverslips	24 x 50 mm	Menzel Gläser
Coverslips	12 mm diameter	Menzel Gläser
Filter paper	Chromatography (3 mm)	Whatman
Injekt	1 ml	Braun
Latex gloves	Satin plus	Kimtech
Microscope slides	Mattrand, geschliffen 76 x 26 mm	Knittel Glaser
Microscope slides	Super frost ultra plus	Menzel Gläser
Nitril gloves	Activ Aloe	Blossom
Nitrocellulose transfer membrane	Protran Nitrocellulose	Whatman
PCR tubes	0.5 ml	Eppendorf
Pipette filter tips	FT10; FT100; FT200; FT1000	Greiner bio-one
Pipette tips	10 µl; 200 µl; 1000 µl	Greiner bio-one
Plastic pipettes	2 ml; 5 ml; 10 ml; 50 ml cell star	Greiner bio-one
PAGE	NuPAGE 4-12% Bis-Tris Gel 1.0 mm x 12 well	Invitrogen
PAGE	NuPAGE 4-12% Bis-Tris Gel 1.5 mm x 10 well	Invitrogen
Reaction tubes 1,5 ml; 2 ml	Safe Lock Tubes	Eppendorf
Reaction tubes 15 ml; 50 ml	Cell Star TUBES	Greiner bio-one
Thin pipette tips for capillary filling	20 µl Physio Care Concept	Eppendorf
Tissue culture flasks	T75	Greiner bio-one

Materials	Type	Supplier
Tissue culture flasks	T25	Greiner bio-one
Transfer pipettes	Transfer pipettes	Sarstedt

2.2.2 Non-disposables

The reusable materials listed in Table 2.5 were used in this work.

Table 2.5: Product, type and supplier of used non-disposable materials.

Materials	Type/Purpose	Supplier
Forceps	Inox.4	Dumont
Forceps	No 4 and No5	Neolab
Glass bottles	DURAN	Schott
Glass erlenmeyer flasks	DURAN	Schott
Glass measuring cylinder	DURAN	Hirschmann
Glass pipettes	2 ml; 5 ml; 10 ml; 25 ml	Brand
Glass beaker	DURAN	Schott
Hemocytometer	0.1 mm depth; 0.0025 mm^2	Marienfeld
ImmEdge pen	Immunostaining	Vector Lab
Micro scale	019.96843 1 mm in 100	Novex

2.3 Chemicals

Product and supplier of the chemicals that were used in this work are listed in Table 2.6.

Table 2.6: Product and supplier of used chemicals.

Product	Supplier	Product	Supplier
Agarose	Roth	Agar	Roth
Ampicillin	Calbiochem	Bromophenol blue	Merck
BSA	Roth	Chloroform	Roth
Collagenase Type II	Gibco	D-Glucose	Sigma
DNA ladder	Bioline	DTT	Roth

Product	Supplier	Product	Supplier
Ethanol	Roth	Ethidium bromide	Fisher Scientific
Formaldehyde (10% without methanol)	Polyscience	Formalin (37% with 10% methanol)	Sigma
FBS gold	PAA Lab	Glycerol	Sigma
Glycine	Roth	Heparin	Fluka
Hydrochloric acid	Roth	Hydrogen peroxide	Sigma
HRP-Substrate	Thermo Scientific	HEPES Na	Sigma
IPTG	Sigma	Kanamycin	Serva
KCl	Roth	KH_2PO_4	Roth
LB agar	Roth	LB medium	Roth
Lysis buffer (10x)	Cell Signaling	Methanol	Roche
$MgCl_2$, $6H_2O$	Roth	MOPS buffer (20x)	NuPage
Mounting medium (Entellan/Xylol-based)	Merck	Mounting medium (Kaiser's glycerol gelatin/water-based)	Merck
NaN_3	Sigma	NaOH	Roth
Na_2HPO_4	Roth	Nitrocellulose membrane	Whatman
Nonidet P40	Sigma	dNTPs	Invitrogen
N-phenylthiourea	Alfa aesar	Oligo dT	Invitrogen
Para-formaldehyde	Sigma	Paraffin	Sigma
PEG-3500	Sigma	Phenol red	Sigma
Propanol	Roche		
Precision Plus Protein Standard	BioRad	Polyacrylamide precast gel	Invitrogen
Protease inhibitor cocktail	Thermo Scientific	2-Propanol	Roche
Reverse transcriptase (MMLV)	Invitrogen	RNase inhibitor	Roche

Product	Supplier	Product	Supplier
Sodium citrate	Roth	Sodium chloride	Sigma
SDS	Fluka	Stripping buffer	NuPage
Sodium acetate	Roth	Tween 20	Sigma
Triton X100	Sigma	Trizol	Invitrogen
Tris base	Roth	Whatman filter paper	Whatman
Xylol	Roth		

2.4 Enzymes

The enzymes listed in Table 2.7 were used in this work. Compatible 10x buffers for different enzymes were supplied with the enzymes.

Table 2.7: Product and supplier of used enzymes.

Product	Supplier	Product	Supplier
DNase I	Roche	MMLV reverse transcriptase	Invitrogen
SalI	NEB	ScaI	NEB
Taq DNA polymerase	Roche	Top-Taq DNA polymerase	Quiagen
T4 DNA ligase	Promega		

2.5 Oligonucleotides

The oligos listed in Table 2.8 were used in this work. All primers were purchased from Sigma-Aldrich GmbH.

Table 2.8: Oligonucleotides used in this study.

Oligo name	Primer sequence (5'-3')	Gene accession
p21	AGGCAGACCAGCCTAACAGA	U24174.1
p21	CAGCACTAAGGAGCCTACCG	U24174.1
c-myc:	CGAGCTGAAGCGTAGCTTTT	NM_012603.2
c-myc:	CTCGCCGTTTCCTCAGTAAG	NM_012603.2
β-catenin	ACAGCACCTTCAGCACTCT	NM_053357.2

Oligo name	Primer sequence (5'-3')	Gene accession
β-catenin	AAGTTCTTGGCTATTACGAC	NM_053357.2
PPARδ	GAACAGCCACAGGAGGAGAC	NM_013141.2
PPARδ	CCCATCACAGCCCATCTG	NM_013141.2
cyclin B	gcgTAAAGTCAGCGAACAGTCAAG	NM_171991.2
cyclin B	gcGGAGAGGGAGTATCAACCAAA	NM_171991.2
cyclin A	gcgTATTTGCCATCGCTTATTGCT	NM_053702.3
cyclin A	gcgCTGTGGTGCTTTGAGGTAGGT	NM_053702.3
cyclin D2	AAGAGAGAGGCGTGTTCGTC	NM_022267.1
cyclin D2	TTCCTTCTTGGGTTCAATGC	NM_022267.1
gapdh	CAGAAGACTGTGGATGGCCC	NM_001115114.1
gapdh	AGTGTAGCCCAGGATGCCCT	NM_001115114.1

2.6 Antibodies

The primary and secondary antibodies used in this study are listed in Table 2.9 including additional information.

Table 2.9: Antibodies used in this study.

Primary antibody			
Antigen	**Purpose/Dilution**	**Isotype**	**Supplier**
Alpha-sarcomeric actinin	ICC, IHC 1:100	Mouse	Abcam
Aurora B	ICC 1:150	Mouse	Transduction Laboratories
BrdU	ICC 1:100	Rat	Abcam
Aurora B	ICC 1:150	Mouse	Transduction Laboratories
Troponin I	ICC 1:50	Rabbit	Santa Cruz
Tropomyosin	ICC 1:200	Mouse	DSHB, J.J.-C. Lin
Pan-actin	ICC 1:1000	Rabbit polyclonal	Cell Signaling
PDK1/PDPK1	ICC 1:1000	Rabbit	Cell Signaling

Primary antibody			
Antigen	**Purpose/Dilution**	**Isotype**	**Supplier**
		polyclonal	
PPARδ	WB- 1:500	Rabbit polyclonal	Santa Cruz
P27 (KIP/p27)	ICC 1:2500	Mouse	Transduction Laboratories
Cyclin A	ICC 1:50	Rabbit monoclonal	Santa Cruz
β-catenin	WB 1:1000	Rabbit monoclonal	Cell Signaling
Mcherry/Ds-Red	ICC 1:200	Mouse	Clontech
anti-mAG (Azami green)	ICC 1:300	Rabbit monoclonal	MBL
GSK3B	WB 1:100-	Rabbit moclonal	Cell Signaling
PS9 GSK3B	WB 1:1000	Rabbit polyclonal	Cell Signaling
Akt	WB 1:1000	Mouse	Cell Signaling
P308 Akt	WB 1:1000	Mouse	Cell Signaling
PARP	WB 1:1000	Mouse	Transduction Laboratories
CDC2	ICC 1:50	Rabbit polyclonal	Santa Cruz
pRB (pRb807/811)	ICC 1:100	Rabbit polyclonal	Cell Signaling
Survivin	ICC 1:100	Mouse	Santa Cruz
Caveolin 3	IHC 1:100	Rabbit polyclonal	Transduction Laboratories

Primary antibody			
Antigen	**Purpose/Dilution**	**Isotype**	**Supplier**
Cyclin D2	WB 1:1000	Rabbit polyclonal	Santa Cruz
Anti-phospho-Histone H3 (Ser10)	ICC, IHC 1:200	Rabbit polyclonal	Cell Signaling

Secondary antibody			
Antigen	**Purpose/Dilution**	**Isotype**	**Supplier**
Alexa Fluor 488 Anti-Rabbit	ICC 1:200	goat IgG	Invitrogen
Alexa Fluor 594 Anti-Rabbit	ICC 1:200	goat IgG	Invitrogen
Alexa Fluor 488 Anti-Mouse	ICC 1:200	goat IgG	Invitrogen
Alexa Fluor 594 Anti-Mouse	ICC 1:200	goat IgG	Invitrogen
Anti-Mouse IgG HRP-linked	WB 1:10000	sheep IgG	GE Health care UK limited
Anti-Rabbit IgG HRP-linked	WB 1:10000	donky IgG	GE Health care UK limited

2.7 Buffer and solutions

The buffer and solutions used in this work are listed in Table 2.10. Unless specified otherwise the solutions were prepared in distilled and autoclaved water. Freshly prepared solutions for an application were not autoclaved.

Table 2.10: Compositions of buffers and solutions.

Buffer/Medium/Solution	Compositions
Agarose gel loading buffer	**0.25% bromophenol blue [w/v]** **0.25% xylene cyanol FF [w/v]** **15% Ficoll 400 [v/v] in dH_2O**
Acetate buffer (pH 4.9)	85 g CH_3COONa, $3H_2O$ 900 ml dH_2O adjust pH with glacial acetic acid dH_2O q.s. to 1 l
Antigen retrivel buffer	0.1 M Tris/HCl buffer (pH 9.0)
B-Block	2% blocking reagent [w/v] 10% goat serum in PBST [v/v] 0.1% Tween 20 [v/v] store at -20°C
Conditioned water	75 g $NaHCO_3$ 18 g sea salt 8.4 g $CaSO_4$ dH_2O water to 1000 ml pH: ≈6.8 -7.5, conductivity: 180-350 µS
DEPC-Water	0.01% DEPC [v/v] in dH_2O incubate overnight at RT and then autoclave for 60 min.
DNase I solution	100 mg DNase I dissolve in 10 ml 10 µM $MgCl_2$ solution, filter and store at -20°C
MOPS Buffer (10x, 1000 ml)	4.18 g 3-[N-morpholino] propanesulfonic acid 680 mg sodium acetate 2 ml 0.5 M EDTA Dissolve in 1 l dH_2O and store at 4°C in the dark without autoclavation (MOPS gets degraded)

PBS (1x)	8 g NaCl 0.2 g KCl 1.44 g Na_2HPO_4 0.24 g KH_2PO_4 Dissolve in 800 ml of dH_2O, adjust pH to 7.4 and add H_2O q.s. to 1 l
PCR buffer (10x) without $MgCl_2$	20 ml KCl (1 M) 4 ml TrisHCl (1 M), pH 9 0.4 ml Triton X-100 Sterile distilled water q.s. to 40 ml
PFA in PBS (4%)	4 g PFA dissolve in 100 ml PBS (add few drops of NaOH). Heat at 55°C until PFA is dissolved. Cool and adjust the pH to 6-7
PBT	0.1% Tween20 in PBS [v/v]
PBA	5% BSA [w/v] 0.02% NaN_3 [w/v] Dissolve in PBS
PBT	0.3% Triton X100 in PBA [v/v]
RIPA buffer	2.5 ml 10% SDS in water 15 ml NaCl (5 M) 5 ml NP40 25 ml 10% deoxycholate in water [w/v] 1 ml EDTA (0.5 M) 25 ml Tris (1M, pH 8.0) Dissolve in DEPC-treated water q.s. to 500 ml. Don't autoclave afterwards
SADO mix	50 ml HEPES Na (200 mM; pH 7.6) 50 ml NaCl (1.3 M) 5 ml KCl (300 mM) 5 ml NaH_2PO_4 (100 mM) 1 ml glucose (2 M) Dissolve in 390 ml dH_2O
TBST (10x)	8 g NaCl

	0.2 g KCl 25 ml Tris (1 M; pH 7.5) 1 ml Tween 20 dH_2O q.s. to 100 ml
TAE running buffer (1x)	0.04 M Tris base 0.002 M glacial acetic acid 0.002 M EDTA, $2H_2O$ Dissolve in dH_2O
TBS	40 g NaCl 1.8 g tris base Dissolve in 4.5 l dH_2O Adjust the pH 7.6 dH_2O q.s. to 5 l
TBST	0.1% Tween 20 in TBS [v/v]
Transformation buffer (KCM buffer)	500 mM KCl 150 mM $CaCl_2$ 250 mM $MgCl_2$
Transfer buffer (20x)	163.2 g bicine 209.3 g bis Tris 12 g EDTA dH_2O q.s. to 2 l
Transfer buffer (1x)	250 ml 20x transfer buffer 1 l methanol dH_2O q.s. to 5 l
TSB buffer	10 g PEG-3500 5 ml DMSO 1 ml 1 M $MgCl_2$ 1 ml 1 M $MgSO_4$ LB medium (pH 6.1) q.s. to 100 ml Sterilize by passing through 0.45 µm filter and store at 4°C
Wash buffer	110 mM NaCl 3.5 mM KCl

	2.7 mM $CaCl_2$ 500 µl 1 M Tris HCl (pH 8.5) dH_2O q.s. to 50 ml
Stock perfusion buffer (KHP):	7.42 g/l NaCl 0.34 g/l KCl 2.08 g/l $NaHCO_3$ 0.27 g/l $MgSO_4x7H_2O$ 0.16 g/l KH_2PO_4 1.5 g/l D-Glucose 20 ml Na Pyruvate 100 mM (solution) 1.31 g/l Creatine 2.5 g/l Taurine
Buffer A	KHP + 100 mM $CaCl_2$ (850 µl/50 ml)
Buffer B	KHP + FAFBSA (0.5 g/500 ml)
Buffer C	KHP + digest buffer (22 mg collagenase Type II + 86 mg FAFBSA + 3.6 ml Buffer A/C)

2.8 Kits

The kits that were used in this work are listed in Table 2.11.

Table 2.11: List of kits used in this study.

Kit	Purpose	Supplier
Agarose gel extraction kit	cDNA isolation	QIAGEN
Bio-Rad Dc protein assay kit	Protein concentration	BIO-RAD
Dual Luciferase Assay System	Luciferase detection	Promega
lipofectamine™ RNAiMAX kit	Cell transfection kit	Invitrogen
NE-PER nuclear and cytoplasmic extraction kit	Protein extraction [112]	Thermo Scientific
Nucleofactor Kit	Cell transfection kit	Lonza
PCR purification kit	PCR product cleanup	QIAGEN
RNA easy	RNA isolation	QIAGEN
SuperSignal West Femto	Chemiluminescence	Thermo

Kit	Purpose	Supplier
substrate		Scientific
QIAprep spin Midiprep	Plasmid extraction	QIAGEN
QIAprep spin Miniprep	Plasmid extraction	QIAGEN

2.9 Antibiotics

Antibiotics that were used in this study are listed in Table 2.12. Ampicillin, kanamycin and G-418 were stored at 4ºC. Chloramphenicol and zeocin were stored at -20ºC

Table 2.12: Antibiotics and their working concentrations.

Antibiotics	Working concentration	
	Liquid culture	Agar plates
Ampicillin	100 µg/ml	100 µg/ml
Chloramphenicol	15 µg/ml	30 µg/ml
Kanamycin	20 µg/ml	20 µg/ml
Zeocin	50-500 µg/ml	100 µg/ml

2.10 Plasmids

Different constructs were used for *in situ* probe synthesis in this work. Gene name, construct backbone and restriction enzymes are listed in Table 2.13.

Table 2.13: List of plasmids, restriction enzymes and respective RNA polymerases.

Gene name	Vector	Resistance to	Enzyme
amhc	Alpha MyHC clone 26	Ampicillin	SalI
mko2-cdt1	Mko2-cdt1(30/120)	zeocin	SalI
mAG-hegeminin	*mAG-hgGeminin (1/110)*	Zeocin	SalI
amhc-mko2-cdt1	*amhc-mko2-cdt1* (30/120)	Zeocin	SalI
Amhc-mAg-hGeminin	*amhc-mAg-hGeminin (1/110)*	Zeocin	SalI

Gene name	Vector	Resistance to	Enzyme
TCF/LEF sites	*Topflash*	Ampicillin	
Mutated TCF/LEF sites	*Fopflash*	Ampicillin	
Luciferase	pGL4.75 (hRluc/CMV) vector (Promega	Ampicillin	

2.11 Adenoviruses

Adenoviruses that were used in this study are listed in Table 2.14. All viruses were stored at -80ºC. (Table 2.14).

Table 2.14: List of adenoviruses, their target sites and sequences.

Adenovirus	Target	MOI (multiple of infection)
Ad-mAG-hgeminin	Fucci construct express In S/G2/M	400
Ad-mko2-cdt1	Fucci construct express In G0/G1	400
Ad-DN-β-catenin	Dominant negative β-catenin	100
Ad-DN-TCF	Dominant negative TCF	100
Ad-DN-Akt	Dominant negative Akt	200

2.12 RNA interference

For siRNA-mediated β-catenin (80 nM) and PPARδ (100 nM) knockdown in cardiomyocytes, we purchased following SiRNA from Qiagen, Germany, All Stars Negative Control siRNA (Qiagen) was used as a negative control.

Table 2.15: List of RNAi, their target sites and sequences.

Cat. No.	Target	Sequence (5'-3')
SIO2012003	β-catenin	UUACAGGUCGGUAUCAAACCA
SIO2012010	β-catenin	UAGUCGUGGGAUCGCACCCTG
SIO1963479	PPARδ	CCAGCGAGGGATGCCAGCAAA

SIO1963486	PPARδ	CCCATGAGTTCTTGCGCAGTA

2.13 Growth media

Different media used for bacterial, cardiomyocyte and non-myocyte culture in this work are listed in Table 2.16.

Table 2.16: Name, purpose and formulation of used media.

Media	Purpose	Formulation
Neonatal medium	Cardiomyocyte isolation from neonatal rat heart	DMEM/F-12 medium supplemented with: 3 mM Na-pyruvate 2 mM L-glutamine 0.1 mM Ascorbic acid 1:100 Insulin/transferin/Na selenite 0.2% BSA penicillin (100 U/ml) streptomycin (100 mg/ml)
Preplating medium	Non-myocyte separation from harvested cells from neonatal rat heart	DMEM/F-12 medium supplemented with 10% FBS 2 mM L-glutamine Penicillin (100 U/ml) Streptomycin (100 mg/ml)
LB agar	Propagation of bacteria	35 g in 1 l H_2O
LB medium	Propagation of bacteria	20 g in 1 l H_2O
SOC medium	Bacterial transformation	Sigma
Adult rat cardiomyocyte medium	Cardiomyocyte isolation from adult rat heart	M199 medium from GIBCO 5 mM Creatine 2 mM L-Carnitine 5 mM Creatine

		Penicillin (100 U/ml) Streptomycin (100 mg/ml) 0.2% BSA

2.14 Competent cells

Different competent bacterial strains were used for transformation (Table 2.17).

Table 2.17: Bacteria used as competent cells for plasmid propagation.

Bacterial Strain	Specification
XL1-Blue	Competent cells
Dh5α	Competent cells

2.15 Software

Software used for data analysis in this study is listed in Table 2.18.

Table 2.18: Software used in this study and its application.

Software	Application
Microsoft Office Excel, Word, Powerpoint	Data anlysis and Documentation
Adobe Photoshop, Illustrator, Reader	Figure preparation
Image J	Image analysis
GraphPad Prism	Graphical representation and statistical analysis

3. Methods

3.1 RNA isolation and reverse transcription (RT)

The cultured cells were first washed 2 times with PBS. The cells were then scrapped from the culture plates using 10 µl of 2-mercaptoethanol + 1 ml lysis RW1 buffer from Qiagen. RNA extraction was carried out using the Qiagen RNA extraction kit. The RNA concentration was measured using Nanodrop and isolated RNA was dissolved in 30 to 50 µl RNase-free water and stored at -80°C.

cDNA was prepared from isolated RNA using MMLV or superscript II reverse transcriptase. For MMLV-mediated reverse transcription 1 µg RNA was incubated with 1 µl dNTP mix (10 mM), 0.5 µg oligo dT and RNase free water q.s. to 10 µl at 65°C for 5 min. Then this reaction mixture was incubated with 2 µl MMLV reverse transcriptase buffer (10x), 7 µl RNase free water and 1 µl MMLV reverse transcriptase at 37°C for 50 min. After 50 min the incubation reaction was inactivated by incubation at 80°C for 10 min and RNase free water was added q.s. to 100 µl. Synthesized cDNA was stored at -80°C for further use.

3.2 cDNA amplification by PCR

For PCR-mediated cDNA amplification, a standard PCR reaction was set up. As a template for the reaction 1 µl cDNA was used. A master mix was prepared by adding 10 pmol forward and reverse primers, 10 nmol dNTPs, 40 nmol $MgCl^{2+}$, 0.5 U Taq polymerase and 1x PCR amplification buffer ($MgCl^{2+}$ free). The amplification was carried out in a Gene Amp PCR System 9700 thermocycler from Applied Biosystems under the following conditions: initial denaturation for 2-5 min at 94°C; 24-35 cycles of 30 s at 94°C, annealing at 56°C to 59°C and extension of 1 min per 1 kb of product size at 72°C. After the last cycle the reaction was held for 7 min at the extension temperature to allow the completion of amplification of all products. Subsequently, the temperature was lowered to 4°C to stop the reaction

3.3 Agarose gel electrophoresis

cDNA was resolved on 1.5-2% agarose gels prepared in TAE buffer containing EtBr. Electrophoresis was run for 30 to 60 min in TAE depending upon PCR product size. cDNA was visualized under UV light, λ =260 nm.

3.4 cDNA elution from agarose gel

Resolved PCR products were purified from agarose gel using the QIAquick gel extraction kit according to manufacturer's instructions (QIAGEN) and eluted with 30 µl nuclease free water.

3.5 Cloning, recombinant adenoviral generation and infection

Cardiomyocyte-specific Fucci constructs were generated by cloning an alpha-MHC promoter in front of mCherry-hCdt1 (30/120) as well as mAG-hGem (1/110). mCherry-hCdt1 (30/120) and mAG-hGem (1/110) constructs were PCR amplified from respective lentiviral vectors provided by A. Miyawaki by using salI restriction containing primers (23). A 1028 bp cDNA fragment (primer pair containing SalI restriction sites) was amplified from mCherry-hCdt1 (30/120) plasmid and a 1058 bp cDNA fragment (primer pair containing SalI restriction sites) from mAG-hGem (1/110). All amplified cDNAs were resolved by agarose gel electrophoresis and eluted from the gel. Then this amplified fragments were kept separate salI restictions and also at the same time pAlpha-MyHC (clone 26) for SalI restriction. This restriction treatment leaves SalI sticky ends at both ends. Separately, SalI-restricted Fucci fragments were ligated with pAlpha-MyHC (clone 26) SalI-restricted fragment by incubating a mixture of 5 μl rapid ligation buffer (2x), 3 µl eluted cDNA, and 1 µl T4 DNA ligase (joins between the 5'-phosphate and the 3'-hydroxyl groups) at 4°C overnight. The plasmids were tested in in neonatal cardiomyocytes for their specificity and expression by Amaxa (electroporation based) transfection system. These constructs were then used to generate adenoviruses (Sirion Biotech GmbH). Neonatal P3 cardiomyocyte cultures were infected with adenoviruses 2 days after isolation at 400 M.O.I. in fresh medium. Infection efficiency of cardiomyocytes was > 90% as determined by live fluorescence imagining and indirect immunofluorescence staining's. For inhibition

experiments neonatal cardiomyocyte cultures were infected with adenoviruses expressing DN-Akt (200 M.O.I) 47, DN-β-catenin and DN-TCF4 (both 100 M.O.I., Vector Biolabs) two days after isolation. Cells were washed after 24 h.

3.6 Preparation of competent *E.coli* cells

A single colony of *E. coli* strain (DH5α or XL1Blue) was inoculated in 5-6 ml LB medium and cultured overnight at 37°C with shaking. The 4 ml of grown culture was added into fresh 250 ml LB and grown to early logarithmic phase (OD600=0.3-.6). The culture was centrifuged for 5 min at 2500 rpm at 4°C in a table top centrifuge. The bacterial pellet was resuspended in 25 ml cold TSB buffer (1/10th volume of the bacterial suspension) and incubated on ice for 10 min. Competent cell suspension was aliquoted into cold eppendorf tubes (100 µl and 200 µl) and snap frozen in liquid nitrogen. Aliquoted frozen competent bacterial cells were stored at -80°C.

3.7 Transformation of *E. coli* competent cells

Part of a ligation reaction mixture (5 µl) or 1-10 ng of plasmid DNA was added to 20 µl KCM buffer; water was added q.s. to 100 µl in a 1.5 ml eppendorf tube. An equal volume of thawed competent cells was added to the reaction mixture and mixed by flicking. The reaction mixture was incubated on ice for 20 min followed by incubation at RT for 10 min. Then 1 ml of LB medium (without any antibiotic) was added to the mixture and incubated for 1 h at 37°C with vigorous shaking. Finally cells were plated on LB Agar plates containing appropriate antibiotic. Plates were incubated at 37°C overnight.

3.8 Plasmid DNA isolation

The “mini-prep” method is useful for preparing partially purified plasmid DNA in small quantities from a number of transformants. It is based on the alkaline lysis method using SDS[113]. A single colony was selected and inoculated in 3 to 5 ml of LB medium containing the appropriate antibiotic with a sterile pipette tip. Bacterial cells were cultured overnight at 37°C with vigorous shaking. The cells were harvested by centrifugation for 4 min at 4000 rpm in a table top centrifuge (Eppendorf 5415C). Plasmid DNA was isolated using the QIAGEN miniprep kit following the manufacturer’s instructions. At last plasmid DNA was extracted

from the affinity column with 30 µl sterile water. Large amount of plasmid DNA was prepared using the QIAGEN Plasmid Midi Kit according to the manufacturer's instructions.

3.9 Determination of the concentration of nucleic acids

The DNA and RNA concentrations in solution were estimated using a spectrophotometer (Nanodrop 2000c-Peqlab). The absorbance of the solution was measured at 260 nm and the concentration of nucleic acids was calculated by the manufacturers software based on the Beer-Lambert Law ($A_\lambda = \varepsilon bc$). Where A_λ is the absorbance ($A_\lambda = log_{10}\ P_0 / P$), ε is the molar absorbtivity (molar extinction coefficient), b is the path length of the sample and c is the concentration of the compound in solution.

The molar absorbtivity of double stranded DNA is ε = 50 cm^{-1} M^{-1}, for single stranded DNA is ε = 33 cm^{-1} M^{-1}, and for RNA is ε = 40 cm^{-1} M^{-1}

3.10 Determination of protein concentration

Protein concentration was estimated using the BioRad DC Protein Assay Kit which is based on the Lowry method[114]. The 5 µl protein extract was mixed with 5 µl water, 20 µl reagent A and 200 µl reagent B and incubated for 15 min at RT. Absorbance of the solution was measured by a microplate reader (spectrophotometer from Tecan) at λ =720 nm. Protein sample concentration was calculated by the manufacturer's software based on a standard curve that was determined using BSA standards.

3.11 Western blot analysis

Rat neonatal cardiomyocytes cultured on 6 well plates were homogenized in lysis buffer (20 mM Tris, pH 7.4, 150 mM NaCl, 1 mM EDTA, 1 mM EGTA, 1% Triton X-100, 2.5 mM sodium pyrophosphate, 1 mM β-glycerol phosphate, 1 mM Na3VO4, 1 mg/ml leupeptin) containing 1 mM PMSF and Protease Inhibitor Cocktail (Roche). Cells were suspended in this buffer. After 15 min incubation on ice, the samples were briefly sonicated and centrifuged at 17,000 x g at 4°C for 10 min. Nuclear extracts were prepared according to the manufacturer instructions (Thermo Scientific). The protein concentration was determined using BioRad DC Protein Assay according to manufacturer's

protocol. Equal amount of proteins were resolved by 10% Novex Bis- Tris Gels (Invitrogen) and blotted on nitrocellulose membranes[115]. Membranes were blocked with 5% non-fat dry milk (DM) or 5% BSA in Tris-buffered saline (TBS) (10 mM Tris–HCl (pH 7.5), 150 mM NaCl) with 0.1% Tween 20 for 1 h at RT and incubated with primary antibodies diluted in 5% milk/TBS/T and/or 5%BSA/TBS/T overnight at 4°C: rabbit polyclonal anti-Cyclin D2 (1:1000), anti-PPARδ (1:500) (both Santa Cruz, DM), anti-phospho-GSK3B (DM), anti-pan-actin (DM), anti-PDK1 (BSA) (all 1:1000, Cell Signaling, DM), rabbit monoclonal anti-β-catenin (1:1000, Cell Signaling, BSA), anti-GSK3B (1:1000, BD Transduction Laboratories, DM), mouse monoclonal phospho (308) anti-Akt (1:1000, BSA), anti-Akt (1:1000, DM) (both Cell Signaling), anti-KIP/p27 (1:2500, DM), anti-PARP (1:1000, DM) (all BD Transduction Laboratories). Antigen/antibody complexes were visualized using horseradish peroxidase-conjugated secondary antibodies (Amersham) and Super Signal @ ECL detection system (BioRad). Chemiluminescence was documented by a blot developing system from FujiFilm, which can detect chemiluminescence.

3.12 Immunofluorescence staining

Staining was performed as previously described[116, 117]. The cells in culture were washed shortly (not > 30 sec) with PBS. For staining cells were fixed for 15 min in 3.7% methanol-free formaldehyde at RT. Cells were washed thrice with PBS and permeabilised in 400 µl / well D-PBS with 0.5% Triton-X100 for 10 min at RT (for BrdU staining cells were afterwards incubated with 2N HCl/1% Triton X-100 and incubated for 30 min at RT, and cells were washed thrice with PBS). Then cells were blocked with 5% goat serum/0.2% Tween-20/PBS for 20 min and incubated 1 h at RT with primary antibodies (for BrdU staining incubated overnight at 4°C with anti-BrdU antibody. Subsequently, samples were washed thrice with with 0.1 % Nonidet P40 in PBS, and incubated with corresponding secondary antibodies conjugated to Alexa Fluor 488 and Alexa Fluor 594 (1:200 Invitrogen) for 45 min at RT. Cells were washed and incubated with DAPI (DNA visualization) for 15 min. subsequentely cells were washed and mounted on glass slide. Primary antibodies: mouse monoclonal anti-mCherry/Ds-Red (1:200, Clontech), anti-Tropomyosin (1:200, Sigma), anti-Actinin (1:100, Abcam), anti-Aurora B (1:200), anti-p27 (1:50) (both BD

Transduction Laboratories), rabbit polyclonal anti-Troponin I, anti-Cyclin A, anti-cdc2, (all 1:50, Santa Cruz), anti-phospho-Histone H3 (Ser10) (1:200, Millipore), antipRb807/ 811 (1:100, Cell Signaling), anti-mAG (1:300, MBL), rat monoclonal anti- BrdU (1:100, Abcam). For BrdU, cells were cultured in 30 µM BrdU (neonatal P3: last 24 hours, P8: last 24 hours, adult: last 5 days)

3.13 Screening of small molecule libraries

Neonatal cardiomyocytes were seeded in 100 µl medium at a density of 15,000 cells per 96 well for 2 days. Then cells were infected with Ad-mAG-hGem(1/110). After 24 h cells were washed and treated with compounds dissolved in DMSO (Nuclear Receptor Ligand Library, 74 compounds, Enzo Life Science; Epigenetics Screening Library, 54 compounds, Cayman Chemicals) at 3 different concentrations (10 nM, 250 nM and 30 µM). AG expression was analyzed every 12 h for the following 4 days by visual inspection using a Leica fluorescence microscope. For quantitative analysis every 12 hours a random field of around 100 cells was evaluated. The maximal number of mAG-hGem(1/110) expressing cells was used to normalize the data against DMSO control as fold change. Hit compounds were defined as those higher than two fold

3.14 RNA interference

For siRNA-mediated β-catenin and PPARδ knockdown, neonatal cardiomyocytes were transfected 48-72 h after seeding and PBS washing by lipofectamine™ RNAiMAX kit (Invitrogen) with 100 nM of validated siRNAs (Qiagen). Cells were washed after 4 h by PBS and stimulated after 48 h with 1. DMSO, 2. Carbacyclin. All Stars Negative Control siRNA (Qiagen) was used as a negative control. Efficiency of siRNAs was verified by RT-PCR analysis using β-catenin and PPARδ specific primers (see Materials).

3.15 Luciferase assay

Cells were assayed for β-catenin-mediated transcriptional activation by using a reporter containing either functional (TOPflash) or mutated (FOPflash) Tcf binding sites A total of 2 µg TOPflash or FOPflash reporter plasmids (Upstate Signaling) were cotransfected with 2 µg pGL4.75 (hRluc/CMV) vector

(Promega) into 2 millions neonatal cardiomyocytes using the Nucleofactor kit (Amaxa) and were plated in 24-well plates. Cells were cultured for 3 days and were subsequently stimulated with selected compounds (1. DMSO, 2. carbacyclin) for 24 h. Reporter activity was measured by using the Dual Luciferase Assay System (Promega). TOPflash or FOPflash activity was normalized to the measured Renilla luciferase activity of pGL4.75, an internal standard for transfection efficiency. The results were showed in fold change in luciferase activity.

3.16 Isolation of neonatal rat heart cells

Neonatal rats (P3 and P8) were decapitated, the chest was opened and hearts were removed with a curved forcep. Isolated hearts (10 to 20) were placed in a petridish containing 20 ml PBS without Ca^{2+} and Mg^{2+} and 5 mM glucose on ice. Using a scalpel blade, the aorta and the atria were removed. The remaining ventricles were gently squeezed with forceps to remove the blood and washed with PBS without Ca^{2+} and Mg^{2+} containing 5 mM glucose. The ventricles were placed on a dry petridish and were minced as small as possible using a scalpel blade. The minced heart tissue was transferred to a Corex glass tube, containing 10 ml of digestion buffer and one magnetic stir bar, in a 37°C water bath on a magnetic stirrer (200 to 300 rpm). After 3 min the Corex glass tube was removed that the tissue could settle on the bottom (3 min tissue sedimentation). Subsequently the supernatant was discarded. This wash step was followed by a series of digestion steps each with 10 ml digestion buffer. The first two digestion steps involved 10 min of digestion followed by 5 min sedimentation. This procedure was continued with 8 min digestion and 5 min sedimentation for 5 steps more. After each sedimentation step, the supernatant containing the cells was collected and transferred to 50 ml falcon tube containing 4 ml ice-cold horse serum (each tube to collect 40 ml supernatant) and kept on ice. The tubes containing the cell suspension in horse serum were centrifuged at 330 x *g* for 3 minutes at 4°C. Subsequently the supernatant was discarded and the cell pellets were resuspended in preheated preplating medium (37°C, 10 ml per 5 hearts). The cell suspension was preplated on 10 cm cell culture dishes (10 ml cell suspension/dish) and incubated for 1h 30 min

at 37°C at 5% CO2 level. During this preplating, non-myocytes attach to the cell culture dish whereas cardiomyocytes get enriched in the medium.

The supernatant from the preplating step was collected in 50 ml falcon tubes. Cells were pelleted at 330 x *g* for 3 min at 4°C and RNA was isolated from the cell pellet (cardiomyocytes) or from the attached non-myocytes after washing twice with PBS using the QIAGEN RNA easy kit according to manufacturer's instructions.

3.17 Isolation of adult rat heart cardiomyocytes

The adult cardiomyocytes were provided by Dr. Felix Engel isolated by collagen-based digestion from 12-week-old rats using langendorff perfusion system[116]. The perfusion system was assembled as shown in figure 3.1. The isolated cells were washed with pre-warmed washing buffer and calcium was re-introduced. Then cell were centrifuged, supernatant removed and replaced with adult cardiomyocytes medium. The cells were plated on previously laminin-coated glass coverslips and incubated at 37^0C in CO2 incubator.

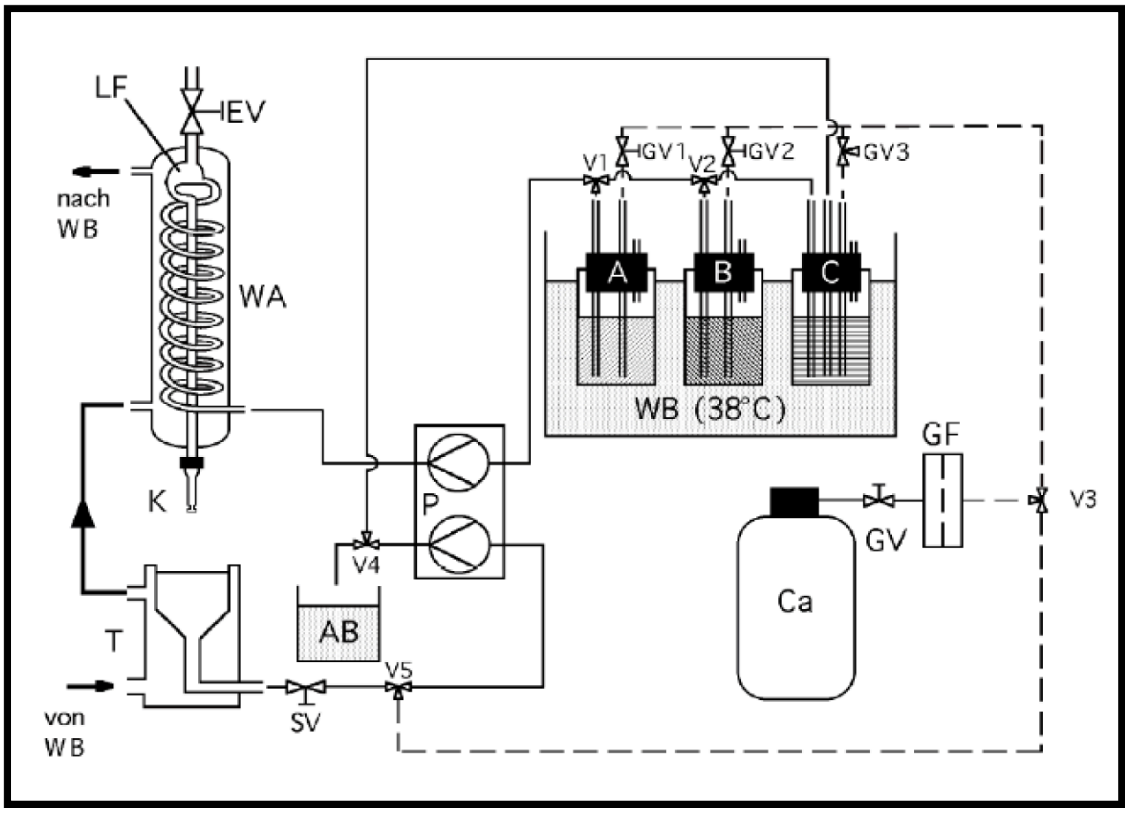

Figure 3.1: Perfusion system for isolation of adult rat cardiomyocytes. (adapted from Dr. Felix Engel PhD thesis)

3.18 PPARδ transgenic mouse model

The transgenic mouse model with tamoxifen inducible cardiomyocyte-restricted overexpression of a constitutively active mutant PPARδ gene (VP16-PPARδ) has been described previously.[21, 22] The transgenic line of VP16-PPARδ driven by the human cytomegalovirus immediate early enhance/chicken β-actin promoter was crossed with the tamoxifen inducible αMyHC-Mer-Cre-Mer (TMCM) transgenic mice[23] to generate the tamoxifen inducible transgenic mice with cardiomyocyte-restricted overexpression of VP16-PPARδ (TMVPD). Tamoxifen (Sigma) (80 μg/g of body weight/day) was administered by intra-peritoneal injection once daily for 5 days to induce cardiomyocyte-restricted PPARδ overexpression in adult mice (3 months). TMCM and TMVPD mice were anesthetized 14 days after tamoxifen induction, hearts were perfused with cardioplegic buffer and fixed with 4% paraformaldehyde. The heart was embedded in paraffin. Paraffin-embedded sections (5 μm thick) were obtained for immunostaining.

3.19 Immunostaining of heart sections

Mounted sections were deparaffinised by washing slides two times with xylol (10 min first and second time for 5 min) and then series of ethanol : water mixtures (99.4:0.6, 96:4, 70:30, 50:50) for 5 min each step. At last sections were washed with distilled water at least for 5 min. Following antigen retrieval in boiling EDTA Buffer (1 M EDTA, pH 8.0) for 8 min, sections were cooled down to RT (keep for 30 min at RT). After cooling down the slides were rinsed thrice with PBS for 5 min. Each tissue section was circumscribed with an ImmEdge pen. The section was blocked with 5% goat serum/0.2% Tween-20/PBS for 30 min, incubated overnight at 4°C with rabbit anti-phospho-Histone H3 (Ser10) (1:200, Millipore) and mouse anti-sarcomeric alpha Actinin (1:100, Abcam), Subsequently, samples were washed thrice with PBS and incubated with corresponding secondary antibodies conjugated to Alexa Fluor 488 and Alexa Fluor 594 (Invitrogen).

3.20 Statistical analysis

For immunofluorescence analyses 50 cardiomyocytes in five random fields of two different subpopulations were counted per experiment equaling a total cell number of 500 cardiomyocytes. Data of at least three independent experiments are expressed as mean ± SEM. Results were analyzed by Graph Pad Prism (version 4.00, Graph Pad Software Inc.). Statistical significance was determined using a two tailed Student's t-test and analysis of variance (ANOVA). The values of $p < 0.05$ were considered statistically significant.

4 Results

4.1 Cloning and generation of cardiomyocyte-specific recombinant adenoviral Fucci constructs

In order to test whether the Fucci system can be utilized to monitor cell cycle re-entry in fully differentiated cardiomyocytes we have overexpressed via adenovirus a non-functional hCdt1 deletion mutant fused to mCherry (mCherry-hCdt1(30/120)) as well as a non-functional human Geminin deletion mutant fused to a monomeric version of Azami Green (mAG-hGem(1/110)) in primary neonatal rat cardiomyocytes under the control of the cardiomyocyte specific alpha-MHC promoter (**Figure 4.1 a**).

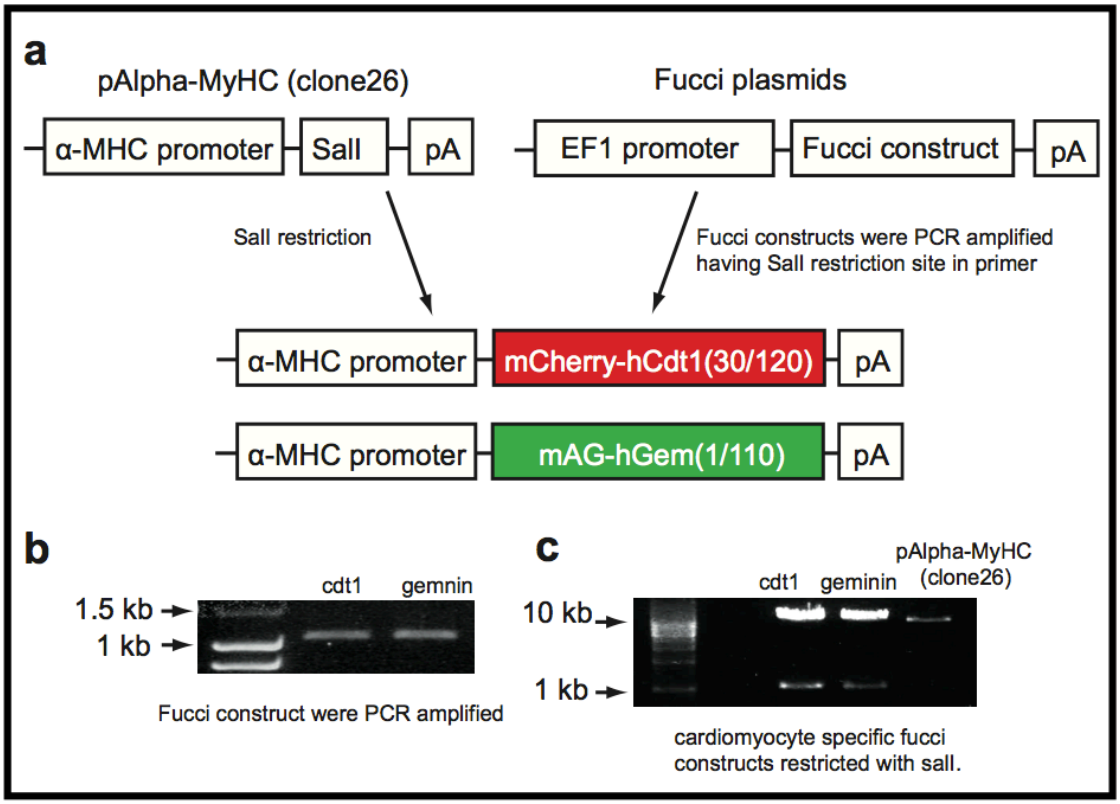

Figure 4.1: Cloning and generation of cardiomyocyte-specific recombinant adenoviral Fucci constructs. (**a**) Diagrammatic representation of cloning and generation of cardiomyocyte specific fucci constructs. **(b)** PCR amplification of Fucci constructs using specific primers containing sall restriction site. **(c)** Cardiomyocyte-specific Fucci constructs alpha-MHC-mCherry-hCdt1(30/120)) and alpha-MHC-mAG-hGem(1/110)) were generated (amplified Fucci sequence and pAlpha-MyHC (clone 26) plasmid was first restricted by SalI separately and Fucci constructs were ligated with sall restricted with pAlpha-MyHC (clone 26) using T4 ligase). Restriction of cardiomyocyte-specific Fucci plasmids and pAlpha-MyHC (clone 26) by SalI restriction **(c).**

To generate cardiomyocyte-specific Fucci constructs, we cloned an alpha-MHC (myosin heavy chain) promoter in front of mCherry-hCdt1 (30/120) as well as mAG-hGem (1/110). mCherry-hCdt1 (30/120) and mAG-hGem (1/110) DNA sequence were PCR amplified from respective vectors provided by Atsushi Miyawaki[105] (**Figure 4.1 b, c**). The primers were designed in a way that both contain a SalI restriction site. These SalI sites were used to insert the amplified sequence from the Fucci plasmids into pAlpha-MyHC (clone 26) plasmid (**Figure 4.1 a**). The constructs were further checked for cardiomyocyte-specific expression in neonatal cardiomyocytes (**Figure 4.2 a, e**). These plasmids have been used to generate adenoviral constructs (Sirion Biotech GmbH).

4.2 Fucci system in primary differentiated rat cardiomyocytes

To investigate the expression of Fucci constructs in neonatal cardiomyocytes, we transfected neonatal cardiomyocytes after 48 h of isolation in cardiomyocyte medium with different M.O.I. of Ad-mCherry-hCdt1 (30/120) and Ad-mAG-hGem (1/110) adenoviral vectors (**Figure 4.2 a, b, e, g**). Ad-mCherry-hCdt1(30/120) infection resulted in the expression of mCherry-hCdt1(30/120) in more than 90% of neonatal cardiomyocytes (95.2% ± 3.0%) based on mCherry staining and counterstaining against cardiomyocyte-specific Troponin I (**Figure 4.2 a**). To verify the specificity of the alpha-MHC promoter we analyzed the expression of mCherry-hCdt1(30/120) also in non-myocytes. For this purpose we used our standard neonatal cardiomyocyte cultures (contain up to 10% of non-myocytes) as well as non-enriched cultures (no pre-plating) containing around 50% of non-myocytes (**Figure 4.2 c, d**). In both cultures we detected less than 1% of mCherry-hCdt1 (30/120)-positive non-myocytes after adenoviral infection confirming the specificity of the alpha-MHC promoter (0.83% ± 0.21%) (**Figure 4.2 c**). Taken together, our data are in agreement with the literature describes that the majority of cardiomyocytes has exited the cell cycle and thus should be Cdt1-positive.

Ad-mAG-hGem(1/110) infection resulted in the expression of mAG-hGem(1/110) of less than 1.5% of cardiomyocytes (1.3% ± 0.2%; (**Figure 4.2 e**). Stimulation with 10% fetal calf serum (FCS), an inducer of cell cycle re-entry, increased the expression of mAG-hGem(1/110) around 10-fold (14.1% ±

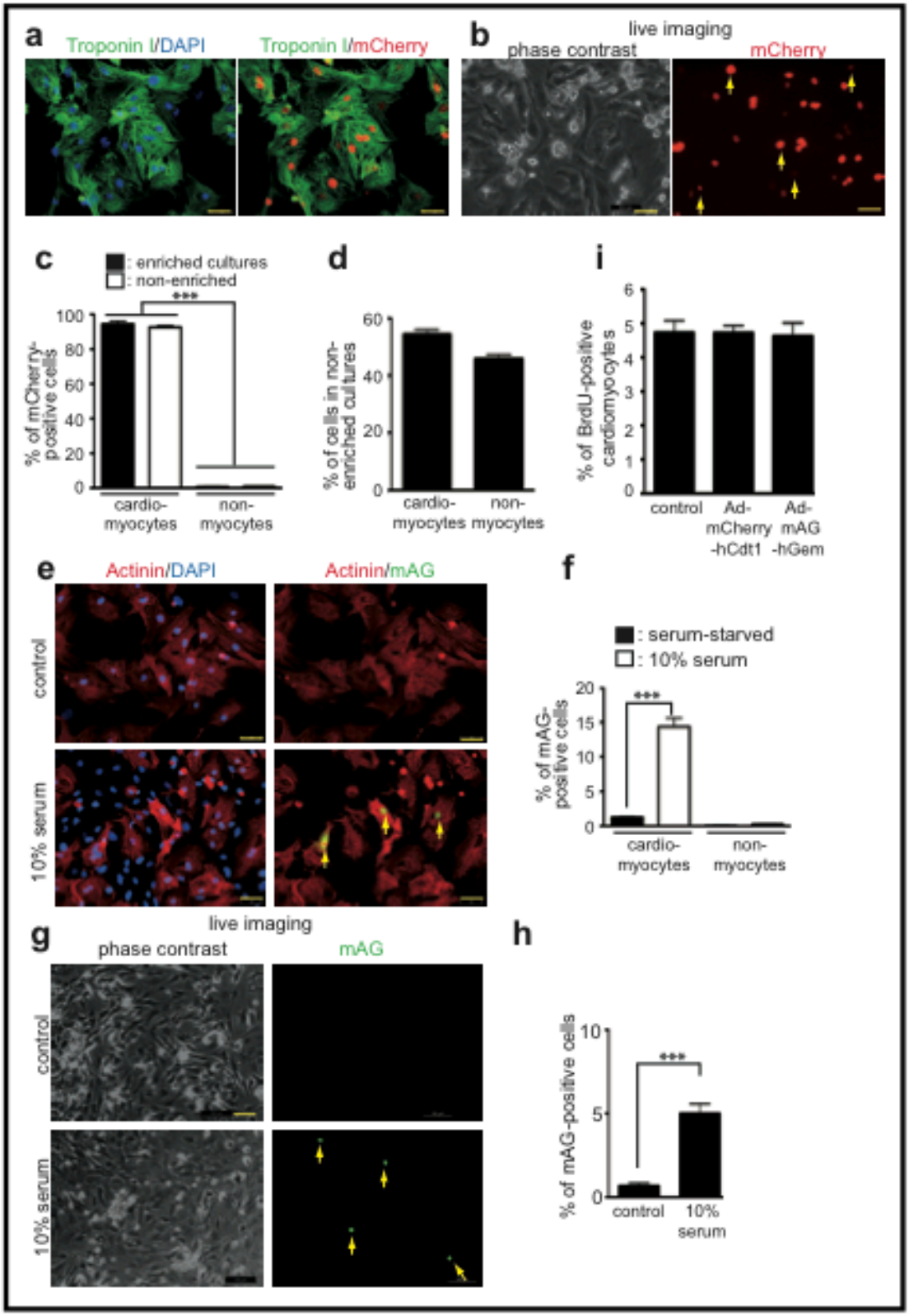

Figure 4.2: Fucci system in primary differentiated neonatal rat cardiomyocytes. **(a)** and **(b)**, Enriched and non-enriched cardiomyocytes cultures infected with Ad-mCherry-hCdt1(30/120) stained for mCherry expression (red) and counter-stained against cardiomyocyte-specific Troponin I (green). DAPI was used to visualize nuclei (blue). (**b**), Representative example for enriched cultures. **(c)**, Quantitative analysis for enriched and non-enriched cultures (n=6). **(d)** Quantitative analysis of cardiomyocytes and non-cardiomyocytes in

non- enriched culture. **(e)**, Ad-mAG-hGem(1/110) infected enriched P3 cardiomyocytes were stimulated with serum starved or 10% fetal calf serum, stained for mAG expression (green) and counter stained against cardiomyocyte-specific actinin (red) and DNA (DAPI, blue). **(f)** Quantitative analysis of (e) in cardiomyocytes and non-cardiomyocytes (n = 6). **(g)** and **(h),** Quantitative analysis (n = 6) and representative live pictures of control or 10% FCS stimulated neonatal cardiomyocyte cultures infected with Ad-mAG-hGem(1/110) (green). : **: $p < 0.01$. Scale bar = 50 µm in **(a)** and 100 µm in **(c)**.

2.1%, $p < 0.01$) (**Figure 4.2 f**), while less than 0.3% of non-myocyte were mAG-positive (**Figure 4.2 f**) (serum starvation: 0.02% ± 0.01%, FCS: 0.27% ± 0.09%). The FCS-induced mAG-hGem(1/110) expression could be easily detected by visual inspection. The number of mAG-hGem(1/110)-positive cells per field was increased more than 5-fold compared to the control (9 ± 3 *vs.* ≤ 1, (**Figure 4.2 g, h**).This suggests that the required degradation machinery is still intact and that the overexpressed mAG-hGem(1/110) is actively degraded in differentiated cardiomyocytes.

Overexpression of neither mCherry-hCdt1(30/120) nor mAG-hGem(1/110) increased DNA synthesis measured by BrdU incorporation confirming that the overexpressed proteins are inactive (**Figure 4.2 i**) Collectively, these data suggest that the Fucci system can be utilized in differentiated cardiomyocytes.

4.3 mAG-hGem(1/110) expression in presence of known inducers of CM proliferation

In order to evaluate our screening strategy we have stimulated neonatal cardiomyocytes with fibroblast growth factor 1 (FGF1) and an inhibitor of the p38 mitogen-activated protein (MAP) kinase (p38i). This combination has been shown to be a potent inducer of cardiomyocytes proliferation[116]. Accordingly it induced Geminin-expression in neonatal cardiomyocytes (25.8% ± 2.7% *vs.* 3.3% ± 0.3%, $p < 0.01$) (**Figure 4.3. e, f**). FGF1/p38i stimulation after Ad-mAG-hGem(1/110) infection increased the expression of mAG-hGem(1/110) in neonatal cardiomyocytes approximately 18-fold compared to the control (20.0% ± 2.6% *vs.* 1.1% ± 0.2%, $p < 0.01$) (**Figure 4.3. c, d**). The FGF1/p38i-induced mAG-hGem(1/110) expression could be easily detected by visual inspection. The number of mAG-hGem(1/110)-positive cells per field was increased more than 9-fold compared to the control (9 ± 3 *vs.* ≤ 1) (**Figure 4.3. a, b**).

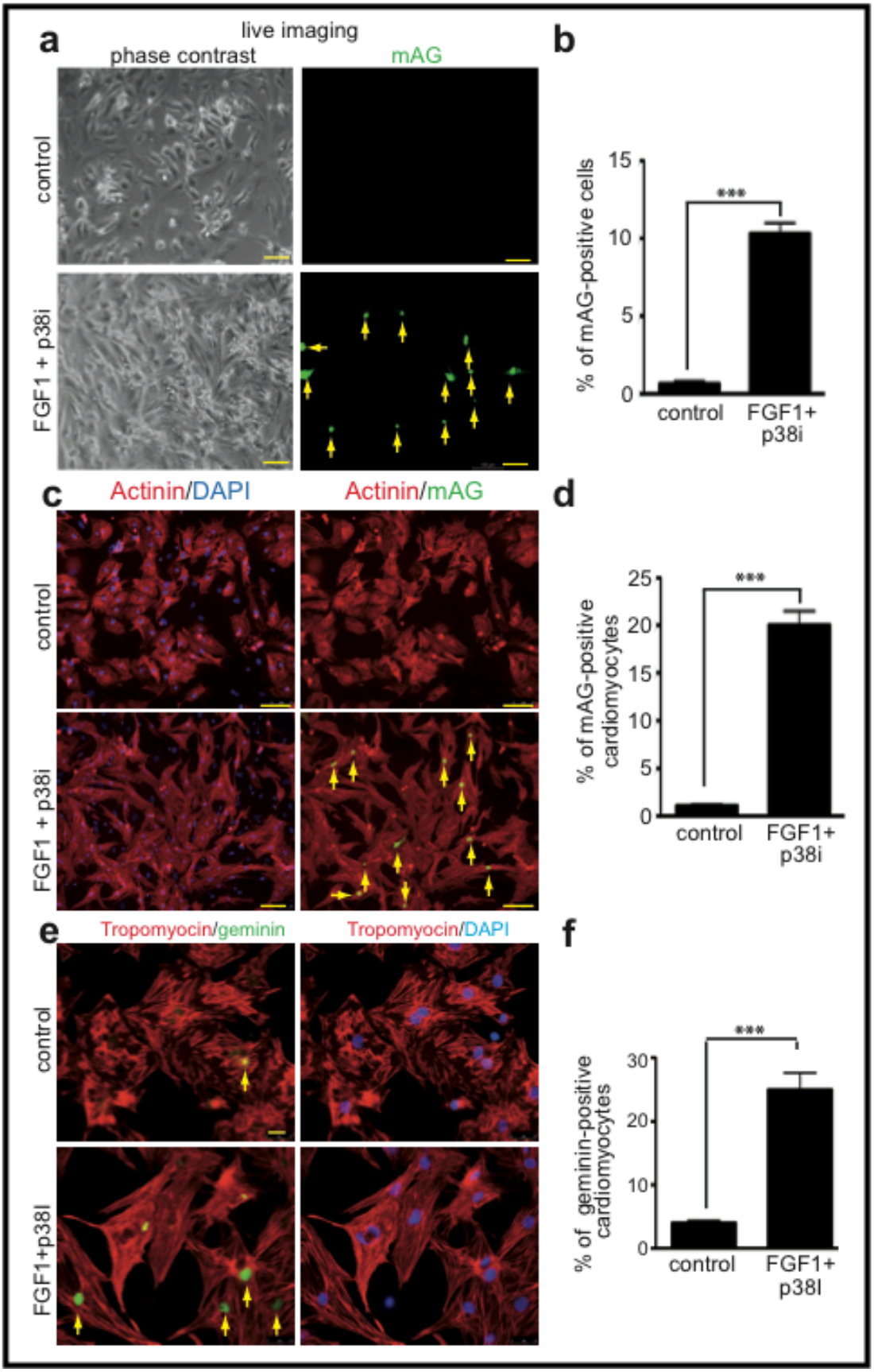

Figure 4.3: mAG-hGem(1/110) expression in presence of known inducers of cardiomyocyte proliferation.

(c) and **(d)** P3 cardiomyocyte cultures infected with Ad-mAG-hGem(1/110) were treated with DMSO or FGF1+p38i and stained for mAG expression (green) and counterstained against cardiomyocyte-specific Actinin (red). DAPI was used to visualize nuclei (blue). **(d)**, Quantitative analysis of (c) (n = 6). **(a)** and **(b)**, Quantitative analysis (n = 6) and representative live pictures of control or FGF1+p38i-stimulated neonatal cardiomyocyte cultures infected with Ad-mAG-hGem(1/110) (green). : **: $p < 0.01$. Scale bar = 100 µm **(e),** Representative examples of enriched neonatal cardiomyocyte cultures serum-starved or stimulated with FGF1 + p38i stained for Geminin (green), Tropomyosin (red) and DNA (DAPI, blue). **(f)**, Quantitative analysis of **(e)** (n = 4).**: $p < 0.01$. Scale bar = 50 µm.

4.4 Screening strategy

The use of the Fucci system to detect the induction of cell cycle re-entry allows two different screening approaches: loss of signal (mCherry-hCdt1(30/120)) or gain of signal (mAG-hGem(1/110)) (**Figure 4.4 a**). Overexpression of mCherry-hCdt1(30/120) resulted in a signal that could be easily detected by visual inspection (**Figure 4.4 b**). However, less mCherry-positive cardiomyocytes were detected during live cell observation than after immunofluorescence staining analysis (**Figure 4.4 a**). In addition, this approach appears to be error-prone due to the unavoidable presence of non-myocytes. Drug-induced increase of the mCherry-hCdt1(30/120)-negative non-myocyte population will result in a “false loss of signal” giving the wrong impression that cardiomyocytes have re-entered the cell cycle (**Figure 4.4 d**). Therefore, this approach appears not optimal.

In contrast, screening based on geminin appears to be very stringent as the noise of the system is very low (<1.5% mAG-hGem(1/110)-positive cardiomyocytes) and proliferating non-myocytes will increase the signal only minimal (< 0.5% mAG-hGem(1/110)-positive non-myocytes) (**Figure 4.4 c**). Collectively, our data suggest that this screening approach based on mAG-hGem(1/110) expression can be utilized to screen small molecule libraries for molecules that induce cardiomyocytes cell cycle re-entry.

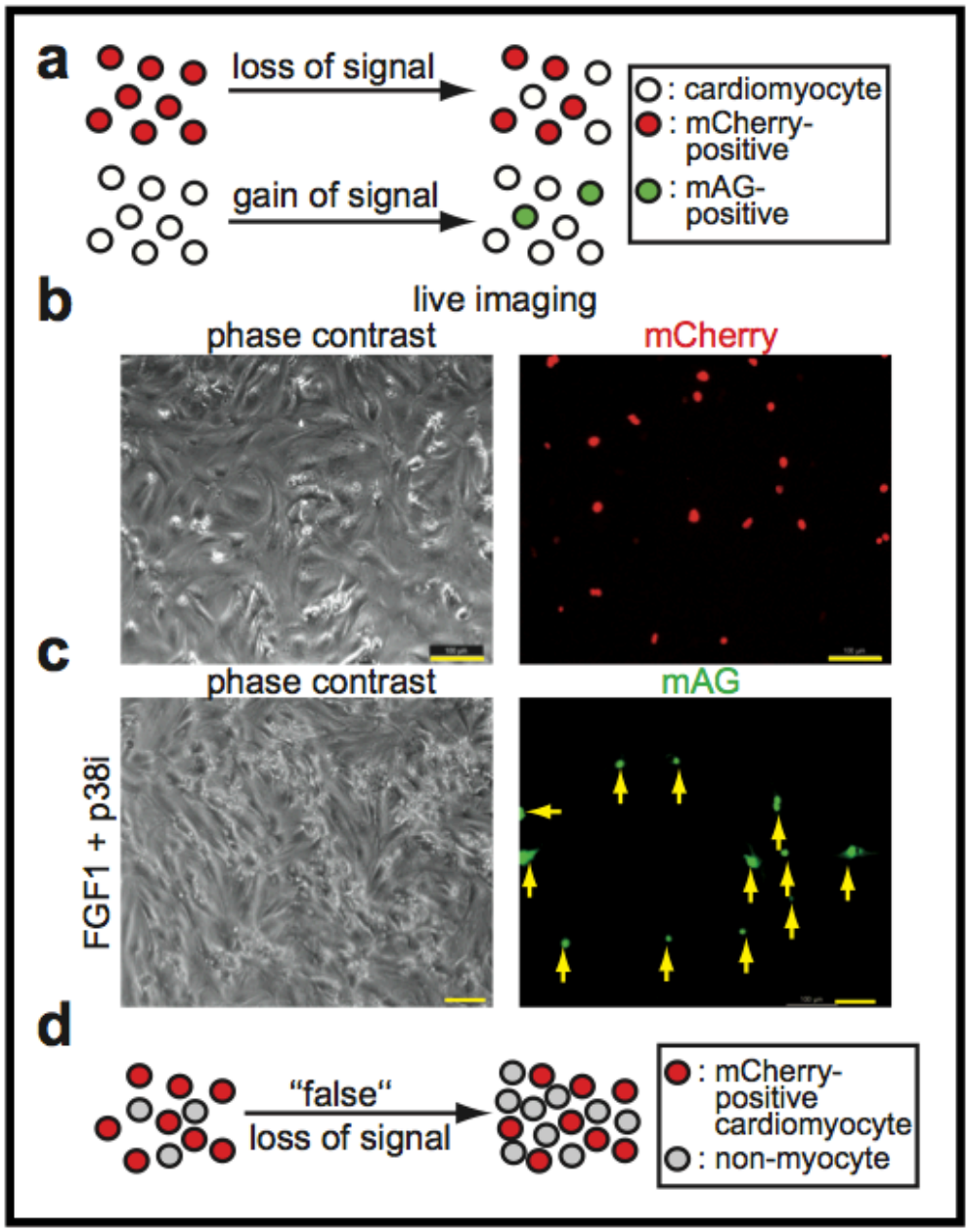

Fig 4.4: Schematic representation of possible screening approaches in which induction of proliferation is associated with a loss or gain of signal (a). (**b**), Representative live pictures of a control neonatal cardiomyocyte culture infected with Ad-mCherry-hCdt1(30/120) (red) **(b)** and Ad-mAG-hGem(1/110) **(c).** (**d),** Schematic representation of the effect of drugs inducing non-myocyte proliferation mocking loss of signal.

4.5 Screening of chemical libraries identifies carbacyclin

Two small molecule libraries were screened for molecules that induce cardiomyocytes cell cycle re-entry: a nuclear receptor ligand library (Enzo Life Sciences) and an epigenetics-screening library (Cayman Chemicals). Cardiomyocytes were isolated from 3-days-old neonatal rats, enriched and seeded at 15,000 cells per well in a 96-well plate. After 2 days the cells were

infected with an adenovirus expressing mAG-hGem(1/110) under the control of the cardiomyocyte specific alpha-MHC promoter. One day later at day 3 cells were washed and treated with the different compounds at three different concentrations (10 nM, 250 nM and 30 µM). DMSO served as negative control, 10% FCS and FGF1/p38i as positive controls. Subsequently, mAG-hGem(1/110)-positive cells per field were recorded for 4 days at intervals of 12 h. Data are represented as fold change increase of the observed maximal number of mAG-hGem(1/110)-positive cells per field in comparison to the average maximal number in DMSO treated cultures over time (**Table 4.1**). The workflow of this screen is summarized in (**Figure 4.5 a**).

The positive control FGF1/p38i treatment induced a 10-fold increase while 10% FCS, a weaker inducer of cell cycle re-entry, a 5-fold increase in mAG-hGem(1/110)-positive cells per field. Most of the tested small molecules had no effect on cardiomyocyte cell cycle re-entry. However, 8 compounds induced at least a 2-fold increase in mAG-hGem(1/110)-positive cells (**Figure 4.5 b** and **Table 4.1**). The most potent treatment was 250 nM carbacyclin inducing a 9-fold increase (**Figure 4.5 b**). These data suggested that carbacyclin is a new inducer of cardiomyocytes proliferation.

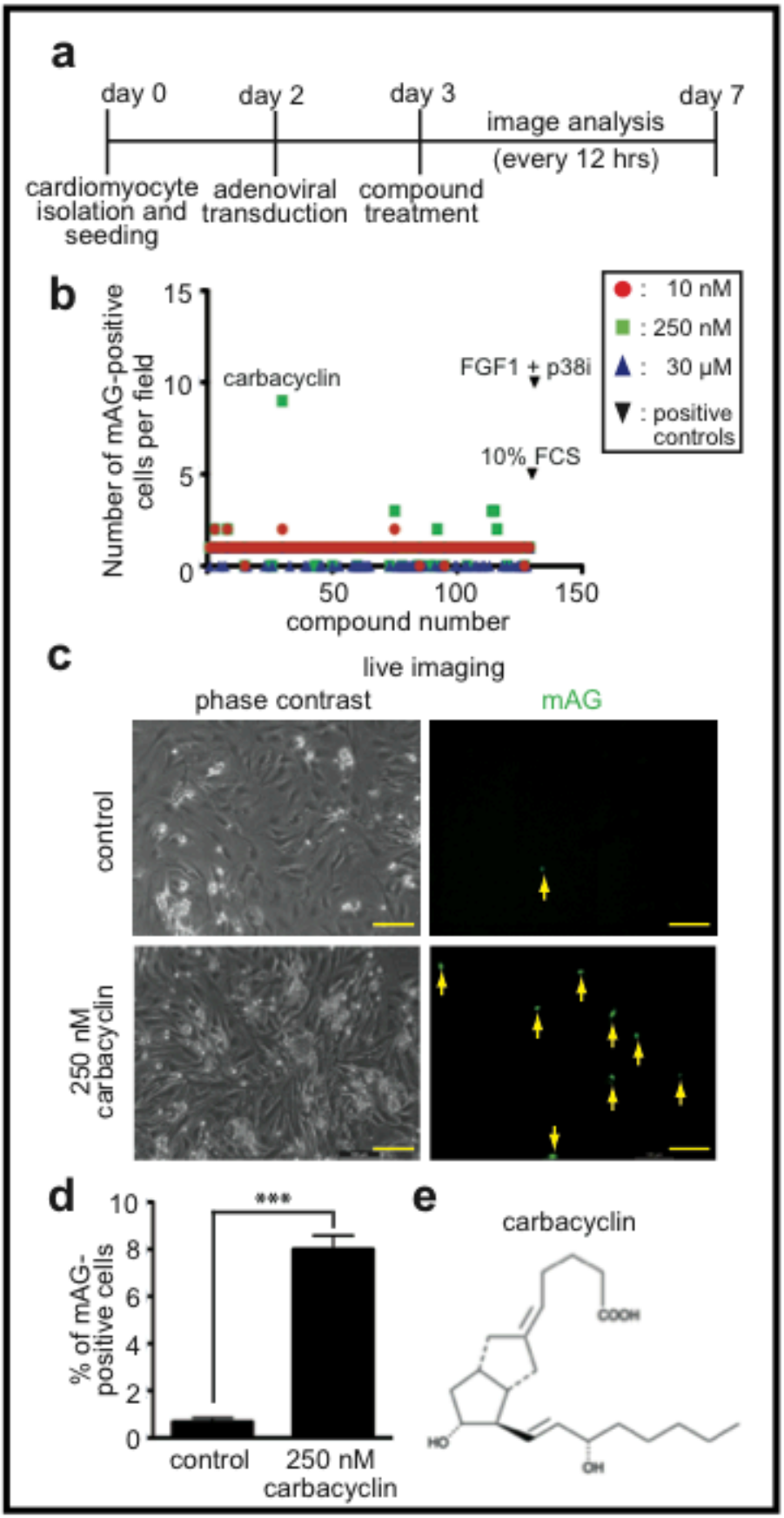

Figure 4.5: Screening of chemical libraries identifies carbacyclin. **(a)**, Work flow of the applied screening strategy. **(b)**, Quantitative analysis of the screen of a nuclear receptor ligand

library and an epigenetics screening library. **(c)**, Representative live pictures of control or carbacyclin-treated neonatal cardiomyocyte cultures infected with Ad-mAG-hGem(1/110) (green). **(d)**, Quantitative analysis of **c** (n = 6). **(e)**, Structure of carbacyclin. **: $p < 0.01$. Scale bar = 100 µm.

4.6 Validation of carbacyclin as inducer of cardiomyocyte proliferation

In order to validate the screening data and to find the optimum concentration of positive hits with regards to induction of cell cycle re-entry, we treated P3 neonatal cardiomyocytes with all positive hits including trans-retinoic acid, 4-hydroxy retinoic acid, TTNPB, RG-108, cay-10433, sinefungin, nicotinamide and cabacyclin at 10 nM, 100 nM, 250 nM, 1 µM and 5 µM. Cells were cultured for 2 days and pulse-labeled with BrdU for the final 24 hours, a marker of DNA synthesis. Carbacyclin induced BrdU incorporation in a dose-dependent manner with an optimal concentration of 1 µM (46.3% ± 3.8% *vs.* DMSO: 3.6% ± 0.6%, $p < 0.01$) (**Figure 4.6 a, b**), while other compounds only moderately induced BrdU incorporation in cardiomyocytes (**Figure 4.6 a, b, c, d, e, f** and **g**).

To determine the effect of carbacyclin on cardiomyocyte proliferation, we assessed its effect on well-characterized cell cycle genes on RNA and protein level. Carbacyclin induced the expression of cell cycle perpetuating factors like phospho-RB, cyclin D2, cyclin A, cyclin B, cdc2, and c-myc (**Figure 4.6 c** to **f**). In addition, carbacyclin stimulation resulted in the downregulation of the cell cycle inhibitors p21 and p27 (**Figure 4.6 c** to **f**). These data suggested that carbacyclin induces cell cycle re-entry of neonatal cardiomyocytes.

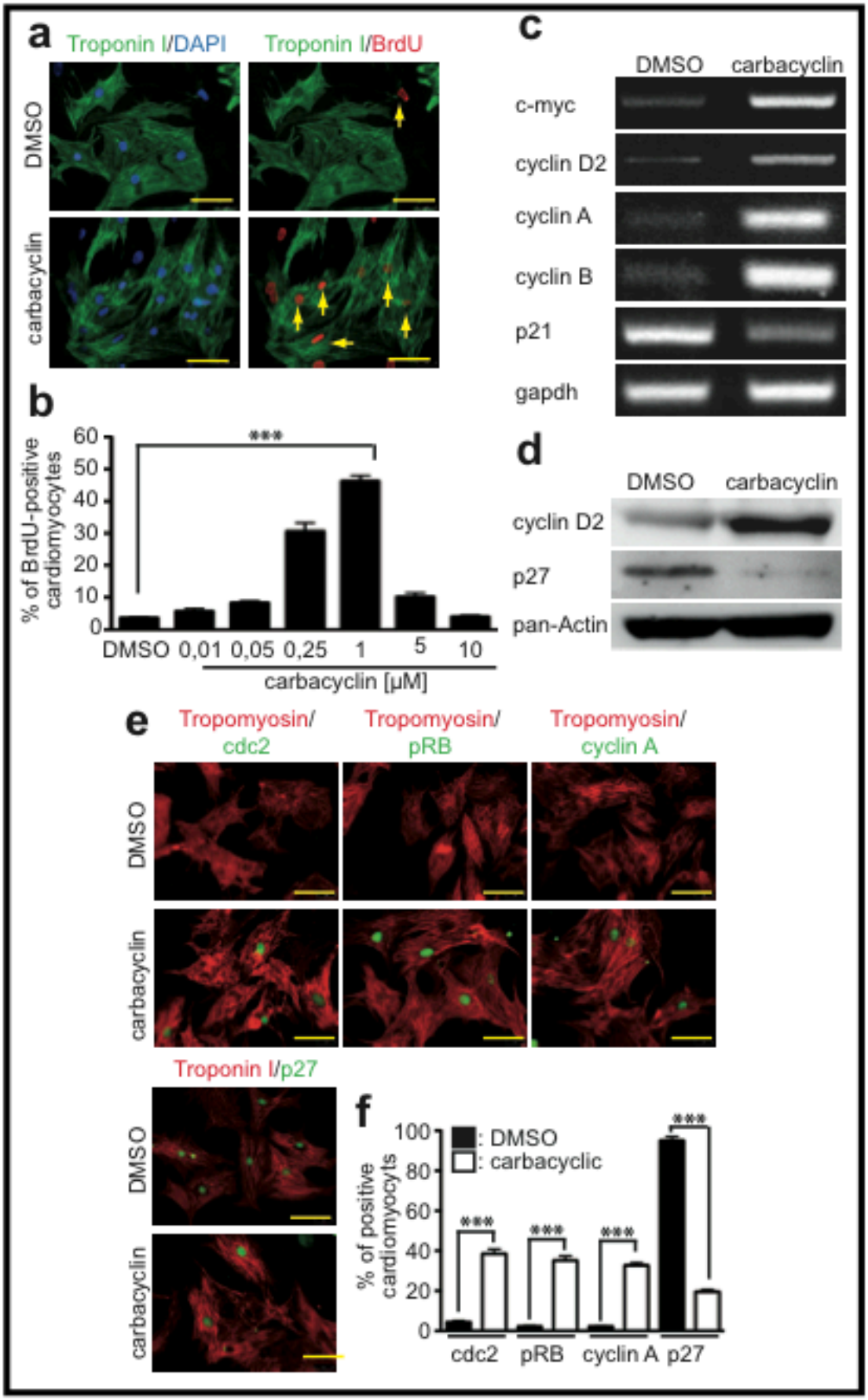

Figure 4.6: Validation of carbacyclin as inducer of cardiomyocytes proliferation. (b), Carbacyclin induced dosage dependent BrdU incorporation of neonatal cardiomyocytes (n = 6).

(a), Representative example of neonatal cardiomyocytes stained for BrdU (red) and Troponin I (green, cardiomyocyte-specific). DNA was visualized using DAPI (blue). (**c** to **e)**, Treatment with carbacyclin induced increased expression of cell cycle promoting factors and a decrease in expression of cell cycle inhibitors. **(c)**, Representative examples of RT-PCR analysis at 48 h. **(d)**, Representative examples of Western blot analysis at 48 h. **(e)**, Representative examples of immunofluorescence analysis at 48 h. Cardiomyocytes were stained for Troponin I or Tropomyosin (red, cardiomyocyte-specific), cell cycle regulators (green) and DNA (blue). **(f)**, Quantitative analysis of **e** (n = 6). **: $p < 0.01$. Scale bar = 50 µm.

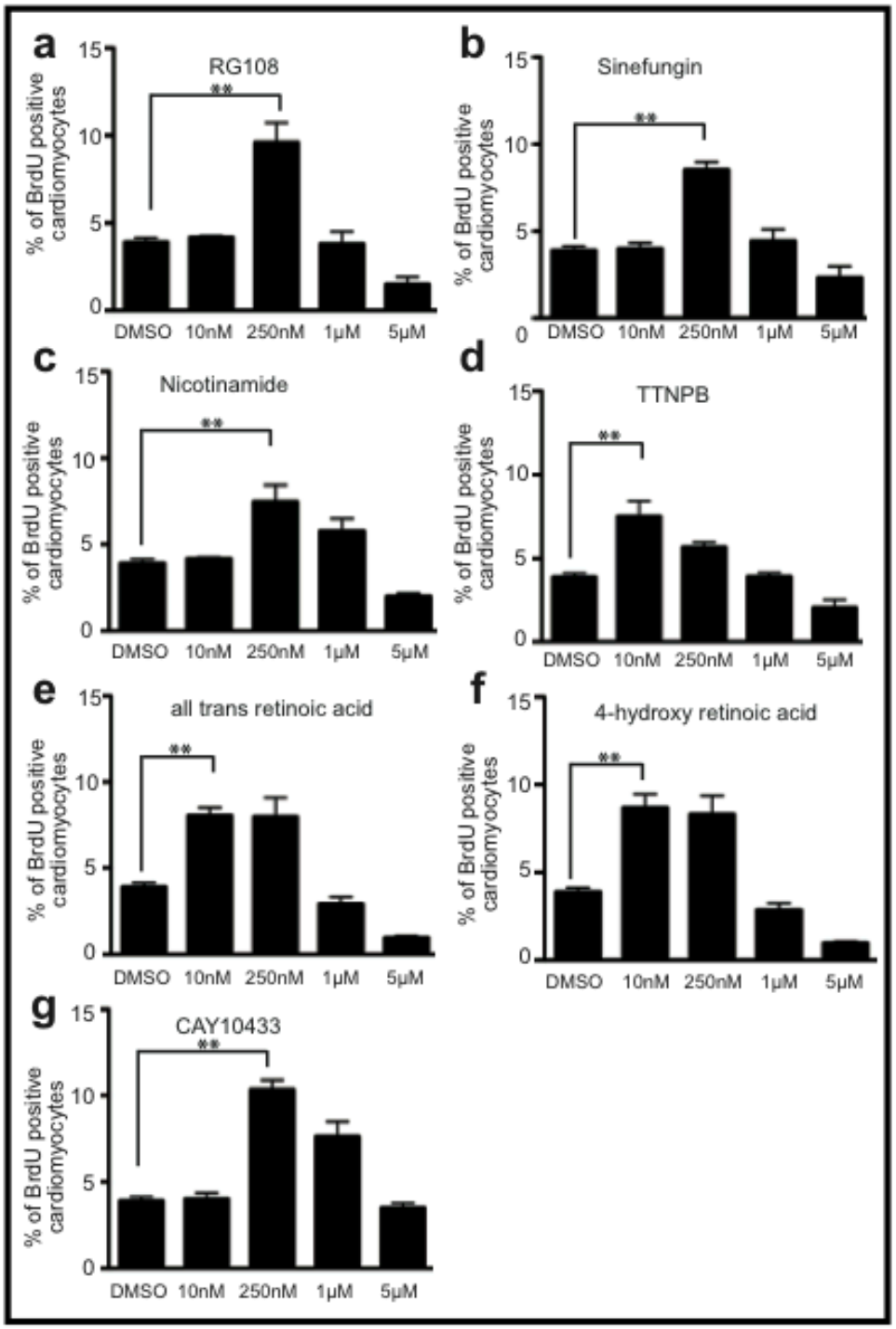

Figure 4.7: Validation of other positive hits as inducer of cardiomyocyte cell cycle re-entry. (a) to **(g)**, Dose-dependent incorporation of BrdU in neonatal cardiomyocytes (n = 4). *: $p < 0.05$; **: $p < 0.01$

4.7 Carbacyclin induces mitosis in neonatal cardiomyocytes

To assess if carbacyclin regulates karyokinesis in neonatal cardiomyocytes, we assayed mitosis by immunofluorescence staining of phosphorylated histone-H3 at ser10 (H3P). Carbacyclin increased the number of H3P-positive cells 11.5-fold resulting in 4.6% ± 0.4% H3P-positive cardiomyocytes compared to 0.4% ± 0.1% in control ($p < 0.01$) at three days after carbacyclin stimulation (**Figure 4.8 a, c**). This value is comparable to that of proliferating cell lines and the mitotic index of fetal cardiomyocytes during embryonic development (E12, 3.7% ± 0.6%)[116]. The H3P-positive cardiomyocytes were also increased after treatment of other positive hits **(Figure 4.8 g).** Thus the carbacyclin induced neonatal cardiomyocyte karyokinesis more efficiently than the other 7 identified compounds.

4.8 Carbacyclin induces cell division in neonatal cardiomyocytes.

To test whether carbacyclin treatment induces cardiomyocyte cell division, we assayed cytokinesis using utilizing Aurora B antibodies. Carbacyclin treatment increased the number of Aurora B-positive cells 11.5-fold compared to control resulting in 4.7% ± 0.4% Aurora B-positive cardiomyocytes (control: 0.4% ± 0.1%, $p < 0.01$) (**Figure 4.8 b, c**). Cardiomyocytes stimulated with carbacyclin were found in all stages of cell division including the final stages of cytokinesis (**Figure 4.8 e, d**). In addition the cells underwent, as previously described transient dedifferentiation of the sarcomeric apparatus during mitosis (**Figure 4.9**). Compared to DMSO carbacyclin treatment did also not induce cardiomyocyte binucleation at day 5. As positive control we utilized 10% FCS (DMSO: 10.6% ± 1.4%; 1 µM carbacyclin: 12.5% ± 1.6%; 10% serum 36.7% ± 3.3%. **: $p < 0.01$; $n = 6$) (**Figure 4.10**). These data indicate that carbacyclin induces neonatal cardiomyocytes to re-enter the cell cycle and then to divide. Moreover, continuous stimulation of neonatal cardiomyocytes resulted in an increase in cardiomyocyte cell density over time (**Figure 4.8 f**). Taken together, carbacyclin is a potent inducer of neonatal rat cardiomyocyte proliferation.

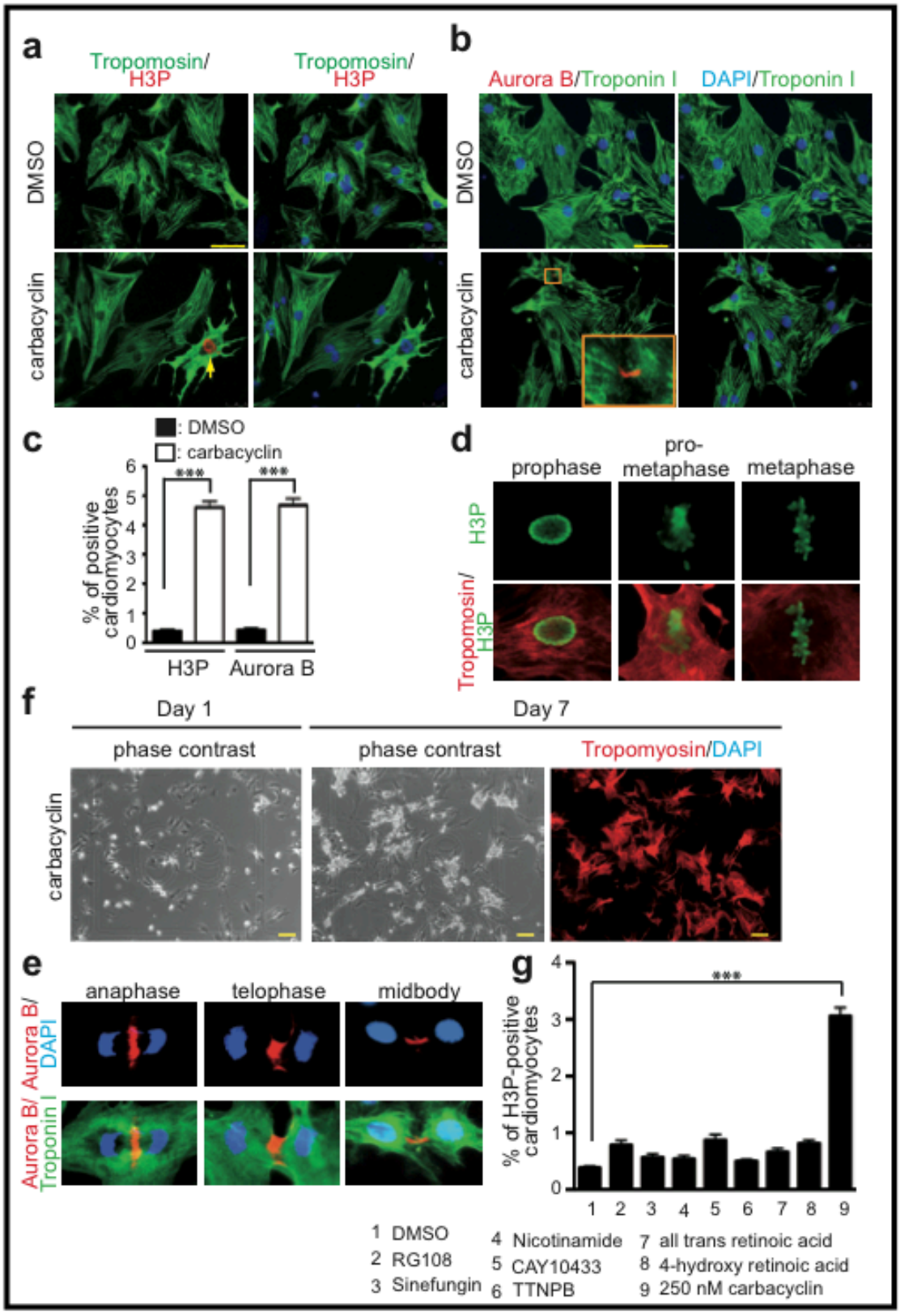

Fig 4.8: Carbacyclin induces Mitosis and cell division in neonatal cardiomyocytes (a, b, c,) Carbacyclin (1 µM) induced H3P and Aurora B positive neonatal cardiomyocytes. Representative examples of neonatal cardiomyocytes stained for Tropomyosin (red, cardiomyocyte-specific) and H3P (green) identifying mitotic neonatal cardiomyocytes. **(b)**

Representative example of neonatal cardiomyocytes stained for Troponin I (green, cardiomyocyte-specific) and Aurora B (red, central spindle) identifying neonatal cardiomyocytes undergoing cytokinesis. DNA was visualized using DAPI (blue). **(c)** Quantitative analysis of a and b (n = 4). **(d** and **e)** Representative pictures of cardiomyocyte are in different phases of mitosis and mid body formation. **(f)** Representative examples of cell density experiments. Continuous stimulation of cardiomyocytes with carbacyclin resulted in cardiomyocyte proliferation. (At day 7 cells were fixed and stained with Tropomyosin (red) and DAPI (blue)). **(g**). Quantitative analysis of H3P-positive cardiomyocytes (n = 4). For each compound the most efficient concentration regarding BrdU incorporation was used (for 7 and 8 10 nM). *: $p < 0.05$; **: $p < 0.01$ Scale bar = 50 µm (**a** and **b**), Scale bar = 100 µm **(f).**

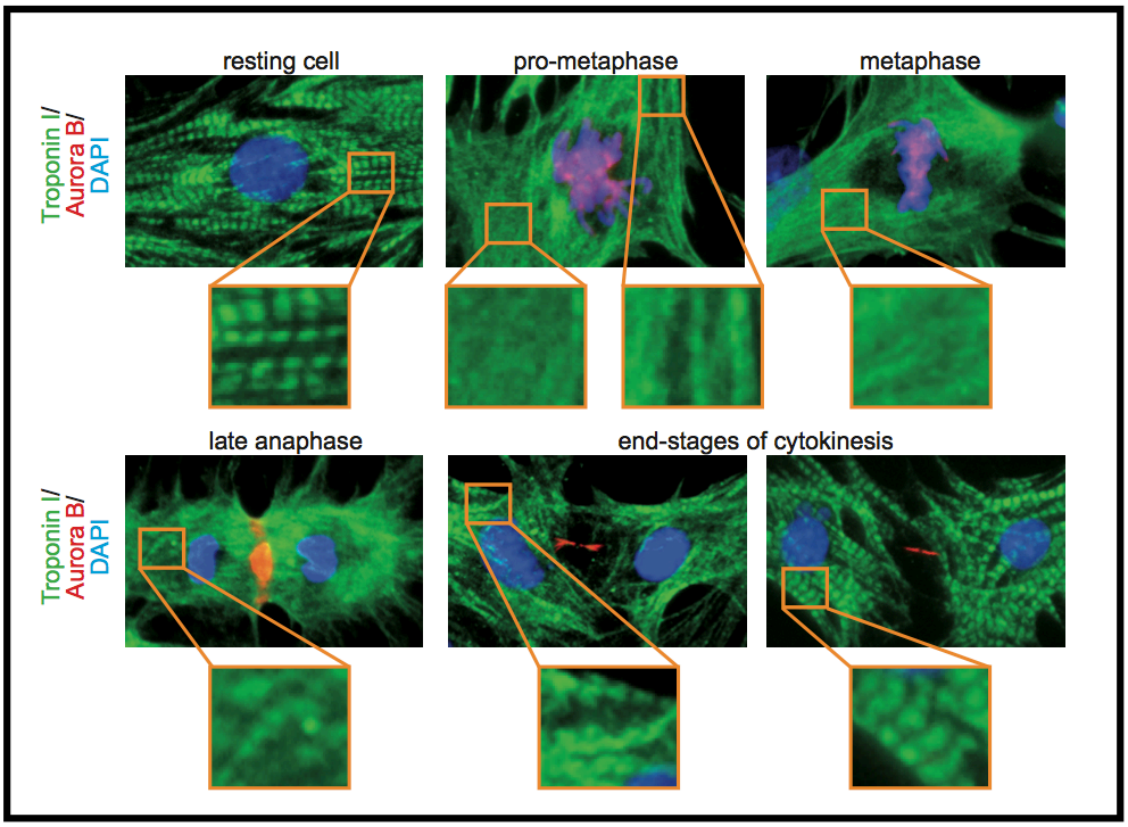

Figure 4.9: Indicators of cardiomyocyte cell division. Disassembly of myofibrils during carbacyclin-induced cardiomyocyte cell division. The extent of sarcomere disassembly was assessed in carbacyclin-treated cardiomyocytes using Troponin I (green). Cells were stained for Aurora B (red) and DNA (DAPI, blue) to assess the cell cycle status. Striations were apparent in resting/unstimulated cells. During pro-metaphase, sarcomeres became disassembled and were reassembled during late anaphase.

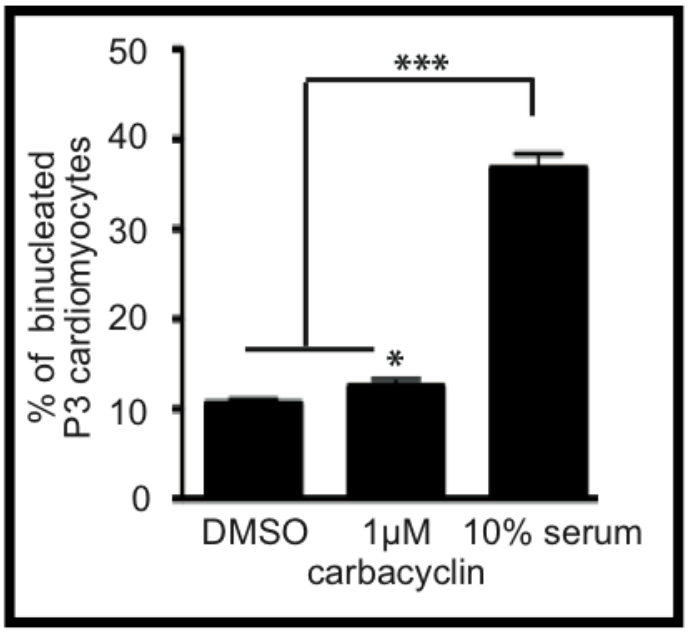

Fig 4.10: Carbacyclin does not induce binucleation in cardiomyocytes. Quantitative analysis of the percentage of binucleated cardiomyocytes after 5 days of treatment with DMSO,, 1 µM carbacyclin and 10% serum. (Cells were treated on day 0 and day 3) (n = 6). **: $p < 0.01$.

4.9 Non-myocytes do not affect carbacyclin-induced neonatal cardiomyocyte proliferation

It is known that the presence of non-cardiomyocytes affects the cardiomyocyte proliferation in culture and also during heart development. Therefore we were interested to determine whether the presence of non-cardiomyocytes in culture affects the potency of carbacyclin to induce P3 neonatal cardiomyocyte proliferation. We used non-enriched cultures containing around 50% of non-cardiomyocytes. Carbacyclin 1 µM treatment induced DNA synthesis in more than 40% of cardiomyocytes (42.2% ± 5.7%; *vs.* DMSO: 4.8% ± 0.8%, $p < 0.01$) (**Figure 4.11 a, b**).

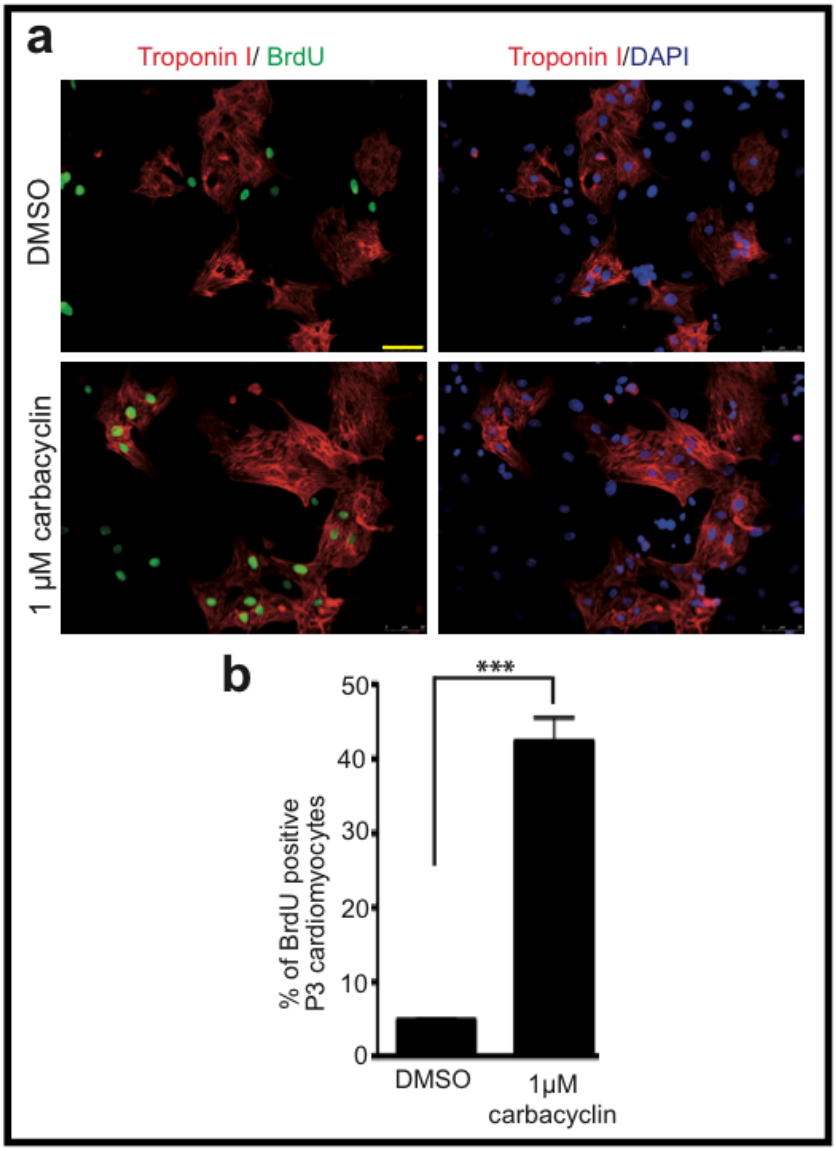

Fig 4.11: Carbacyclin induced cardiomyocyte cell cycle re-entry does not correlate/affected with abundance of non-cardiomyocytes. **(a)** Non-enriched P3 cardiomyocyte culture (around 50% non-cardiomyocytes) were treated with DMSO or carbacyclin and stained for BrdU (green) and counter stained against cardiomyocyte-specific Troponin I (green). DAPI was used to visualize nuclei (blue). **(b)**, Quantitative analysis of **(a)** (n = 6). **: $p < 0.01$. Scale bar = 100 µm.

4.10 Activation of the PPARδ-induced pathway is required for cardiomyocyte proliferation

Carbacyclin is a chemically stable carbocyclic analog of prostacyclin, a known potent agonist of PPARδ, which is associated to 3-phosphoinositide-dependant protein kinase-1 (PDK1)/p308Akt and pGSK3B/β-catenin signaling as well as promotion of proliferation. Thus, we wondered if carbacyclin activates the

PPARδ/PDK1/p308Akt/pGSK3B/β-catenin-pathway in neonatal cardiomyocytes, we utilized different small molecules, dominant negative proteins and siRNAs and assayed for induction of DNA synthesis by BrdU incorporation in neonatal cardiomyocytes (**Figure 4.12**). Stimulation of cardiomyocytes with 1 µM carbacyclin resulted in the up regulation of PPARδ, PDK1 and an increase in nuclear PPARδ and β–catenin (**Figure 4.13 a, b**). Taken together, these data show that carbacyclin activates PPARδ signaling in cardiomyocytes.

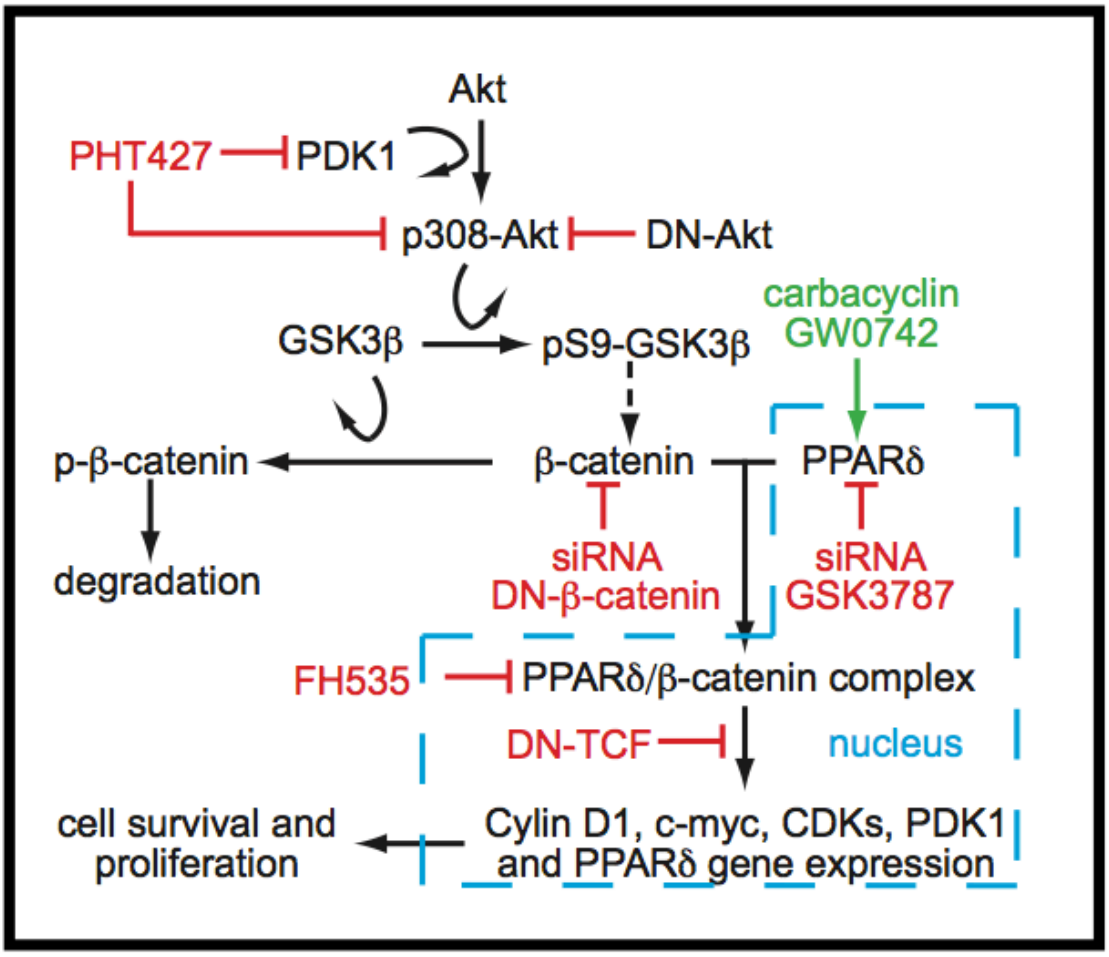

Figure 4.12: Model of the carbacyclin-induced signaling pathway in neonatal cardiomyocytes.

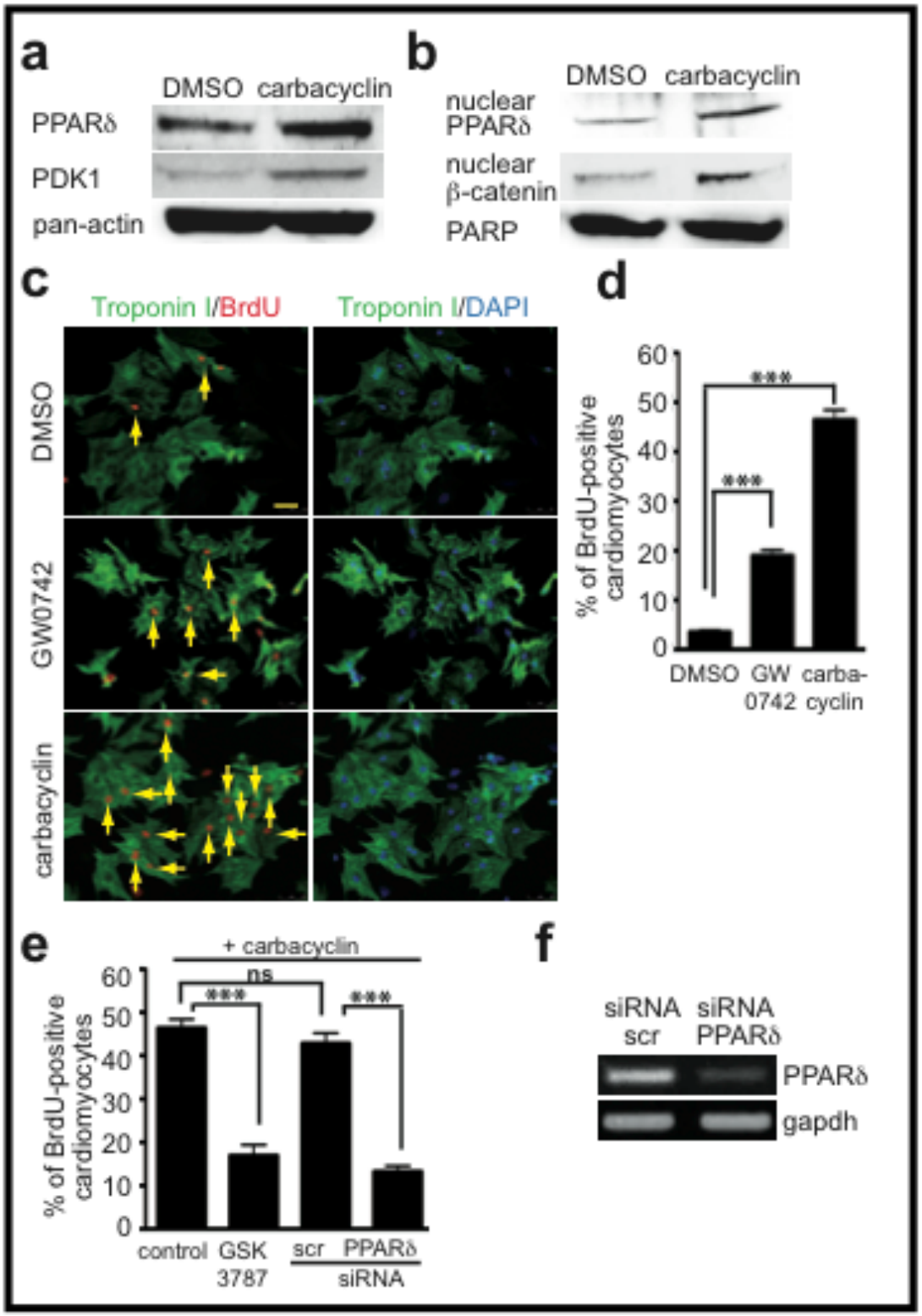

Figure 4.13: Activation of the PPARδ -pathway is required for cardiomyocyte proliferation. To determine whether the activation of the PPARδ /PDK1/p308Akt/pGSK3B/β-catenin pathway by carbacyclin is required for the induction of cardiomyocyte proliferation we utilized different small molecules, dominant negative proteins and siRNAs and assayed for induction of DNA synthesis by BrdU incorporation in neonatal cardiomyocytes. **(a)**, Representative examples of Western blot analysis showing that carbacyclin increased the

expression of PPARδ at 48 h and PDK1 at 24 h. **(b)** The increase in nuclear PPARδ and β-catenin at 48 h after carbacyclin treatment. **(c)** and **(d)**, Two agonist of PPARδ , carbacyclin and GW0742 significantly increased DNA synthesis in neonatal cardiomyocytes. **(d)** Quantitative analysis of c. (n=6) **(e),** Inhibition of PPARδ by siRNA or the antagonist GSK3787 abolished the effect of carbacyclin on cardiomyocyte DNA synthesis (scr: scrambled). (n=6) **(f)** The siRNA-mediated knockdown of PPARδ mRNA was checked by PCR. *: $p < 0.05$; **: $p < 0.01$ Scale bar = 50 µm.

GW0742, another agonist of PPARδ , also induced BrdU incorporation in neonatal cardiomyocytes (17.8% ± 3.2% *vs.* DMSO: 3.4% ± 0.5%; $p < 0.01$, (**Figure 4.13 c, d**) suggesting that carbacyclin-mediated cell cycle re-entry requires activation of PPARδ. This conclusion was further supported by the fact that carbacyclin-mediated induction of BrdU incorporation was significantly reduced by 100 nM GSK3787, a specific inhibitor of PPARδ (46.9% ± 4.2% to 18.3% ± 3.4%; $p < 0.01$, (**Figure 4.13 e**), as well as by siRNA-mediated knock down of PPARδ (46.9% ± 4.2% to 13.2% ± 3.9%; $p < 0.01$, (**Figure 4.13 e**). The siRNA-mediated knockdown of PPARδ mRNA was checked by PCR (**Fig 4.13 f**). Collectively, these data suggest that carbacyclin induces cardiomyocyte proliferation by activating PPARδ .

4.11 Role of PDK1-Akt-β-catenin axis in carbacyclin induced cardiomyocyte proliferation

Previously, it has been shown that activation of different signaling pathways, including PI3 kinase and extracellular-signal-regulated kinases (ERKs), can mediate cardiomyocyte proliferation[99]. However, neither 20 µM PD98059, an inhibitor of ERKs, nor 10 µM LY294002, an inhibitor of PI3 kinase, affected carbacyclin-mediated induction of BrdU incorporation (**Figure 4.14 a, b**). In contrast, overexpression of dominant negative Akt (DN-Akt) markedly decreased BrdU incorporation (45.3% ± 3.0% to 14.2% ± 2.9%; $p < 0.01$, (**Figure 4.14 a, b**). Moreover, BrdU incorporation was also decreased after addition of 20 µM PHT427, a dual inhibitor of PDK1/Akt (20.8% ± 2.4%; $p < 0.01$, (**Figure 4.14 b**). Stimulation of cardiomyocytes with 1 µM carbacyclin resulted in the up-regulation of phosphorylation of Akt at Thr308 and GSK3B.

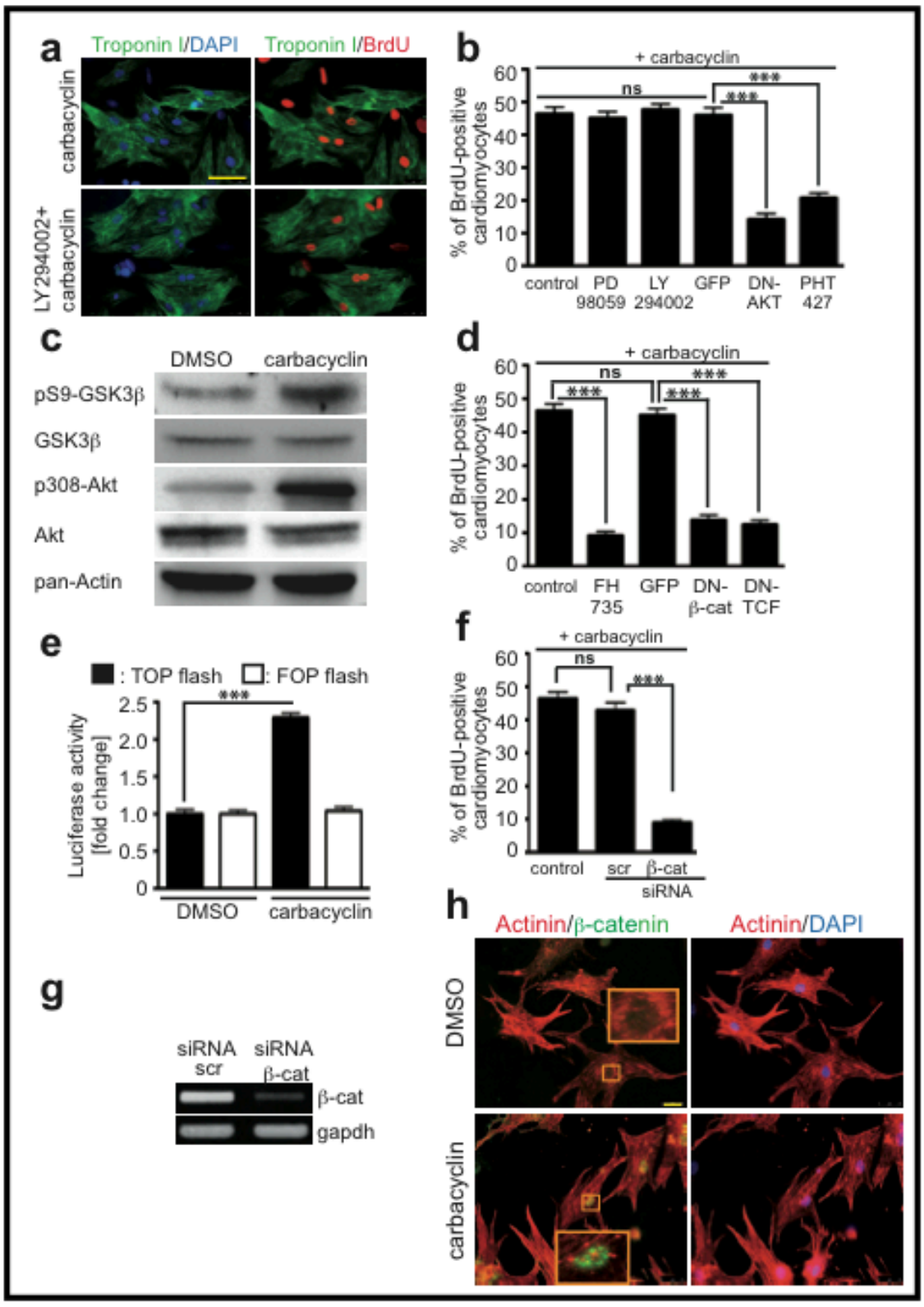

Fig 4.14: PDK1-Akt-β-catenin axis required for carbacyclin induced cardiomyocyte proliferation (a) and **(b)** Akt phosphorylation at position 308 is required for carbacyclin-induced DNA synthesis but not PI3 kinase-induced AKT phosphorylation (LY 294002) or ERK activity (P 98059). These inhibitors do not significantly decrease DNA synthesis in neonatal cardiomyocytes**. (b)** Quantitative analysis of a. (n=6). **(a)** and **(b)** The DN-Akt as well as PDK1 and Akt dual inhibitor PHT427 inhibited carbacyclin induced BrdU incorporation. (Adenoviral

GFP is used as control for DN-Akt) (n=6). **(c)** Representative examples of Western blot analysis showing that carbacyclin increased the phosphorylation of p308 Akt and pS9-GSK3B at 48 h. **(d)** and **(f)** Inhibition of β-catenin signaling by siRNA (β-cat), adenoviral overexpression of dominant negative β-catenin or TCF as well as blocking the activity of β-catenin/ PPARδ complexes by FH535 abolished the effect of carbacyclin on cardiomyocyte DNA synthesis. **: $p < 0.01$, $n = 6$. **(g)** The siRNA-mediated knockdown of PPARδ mRNA was checked by PCR. *: $p < 0.05$; **: $p < 0.01$ Scale bar = 50 µm. **(e),** In addition, carbacyclin induced β-catenin-mediated transcriptional activation, which was assayed by using reporter containing either functional (TOPflash) or mutated (FOPflash) Tcf binding sites. **(h)** Representative examples of neonatal cardiomyocytes stained for actinin (red, cardiomyocyte-specific) and β-catenin (green) showing increase in nuclear β-catenin in cardiomyocytes at 48 h after carbacyclin treatment. DNA was visualized using DAPI (blue). Scale bar = 50 µm.

at Ser9 (**Figure 4.14 c**). These data suggest that not PI3 kinase-mediated but PDK1-mediated phosphorylation of Akt is required for carbacyclin-mediated cell cycle re-entry of postnatal cardiomyocytes.

Finally, also inhibition of β-catenin signaling by siRNA-mediated knock down of β-catenin significantly reduced BrdU incorporation (8.9% ± 1.3% *vs.* scrambled siRNA: 42.8% ± 4.0%, $p < 0.01$, (**Figure 4.14 f**). The siRNA mediated knockdown of β-catenin mRNA was confirmed by PCR (**Figure 4.14 g**). In addition, BrdU incorporation was also inhibited by overexpression of dominant negative β-catenin (DN-β-cat) (46.4% ± 5.2% to 14.8% ± 2.2%, $p < 0.01$), addition of 15 µM FH 535, an inhibitor of nuclear PPARδ/β-catenin complexes (9.3% ± 1.3%, $p < 0.01$), or overexpression of dominant negative TCF (DN-TCF) (12.3% ± 4.3%, $p < 0.01$, (**Figure 4.14 d**). It has been shown before that translocation of β-catenin in to the nucleus and inhibition of its ubiquitinization induces cardiomyocytes proliferation[118, 119]. Also carbacyclin treatment resulted in nuclear translocation of β-catenin compared to DMSO (**Figure 4.14 h**). In addition, we assayed for β-catenin-mediated transcriptional activation by using a reporter containing either functional (TOPflash) or mutated (FOPflash) Tcf binding sites. Cells stimulated with carbacyclin increased reporter activity 2.3-fold compared to control $p < 0.01$) (**Figure 4.14 e**).

Finally, we tested whether the effect of carbacyclin on cardiomyocyte cell cycle entry can be further enhanced by FGF1, p38i or the GSK3B inhibitor BIO (which are known to induce cardiomyocytes proliferation). Our data

demonstrate that carbacyclin only in combination with 5 µM of BIO significantly increased the number of BrdU-positive (63% ± 7.4 *vs.* 46.4% ± 4.3, $p < 0.01$) as well as H3P-positive cardiomyocytes (5.89% ± 0.53% *vs.* 4.48% ± 0.38%, $p < 0.01$) compared to carbacyclin treatment (**Figure 4.15 a, b**).

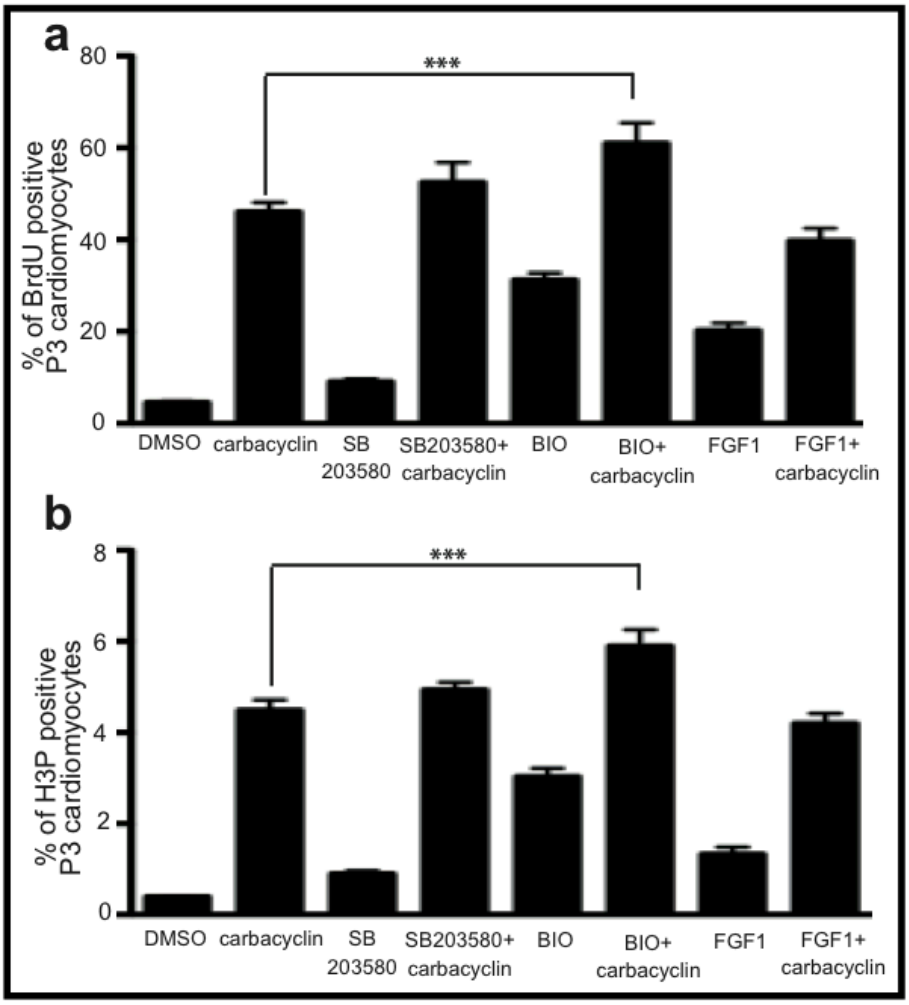

Figure 4.15: BIO enhanced carbacyclin induced cardiomyocyte proliferation. The effect of carbacyclin on neonatal cardiomyocyte cell cycle reentry is significantly increased in the presence of 5 µM BIO but not FGF1/p38 inhibitor. **(a)**, Quantitative analysis of BrdU incorporation (n = 6). **(b),** Quantitative analysis of mitosis by H3P staining (n = 6). **: $p < 0.01$.

Collectively, these data suggest that carbacyclin induces cardiomyocytes proliferation by activating the PPARδ-PDK1 autoregulatory pathway and β-catenin signaling.

4.12 Carbacyclin induces adult cardiomyocyte mitosis

Previously, it has been shown that newborn mice can regenerate their heart. However, this ability is lost in postnatal day 7 mice[75]. Therefore, we tested

whether carbacyclin can also induces cell cycle re-entry in postnatal day 8 (P8) rat cardiomyocytes. The BrdU incorporation was increased by more than 5-fold upon carbacyclin treatment (14.5% ± 1.7%*vs.* 2.73% ± 0.4%, $p < 0.01$; (**Figure 4.16 a, b**). A closer analysis revealed that carbacyclin mainly induced mono-nucleated cardiomyocytes to enter the cell cycle (**Figure 4.16 c**), content of binucleated cells: 41.5% ± 6.1%). The mitotic index (H3P-positive cardiomyocytes) was almost 7-fold increased (1.16% ± 0.13% *vs.* 0.17% ± 0.04%, $p < 0.01$; (**Figure 4.16 d, e**).

To determine if carbacyclin can induce cell cycle re-entry also in adult cardiomyocytes we repeated cell proliferation assays using ventricular cardiomyocytes from 12-weeks-old rats. Carbacyclin treatment increased the expression of mAG-hGem(1/110) at day 5 from less than 0.01% (DMSO) to 1.5% ± 0.2% ($p < 0.01$, (**Figure 4.17 a, b**) and resulted in 1.4% ± 0.2% BrdU-positive cardiomyocytes at day 6 (pulse-labeled final 5 days, control: < 0.001%, $p < 0.01$) (**Figure 4.17 a, b**). For the assessment of cell division we analyzed 100.000 adult cardiomyocytes from 4 independent experiments and found in the control in total 1 H3P and 1 Aurora B-positive c. In contrast, we detected after carbacyclin stimulation in total 58 H3P- and 34 Aurora B-positive adult cardiomyocytes (**Figure 4.17 c, d**).

Carbacyclin induced cell cycle re-entry preferentially in mononuclear cells. Of all positive adult cardiomyocytes 58.6% ± 5.0% of BrdU-positive, 58.1% ± 6.4% of H3P-positive and 61.7% ± 7.3% of Aurora B-positive cells were mono-nucleated (**Figure 4.17 e**). Taken together, our data demonstrate that carbacyclin is a potent inducer of mononuclear adult rat cardiomyocyte cell cycle re-entry and that our screening system allows the identification of small molecules that promote cardiomyocyte proliferation.

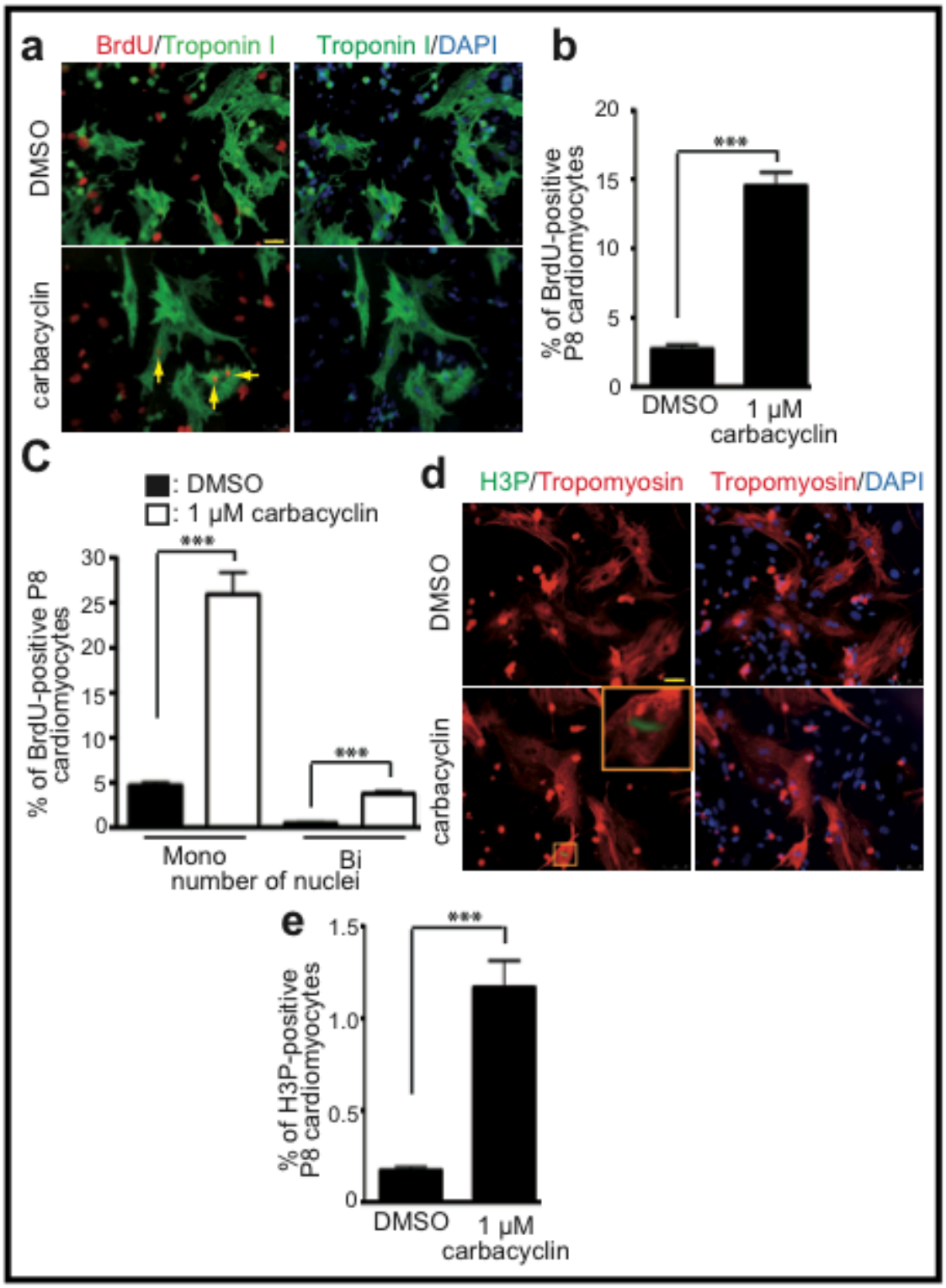

Fig 4.16: Carbacyclin induces P8 cardiomyocyte proliferation, preferentially in mono-nucleated cells. (**a** to **c)**, Carbacyclin induces P8 neonatal cardiomyocyte cell cycle re-entry. (**b** and **c),** Quantitative analysis of BrdU incorporation (n = 4). **(a)** Representative example of P8 cardiomyocytes stained for BrdU (red) and Troponin I (green, cardiomyocyte-specific). Nuclei were visualized using DAPI (blue). **(d** and **e),** Carbacyclin induces P8 cardiomyocyte mitosis.

(d) Representative example of P8 cardiomyocytes stained for H3P (green) and Tropomyosin (red, cardiomyocyte-specific). Nuclei were visualized using DAPI (blue). **(e)** Quantitative analysis of mitosis by H3P staining (n = 4). **: $p < 0.01$.

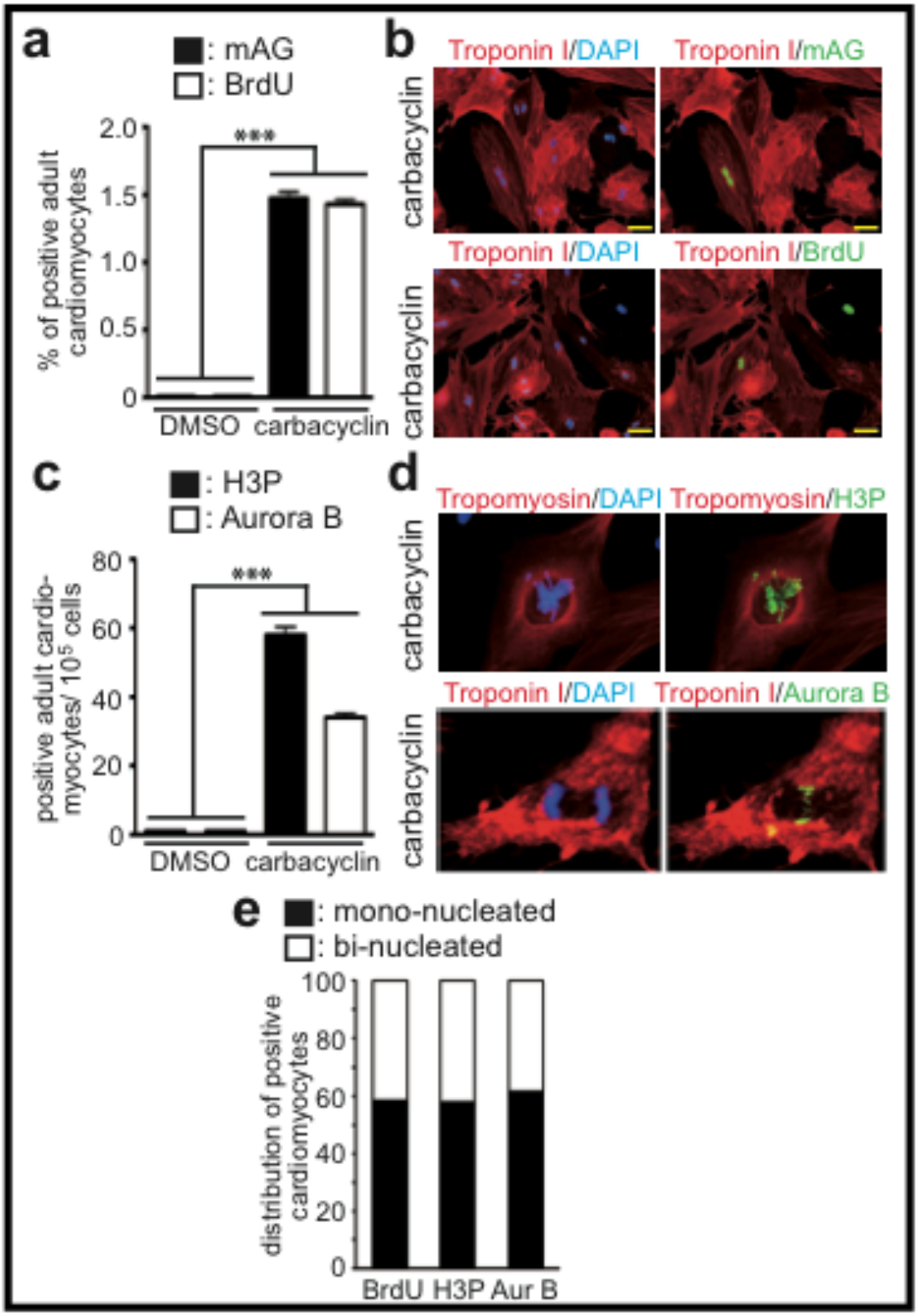

Figure 4.17: Carbacyclin induces adult cardiomyocyte cell cycle and mitosis, preferentially in mono-nucleated cells. **(a)** Carbacyclin induced mAG expression after

infection with Ad-mAG-hGem(1/110) as well as BrdU incorporation in adult (n = 6). **(b)**, Representative example of adult cardiomyocytes stained for mAG or BrdU (green) and Troponin I (red, cardiomyocyte-specific). Nuclei were visualized using DAPI (blue). **(c** and **d)** Carbacyclin treatment induced mitosis and cytokinesis in adult cardiomyocytes. (**c)**, Quantitative analysis (n = 6). **(d)**, Representative examples of adult cardiomyocytes undergoing mitosis and cytokinesis stained for Tropomyosin or Troponin I (red, cardiomyocyte-specific) and H3P or Aurora B (green). **(e)**, Carbacyclin induced cell cycle re-entry preferentially in mononuclear cells. Of all positive adult cardiomyocytes 58.6% ± 5.0% of these cells were BrdU-positive, 58.1% ± 6.4% were H3P-positive and 61.7% ± 7.3% Aurora B (Aur B)-positive **: $p < 0.01$. Scale bar = 50 µm.

4.13 Dominant active PPARδ induces cardiomyocyte mitosis *in vivo*

To determine whether PPARδ activation can induce adult cardiomyocyte cell cycle re-entry also *in vivo*, we utilized a transgenic mouse model with tamoxifen inducible cardiomyocyte-restricted overexpression of a constitutively active mutant PPARδ gene (VP16-PPARδ)[120, 121] The transgenic line of VP16-PPARδ driven by the human cytomegalovirus immediate early enhance/chicken β-actin promoter was crossed with the tamoxifen inducible alpha-MyHC-Mer-Cre-Mer (TMCM) transgenic mice[122] to generate tamoxifen inducible transgenic mice with cardiomyocyte-restricted overexpression of VP16-PPARδ (TMVPD). Adult mice (3 months old) were injected with tamoxifen into TMCM and TMVPD and analyzed for adult mitotic cardiomyocytes (H3P-positive) after 14 days. Cardiac-specific overexpression of dominant active PPARδ resulted in a more than 8-fold higher number of mitotic adult cardiomyocytes (**Figure 4.18 a, b, c, d**).

Taken together, our screening tool enabled us to identify carbacyclin as a potential inducer of cardiomyocyte cell cycle re-entry. Moreover, we validated our system by demonstrating that activation of PPARδ, the target of carbacyclin, induces cell cycle activity in neonatal as well as adult cardiomyocytes *in vitro* and *in vivo*.

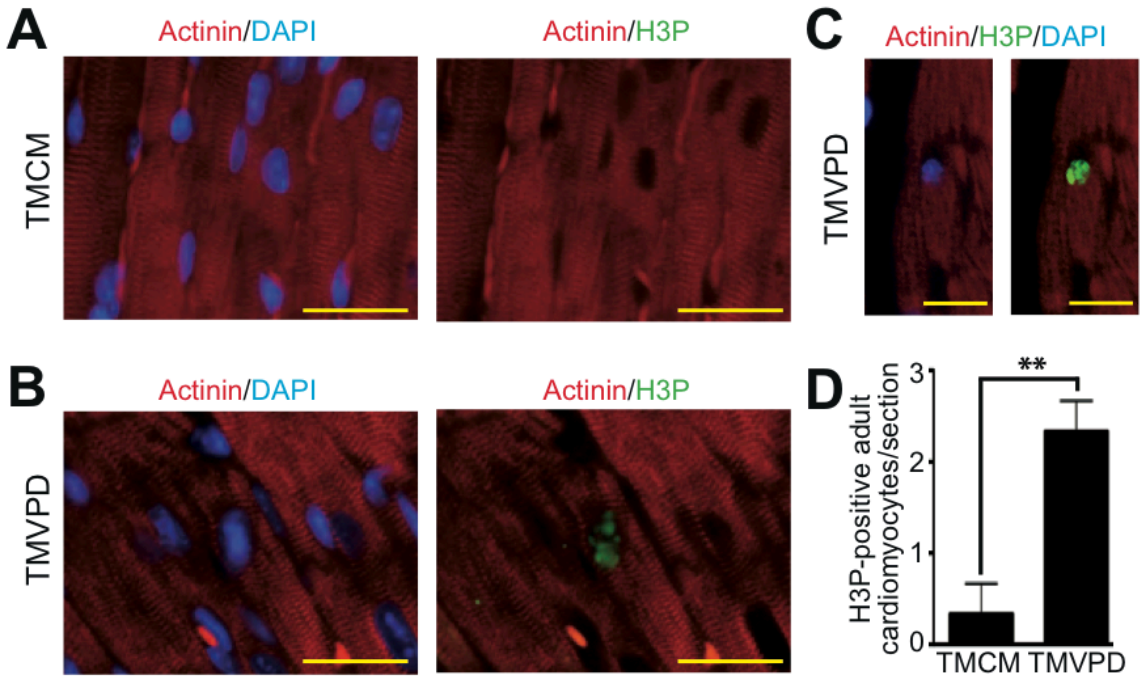

Figure 4.17. Dominant-active PPARδ induces cardiomyocyte mitosis *in vivo*. (**a** to **c**), Representative sections of hearts from control mice (tamoxifen inducible alpha-MyHC-Mer-Cre-Mer, TMCM) and tamoxifen inducible transgenic mice with cardiomyocyte-restricted overexpression of VP16-PPARδ (TMVPD) two weeks after tamoxifen injection. Sections were stained with anti-Actinin (red, cardiomyocytes-specific) and anti-H3P (green, stains mitotic cells) antibodies. Nuclei were visualized with DAPI. **(d),** Quantitative analysis of mitotic cardiomyocytes (n = 4, 3 sections per heart). **: $p < 0.01$. Scale bar = 25 µm.

DISCUSSION

5.1 Fucci system for screening new inducers of cardiomyocyte proliferation

To the best of our knowledge, there is no system available to efficiently screen for new inducer of proliferation of differentiated mammalian cardiomyocytes. Our study describes a new fluorescence-based live imaging-screening assay allowing the efficient identification of small molecules promoting cardiomyocyte proliferation. This system eliminates the need of laborious and expensive techniques like immunofluorescence staining, incorporation of nucleotide analogues, metabolic activity or cell count assays. These assays have their own limitations for screening drug libraries. The system can be applied to neonatal as well as adult mammalian cardiomyocytes. We validated our model through a small-molecule screen in two ways: first, we used well-known inducers of cardiomyocyte proliferation, and second, through the identification and characterization of compounds with previously unknown actions on mammalian cardiomyocyte proliferation.

We screened two chemical libraries containing 134 compounds identifying carbacyclin, a potent agonist of PPARδ, as potent inducer of cardiomyocyte proliferation. Several lines of evidence support this conclusion. First, carbacyclin regulates the expression of genes required for cell cycle progression. Second, it activates β-catenin signaling, which is known to be involved in cardiomyocyte proliferation[118]. Third, it induces DNA synthesis, mitosis and cytokinesis but not binucleation in postnatal cardiomyocytes. Fourth, mitosis is associated with transient dedifferentiation of the contractile apparatus. Finally, its effect on cardiomyocytes was more potent than 10% serum, which is known to induce cycle re-entry but induces rather binucleation than proliferation[60]. In fact the effect of carbacyclin was comparable to the effect of FGF1+p38i, which has previously been shown to induce cardiomyocyte mitosis, to reduce scarring and to rescue function after myocardial infarction[87]. Thus, carbacyclin is a potent inducer of postnatal cardiomyocyte proliferation.

It is important to note that we screened with 3 different concentrations because the potencies of the molecules in our library (effector concentration for half-maximum response (EC_{50})) can vary from the nM range to greater than 30

µM. If a compound is used at a too low or too high concentration its specific, or on-target effect might be lost or it might act toxic, respectively. For example, if we had chosen the typical standard concentration of 10 µM or 10 nM for all drugs we would have overlooked carbacyclin. Thus screening at multiple concentrations, ranging from low to high, maximizes the probability of testing each compound at a near-optimal concentration. In the ideal case, as noted by many others, small-molecule inducers would be less expensive, more easily controlled and possibly more efficient than growth factors in cardiomyocyte proliferation[123 124].

However, one disadvantage of our system is that use of primary cells do not allow to screen large compound libraries. The establishment of a stem cell line that stably expresses the Fucci system might be an alternative. This line could be expanded to large amounts, differentiated selectively into cardiomyocytes and utilized to screen large compound libraries. However, as stem cell-derived cardiomyocytes do not reach a high degree of differentiation[125 126], it remains unclear whether such a screen will indeed identify compounds that have an effect on adult cardiomyocyte proliferation. For example it is known that c-myc can enhance cardiomyocyte proliferation in development but in the adult heart it induces hypertrophy [127 128]. This suggests that unknown mechanisms are activated in the adult cardiomyocyte that divert developmental signaling pathways usually resulting in cardiomyocyte proliferation. Thus, it is important to have a screening system that is based on primary postnatal cardiomyocytes.

5.2 Mono-nucleated cardiomyocytes are more competent to proliferate

A closer analysis of the P8 and adult cardiomyocyte cultures treated with carbacyclin revealed that the majority of cardiomyocytes that entered the cell cycle and mitosis were mono-nucleated. Similar observations have been made in neuregulin-treated cardiomyocytes[102]. These data suggest that there are different populations of cardiomyocytes with different proliferative potentials. It is well established that different populations of cardiomyocytes exist[129] and that they differ in their proliferation potential[130], a finding consistent with the idea that some cardiomyocytes are more receptive to regeneration signals. This might be especially important for human therapy as a significant amount of

human cardiomyocytes is mono-nucleated[103]. In the future it will be important to determine whether a subpopulation of cardiomyocytes with a higher proliferation potential exists in order to better elucidate the signaling pathways to stimulate their proliferation.

The carbacyclin-induced proliferation rate of cardiomyocytes decreases from P3 neonatal cardiomyocytes to P8 and adult cardiomyocytes. This decrease values were correlated with an increase in binucleated cardiomyocytes. In P3 neonatal cardiomyocytes more than 90% of the cardiomyocytes were mono-nucleated and carbacyclin treatment resulted in around 45% BrdU-positive cells. In contrast, P8 cardiomyocytes more than 40% of the cardiomyocytes were binucleated and only 15% were BrdU-positive. In adult rat cardiomyocytes, of which around 90% are binucleated, carbacyclin induced less than 1.5% BrdU incorporation in 5 days. Importantly, the majority of cycling cardiomyocytes were mono-nucleated, indicating that mono-nucleated cardiomyocytes have a higher proliferation competent than binucleated cardiomyocytes. However, the BrdU incorporation rate in the population of mono-nucleated cardiomyocytes decreased with age, too. This might be due to an increase in the expression of inhibitory molecules of PPARδ such as NCOR2/SMRT (silencing mediator for retinoid or thyroid-hormone receptors), SMRT and histone deacetylase-associated repressor protein (SHARP)[131] and class I histone deacetylases. In future experiments it will be important to determine their expression in cardiomyocytes and to assess whether their inhibition or knockdown enhances the proliferation competence of adult cardiomyocytes. Finally, our data support the idea of a mono-nucleated subpopulation of adult cardiomyocytes that appears to be more responsive to regenerative signals.

5. 3 Carbacyclin acts through the nuclear receptor PPARδ

Carbacyclin is a chemically stable carbocyclic analog of prostacyclin, a known potent agonist of PPARδ. Hence, we have demonstrated that carbacyclin induces PPARδ expression as well as downstream signaling resulting in cardiomyocyte proliferation. PPARs are best known as regulators of energy homeostasis[132, 133]. They have many beneficial physiological functions ranging from enhancing fatty acid catabolism, improving insulin sensitivity, inhibiting

inflammation and thrombosis, and promoting angiogenesis[134-136]. It is shown that cardiomyocyte-restricted PPARδ deletion in mice perturbs accordingly myocardial fatty acid oxidation causing cardiac dysfunction, hypertrophy, and lipotoxic cardiomyopathy[137]. In contrast, cardiac-specific overexpression of PPARδ has been shown to be protective to ischemia/reperfusion (I/R) injury[138]. Moreover, mice overexpressing dominant active PPARδ in adult cardiomyocytes are protected from TAC-induced pressure overload[120]. Our analyses demonstrate that cardiac-specific overexpression of dominant active PPARδ *in vivo* induces adult cardiomyocyte mitosis.

There is so far no report regarding the function of PPARδ in cardiomyocyte proliferation. However, PPARδ has been associated with different proliferative diseases like hyperproliferative skin disorders and cancer as well as with proliferation of several cell types[139, 140]. It will be interesting in the future to determine if PPARδ-induced cardiomyocyte cell cycle re-entry contributes to the protective effects of PPARδ in I/R- and TAC-induced injury.

5.4 PPARδ signaling inducing cardiomyocytes proliferation through PPARδ/PDK1/p308Akt/pGSK3B/β-catenin

In some cancers PPARδ levels were increased correlating with a role in cell proliferation. The PDK1 is target gene of PPARδ. PPARδ activates PDK1/Akt signaling in diverse cell types to enhance cell survival and proliferation[132 140]. It has been shown that PDK1 and PPARδ do auto regulatory cascade[141]. We found increased expression of PPARδ after treatment with PPARδ agonists. This leads to activation PDK1, Then PDK1 induced Akt signaling by Akt phosphorylation at P308. Subsequently it induces phosphorylation of GSK3B at Ser9. Then GSK3B phosphorylation inhibits the ability of GSK3B to phosphorylate β-catenin and its destabilization by proteasomal degradation. This results into stabilization and nuclear accumulation of β-catenin. It known that the nuclear accumulation of β-catenin results to enhanced expression of TCF/ LEF target genes include cyclin D1, c-Myc, and PPARδ itself[142]. The increased expression of cell cycle genes results into cell proliferation. PPARδ trans-activates PDK1, which in turn perpetuates the proliferative signaling cascade[143].

Recent work shows that PPARδ regulates bone turnover[144]. The activation of PPARδ amplified Wnt signaling activity and TCF-dependent transcription in osteoblasts and MSCs through two mechanisms, including transcriptional regulation of Wnt co-receptor having PPARδ responsive element (*Lrp5*) and direct interaction with β-catenin. It is interesting in the future to determine the role of *Lrp5* in cardiomyocyte proliferation.

Besides regulating the Akt-β-catenin signaling, PPARδ is also involved in Retinoic acid (RA) signaling, which is a very important regulation of cardiomyocyte proliferation in early heart development[145, 146]. RA can promote as well as inhibit growth depend on activation of two different alternative nuclear receptors PPARδ and retinoic acid receptor respectively[147]. Partitioning of RA between the two receptors is regulated by the intracellular lipid binding proteins CRABP-II and FABP5 and they drive RA from the cytosol to nuclear RAR and PPARδ receptors, respectively and enhances the transcriptional activity of their cognate receptors. Thus the effect of RA depends on the ratio of CRABP-II/FABP5 (**Figure 5.1**). In our screen we found the retinoic acid and their mimics induced moderate cardiomyocytes proliferation and are less potent than carbacyclin. This might be due to a non-favourable CRABP-II/FABP5 ratio.

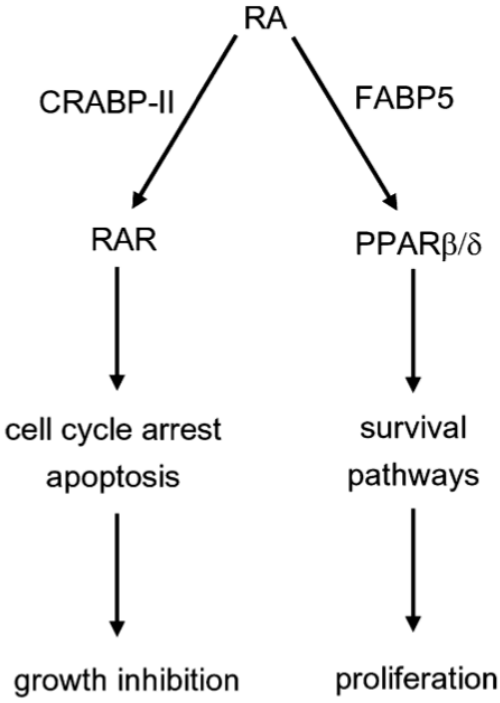

Figure 5.1: Retinoic acid induces cell growth via PPARδ activation. Retinoic acid activates two alternative nuclear receptors RAR or PPARδ to inhibit or induce proliferation.

5.5 PPARδ, energy metabolism and cardiomyocyte proliferation

So far, PPARδ has been implicated mainly as a regulator of energy metabolism in adipose tissue and muscle, where it acts as a sensor for metabolic substrates in the form of fatty acids and enhances thermogenesis, fatty acid catabolism and mitochondrial function[120, 148]. In the skeleton PPARδ itself has recently emerged as an important factor in the regulation of energy homeostasis[122]. It has been shown that activation PPARδ by its agonist can increase glycolysis and fatty acid synthesis as well as glucose and fatty acid transport and fatty acid oxidation supporting cell growth[138]. During embryonic heart development, energy metabolism in highly proliferative fetal cardiomyocytes is mainly based on glycolysis while during postnatal development it shifts to oxidative phosphorylation (non-proliferative)[149]. Thus, changes in energy metabolism might be a way to overcome the cell cycle arrest in cardiomyocytes. This is supported by the fact that adult cardiomyocytes change their metabolism in a variety of pathophysiologic conditions when they re-express fetal genes, change their energy metabolism and partially re-enter the cell cycle[62 24 149]. In addition, recent work has demonstrated that deletion of Meis1 is sufficient to extend the proliferation potential of postnatal cardiomyocytes beyond day 1 to day 7. Meis1 is known to regulate energy metabolism. Loss of meis1 induces switching of the energy metabolism from glycolysis to oxidative phosphorylation in hematopoietic stem cells[79]. Furthermore, inducible Meis1 deletion induced adult cardiomyocyte mitosis *in vivo*[78]. In carbacyclin induced neonatal cardiomyocyte proliferation might be due to abundance of favourable energy after PPARδ activation.

Furthermore it has recently been shown that 5' adenosine monophosphate-activated protein kinase (AMPK) activation of FoxOs promotes cell-cycle withdrawal and inhibits Igf1 gene expression in neonatal cardiomyocytes. Igf1 is a direct downstream target of cardiac Fox transcription factors, which is negatively regulated by FoxOs and positively regulated by FoxM1, dependent on AMPK activation status (indicator of metabolic stress)[150]. This indicates Fox's integrate metabolic status and cell cycle withdrawal in neonatal cardiomyocytes. Immediately after birth and prior to feeding, the mammalian heart is subjected to a period of starvation in which growth factor

signaling is reduced and cardiomyocytes are under metabolic stress. At the same time, expression of FoxM1, which promotes cardiomyocyte proliferation, is down regulated and FoxOs are activated, concomitant with induction of cell cycle inhibitors. Mice lacking FoxM1 in cardiomyocytes exhibit decreased cell proliferation after birth, whereas cardiomyocyte-specific loss of FoxO1 and FoxO3 delays neonatal cell cycle withdrawal. In the future it will be important to elucidate the role of PPARδ in the integration of metabolism and cell cycle progression in cardiomyocytes.

Finally pharmacological PPARδ agonists have entered the stage of clinical trials as lipid-lowering drugs, our findings open potential new therapeutic avenues for the treatment of heart diseases based on energy and metabolic adjustments.

Our screen has identified carbacyclin as a potential inducer of cardiomyocyte proliferation and its target PPARδ as a new regulator of cardiomyocyte proliferation.

Summary

Cardiovascular diseases remain among the leading cause of deaths worldwide accounting for about 40% of all postnatal deaths. Though the current therapies offer a temporary cure, owing to their limitations, there is still a need to develop alternative therapies. Adult mammalian hearts cannot regenerate as zebrafish, newt, and 1-day-old mice hearts do after an injury[22, 24, 75]. Heart regeneration occurs in these animals by proliferation of pre-existing cardiomyocytes. During mammalian heart development the heart grows through cardiomyocyte proliferation, which rapidly ceases after birth[62, 65]. Therefore, we were interested in inducing postnatal cardiomyocyte proliferation in mammals by utilizing a chemical biology approach.

We established a cardiomyocyte-specific live fluorescent-based fucci technique to screen small molecules to induce cardiomyocyte proliferation. We validated the platform first with known inducers and then screened two small molecule libraries containing modulators of nuclear receptor and epigenetic signatures in neonatal cardiomyocytes. Positive hits were further analyzed for their capacity to induce cell cycle re-entry and mitosis in P3 rat cardiomyocytes by for example BrdU incorporation and histone H3 phosphorylation analyses. We found that carbacyclin, an agonist of PPARδ, induces robust cell cycle re-entry of cardiomyocytes.

Carbacyclin in neonatal cardiomyocytes induced DNA synthesis, mitosis and cytokinesis but not binucleation. The effect of carbacyclin on cardiomyocytes was more potent than 10% serum (induces rather binucleation than proliferation)[60]. In fact it was comparable to the effect of FGF1+p38i, which has previously been shown to induce cardiomyocyte mitosis, to reduce scarring and to rescue function after MI[87, 116 .

It has been shown that 1-day-old, but not 7-day-old, mice can regenerate their heart[75]. Therefore, we tested whether carbacyclin can induce P8 and adult cardiomyocytes cell cycle re-entry. Carbacyclin induced both BrdU incorporation and mitosis in P8 and adult cardiomyocytes *in vitro*. A closer analysis of P8 and adult cardiomyocytes revealed that the majority of cardiomyocytes that entered the cell cycle were mono-nucleated. Similar observations have been made in Neuregulin-treated cardiomyocytes[102]. This

result might be important for human therapy, as a majority of human cardiomyocytes is mono-nucleated[103]. These data suggest that different populations of cardiomyocytes with different proliferative potential exist[129 130].

The PPARs are best known as regulators of energy homeostasis and have many beneficial physiological functions[132, 133, 148]. The cardiomyocyte-restricted PPARδ deletion causes cardiac dysfunction, hypertrophy, and lipotoxic cardiomyopathy[137]. In contrast, overexpression of PPARδ has been shown to be protective to ischemia/reperfusion (I/R) injury and TAC-induced pressure overload[120, 138]. We found cardiomyocyte-restricted inducible dominant-active PPARδ *in vivo* induces adult cardiomyocyte mitosis.

PPARδ increases fatty acid synthesis and catabolism as well as glucose and fatty acid transport and glycolysis, which might support cardiomyocyte cell cycle re-entry. Recently, it has been shown that deletion of Meis1, which is known to shift energy metabolism from glycolysis to oxidative phosphorylation, is sufficient to extend the proliferation potential of postnatal cardiomyocytes beyond day 1 to day 7[78]. Thus, changes or shift in energy metabolism might be a way to overcome the cell cycle arrest in cardiomyocytes.

We have shown that activation of PPARδ by carbacyclin induces the PPARδ/PDK1/p308Akt/pGSK3β/β-catenin pathway. This data coincides with recently published data that PPARδ governs Wnt signaling and bone turnover by activation of direct interaction with β-catenin and activation of Lrp5[144]. The stabilization and translocation of β-catenin to nucleus is important to induce cardiomyocyte proliferation and we found enhanced carbacyclin-induced cardiomyocyte proliferation in the presence of BIO[118, 119].

Taken together, our data indicate that the fucci system can be utilized as screening platform for chemical libraries, natural compound libraries and whole genome siRNA libraries to identify critical signaling pathways, druggable targets and compounds to promote cardiac regeneration based on cardiomyocyte proliferation; if this is possible. The presented screening system eliminates the need of laborious and expensive techniques like immunofluorescence staining, incorporation of nucleotide analogues or cell count and metabolic assays. Our initial screen has identified carbacyclin as a potential inducer of cardiomyocyte proliferation and its target PPARδ as a new regulator of cardiomyocyte proliferation and as a new target for regenerative

heart therapies. To our knowledge, this is the first live-imaging screening tool to identify inducers of cardiomyocyte proliferation and the first description that carbacyclin induces cardiomyocyte proliferation. We have dissected the carbacyclin-induced PPARδ/PDK1/p308Akt/pGSK3β/β-catenin signaling pathway. Our data suggest moreover that carbacyclin induces cell cycle re-entry specifically in mono-nucleated cardiomyocytes *in vitro* and that overexpression of dominant-active PPARδ induces adult cardiomyocyte mitosis *in vivo*.

Outlook

In the future, it will be interesting to determine whether PPARδ-induced cardiomyocyte cell cycle re-entry contributes to the protective effects of PPARδ in I/R- and TAC-induced injury. It will be important to determine how activation of PPARδ by its agonist carbacyclin or overexpression of dominant-active PPARδ regulates Wnt and other signaling pathways to induce cardiomyocyte cell cycle re-entry. In addition, it appears worthwhile to determine how the metabolic status of cardiomyocytes influences their proliferation competence. Finally, our results warrant further preclinical investigations towards a carbacyclin-based strategy to treat cardiac disease.

Zusammenfassung

Herz-Kreislauf-Erkrankungen gehören nach wie vor zu den häufigsten Ursachen für Todesfälle weltweit, die rund 40% aller postnatalen Todesfälle zugrunde liegen. Gegenwärtige Therapien bieten in der Regel nur eine vorübergehende symptomatische Behandlung, da sie die primäre Ursache der meisten Herzerkrankungen, den Verlust an Herzmuskelzellen, nicht beheben können. Aus diesem Grund gibt es die Notwendigkeit neue Therapien zu entwickeln. Adulte Säugetierherzen können nicht wie der Zebrafisch, der Lurch bzw. 1 Tage-alte Mäuse ihr Herz nach eine Verletzung regenerieren[22, 24, 75]. Die Herzregeneration erfolgt bei diesen Tieren durch die Proliferation von bereits vorhandenen Herzmuskelzellen. Zudem wächst das Herz während der Säugertierentwicklung ebenfalls durch die Proliferation von Herzmuskelzellen. Aus einem unbekannten Grund hören die Zellen jedoch kurz nach der Geburt auf zu proliferieren[62, 65]. Deshalb sind wir daran interessiert mittels eines chemisch-biologischen Ansatzes neue Induktoren der Herzmuskelzellproliferation zu identifizieren.

Hier haben wir eine Herzmuskelzell-spezifische Fluoreszenz-basierte Methode entwickelt, um kleine chemische Moleküle effizient auf ihre Fähigkeit Herzmuskelzellproliferation zu induzieren zu untersuchen. Die Methode wurde zunächst mit bekannten Induktoren validiert und dann genutzt, um zwei Molekül-Bibliotheken (1: Modulatoren nukleärer Rezeptoren; 2: Epigenetische Modulatoren) nach Kandidaten zu untersuchen. Identifizierte Kandidaten wurden weiter auf ihre Fähigkeit analysiert, den Zellzyklus in Herzmuskelzellen zu reaktivieren (z.B. BrdU-Einbau), Mitose zu induzieren (Histon H3 Phosphorylierung). In dieser Arbeit wurde Carbacyclin, ein Agonist von PPARδ, als robuster Aktivator des Zellzyklus in Herzmuskelzellen identifiziert.

Carbacyclin induzierte in Herzmuskelzellen DNA-Synthese, Mitose und Cytokinese, aber nicht Binukleation. Die Wirkung von Carbacyclin auf Herzmuskelzellen war stärker als 10% Serum (induziert eher Binukleation als Proliferation)[60]. In der Tat war die Wirkung von Carbacyclin vergleichbar mit der von FGF1 + p38i, welche bekanntermaßen Mitose in Herzmuskelzellen *in vivo* induzieren und zur Verringerung der Narbenbildung und einer verbesserten Herzfunktion nach einem Herzinfarkt führen[87, 113].

Es hat sich gezeigt, daß 1-Tage-alte, nicht aber 7-Tage-alte Mäuse ihre Herzen regenerieren können[75]. Deshalb haben wir getestet, ob Carbacyclin auch in Herzmuskelzellen von 8-Tage-alten und adulten Ratten den Zellzyklus aktivieren können. Carbacyclin induzierte sowohl BrdU-Einbau als auch Mitose in P8 und adulten Herzmuskelzellen *in vit*ro. Eine genauere Analyse der P8 und adulten Herzmuskelzellen offenbarte, dass die Mehrheit der Herzmuskelzellen, die den Zellzyklus aktiviert haben, mononuklär waren. Ähnliche Beobachtungen wurden in Neuregulin-behandelten Herzmuskelzellen gemacht[102]. Dieses Ergebnis könnte für menschliche Therapieansätze von Bedeutung sein, da ein Großteil der menschlichen Herzmuskelzellen mononukleär ist[103]. Diese Daten deuten darauf hin, dass verschiedene Populationen von Herzmuskelzellen mit verschiedenen Proliferationspotential existieren[127, 128].

PPARs sind am besten als Regulatoren der Energie-Homöostase bekannt und haben viele positive physiologische Funktionen[132, 133, 148]. Die Herzmuskelzell-spezifische Eliminierung von PPARδ resultiert in kardialer Dysfunktion, Hypertrophie und lipotoxischer Kardiomyopathie[137]. Im Gegensatz dazu wirkt die Überexpression von PPARδ schützend hinsichtlich Ischämie/Reperfusion Schädigung und TAC-induzierter Drucküberlastung[120, 138]. Unsere Daten zeigen, dass die induzierbare, Herzmuskelzell-spezifische Überexpression einer dominant-aktiven Form von PPARδ *in vivo* die Mitose von erwachsenen Herzmuskelzellen induziert.

PPARδ erhöht die Fettsäure-Synthese und -Abbau sowie Glukose und Fettsäure Transport und Glykolyse. Das könnte zum Effekt von Carbacylin hinsichtlich der Aktivierung des Zellzyklus beitragen. Vor kurzem wurde z.B. gezeigt, dass die Deletion von Meis1, welches bekanntlich den Energiestoffwechsel der Glykolyse zur oxidative Phosphorylierung verschiebt, ausreicht, um das Proliferationspotential postnataler Herzmuskelzellen über Tag 1 bis Tag 7 auszudehnen[78]. So könnten Änderungen oder Verschiebungen im Energiestoffwechsel eine Möglichkeit sein, den Zellzyklusarrest in Herzmuskelzellen zu überwinden.

Wir haben gezeigt, dass die Aktivierung von PPARδ durch Carbacyclin den PPARδ/PDK1/p308Akt/pGSK3β/β-Catenin Signalweg induziert. Diese Daten decken sich mit kürzlich veröffentlichten Daten, welche beschreiben,

dass PPARδ den Wnt-Signalweg und den Knochenstoffwechsels durch Aktivierung der direkten Interaktion mit β-Catenin und Aktivierung von Lrp51 reguliert[144]. Die Stabilisierung und Translokation von β-Catenin zum Kern erscheint wichtig für die Induktion der Herzmuskelzellproliferation. Diese Annahme wurde bestärkt durch die Beobachtung, dass die Carbacyclin-induzierte Proliferation von Herzmuskelzellen in der Gegenwart von BIO deutlich erhöht war[118, 119].

Zusammengenommen legen unsere Daten Nahe, dass ein Fucci-basiertes System als Screening-Plattform genutzt werden kann, um chemische Bibliotheken, natürlichen Substanzbibliotheken und ganze Genom siRNA-Bibliotheken zu analysieren, um kritische Signalwege, therapeutische Ziele und neue Moleküle zu identifizieren, die zur Entwicklung von Strategien zur Behandlung von Herzerkrankungen wesentlich beitragen. Das vorliegende Screening System eliminiert die Notwendigkeit von aufwendigen und teuren Verfahren wie Immunfluoreszenzfärbung, Einbau von Nukleotid-Analoga, Zellzahlbestimmungen oder metabolischer Untersuchungen. Unsere ersten Untersuchungen haben Carbacyclin als potenzieller Regulator der Herzmuskelzellproliferation identifiziert und PPARδ als neues Ziel für die Etablierung regenerativer Therapien für Herzerkrankungen. Unserem Wissen nach ist dies das erste „Live-Imaging Screening-Tool“ zur Identifikation von Induktoren der Herzmuskelzellproliferation sowie die erste Beschreibung bzgl. des Effektes von Carbacyclin auf die Herzmuskelzellproliferation. Wir haben den Carbacyclin-induzierten PPARδ/PDK1/p308Akt/pGSK3β/β-Catenin-Signalweg analysiert. Darüber hinaus deuten unsere Daten darauf hin, dass Carbacyclin spezifisch Proliferation in mononukleären Herzmuskelzellen *in vitro* induziert und dass die Überexpression von dominant-aktiven PPARδ *in vivo* in mitotischen adulten Herzmuskelzellen resultiert.

6. References

1. Fishman, M.C. & Chien, K.R. Fashioning the vertebrate heart: earliest embryonic decisions. *Development* **124**, 2099-2117 (1997).
2. Viragh, S., Szabo, E. & Challice, C.E. Formation of the primitive myo- and endocardial tubes in the chicken embryo. *J Mol Cell Cardiol* **21**, 123-137 (1989).
3. DeRuiter, M.C., Poelmann, R.E., VanderPlas-de Vries, I., Mentink, M.M. & Gittenberger-de Groot, A.C. The development of the myocardium and endocardium in mouse embryos. Fusion of two heart tubes? *Anat Embryol (Berl)* **185**, 461-473 (1992).
4. Bruneau, B.G. Transcriptional regulation of vertebrate cardiac morphogenesis. *Circ Res* **90**, 509-519 (2002).
5. McDermott, B.J. et al. Protection of cardiomyocyte function by propofol during simulated ischemia is associated with a direct action to reduce pro-oxidant activity. *J Mol Cell Cardiol* **42**, 600-608 (2007).
6. Olson, E.N. & Srivastava, D. Molecular pathways controlling heart development. *Science* **272**, 671-676 (1996).
7. Srivastava, D. & Olson, E.N. A genetic blueprint for cardiac development. *Nature* **407**, 221-226 (2000).
8. Christoffels, V.M. et al. Chamber formation and morphogenesis in the developing mammalian heart. *Dev Biol* **223**, 266-278 (2000).
9. Lyons, I. et al. Myogenic and morphogenetic defects in the heart tubes of murine embryos lacking the homeo box gene Nkx2-5. *Genes Dev* **9**, 1654-1666 (1995).
10. Lin, Q., Schwarz, J., Bucana, C. & Olson, E.N. Control of mouse cardiac morphogenesis and myogenesis by transcription factor MEF2C. *Science* **276**, 1404-1407 (1997).
11. Srivastava, D., Cserjesi, P. & Olson, E.N. A subclass of bHLH proteins required for cardiac morphogenesis. *Science* **270**, 1995-1999 (1995).
12. Hatcher, C.J. et al. TBX5 transcription factor regulates cell proliferation during cardiogenesis. *Dev Biol* **230**, 177-188 (2001).
13. Nakagawa, O., Nakagawa, M., Richardson, J.A., Olson, E.N. & Srivastava, D. HRT1, HRT2, and HRT3: a new subclass of bHLH transcription factors marking specific cardiac, somitic, and pharyngeal arch segments. *Dev Biol* **216**, 72-84 (1999).
14. Severs, N.J. The cardiac muscle cell. *Bioessays* **22**, 188-199 (2000).
15. Schoen, F.J. Future directions in tissue heart valves: impact of recent insights from biology and pathology. *J Heart Valve Dis* **8**, 350-358 (1999).
16. Seidman, J.G. & Seidman, C. The genetic basis for cardiomyopathy: from mutation identification to mechanistic paradigms. *Cell* **104**, 557-567 (2001).
17. Uusimaa, P. et al. Collagen scar formation after acute myocardial infarction: relationships to infarct size, left ventricular function, and coronary artery patency. *Circulation* **96**, 2565-2572 (1997).
18. Laflamme, M.A. et al. Cardiomyocytes derived from human embryonic stem cells in pro-survival factors enhance function of infarcted rat hearts. *Nat Biotechnol* **25**, 1015-1024 (2007).
19. McMurray, J. & Pfeffer, M.A. New therapeutic options in congestive heart failure: Part II. *Circulation* **105**, 2223-2228 (2002).
20. Gonzalez, A. et al. Cardiomyocyte apoptosis in hypertensive cardiomyopathy. *Cardiovasc Res* **59**, 549-562 (2003).
21. Poss, K.D., Wilson, L.G. & Keating, M.T. Heart regeneration in zebrafish. *Science* **298**, 2188-2190 (2002).

22. Kikuchi, K. et al. Primary contribution to zebrafish heart regeneration by gata4(+) cardiomyocytes. *Nature* **464**, 601-605 (2010).
23. Jopling, C. et al. Zebrafish heart regeneration occurs by cardiomyocyte dedifferentiation and proliferation. *Nature* **464**, 606-609 (2010).
24. Oberpriller, J.O. & Oberpriller, J.C. Response of the adult newt ventricle to injury. *J Exp Zool* **187**, 249-253 (1974).
25. Oberpriller, J.O., Oberpriller, J.C., Matz, D.G. & Soonpaa, M.H. Stimulation of proliferative events in the adult amphibian cardiac myocyte. *Ann N Y Acad Sci* **752**, 30-46 (1995).
26. Nurse, P. Ordering S phase and M phase in the cell cycle. *Cell* **79**, 547-550 (1994).
27. Heichman, K.A. & Roberts, J.M. Rules to replicate by. *Cell* **79**, 557-562 (1994).
28. King, R.W., Jackson, P.K. & Kirschner, M.W. Mitosis in transition. *Cell* **79**, 563-571 (1994).
29. Vidal, A. & Koff, A. Cell-cycle inhibitors: three families united by a common cause. *Gene* **247**, 1-15 (2000).
30. Glotzer, M. The molecular requirements for cytokinesis. *Science* **307**, 1735-1739 (2005).
31. Adams, R.R., Maiato, H., Earnshaw, W.C. & Carmena, M. Essential roles of Drosophila inner centromere protein (INCENP) and aurora B in histone H3 phosphorylation, metaphase chromosome alignment, kinetochore disjunction, and chromosome segregation. *J Cell Biol* **153**, 865-880 (2001).
32. Cooke, C.A., Heck, M.M. & Earnshaw, W.C. The inner centromere protein (INCENP) antigens: movement from inner centromere to midbody during mitosis. *J Cell Biol* **105**, 2053-2067 (1987).
33. Bischoff, J.R. & Plowman, G.D. The Aurora/Ipl1p kinase family: regulators of chromosome segregation and cytokinesis. *Trends Cell Biol* **9**, 454-459 (1999).
34. Silke, J. & Vaux, D.L. Two kinds of BIR-containing protein - inhibitors of apoptosis, or required for mitosis. *J Cell Sci* **114**, 1821-1827 (2001).
35. Williams, B.C., Riedy, M.F., Williams, E.V., Gatti, M. & Goldberg, M.L. The Drosophila kinesin-like protein KLP3A is a midbody component required for central spindle assembly and initiation of cytokinesis. *J Cell Biol* **129**, 709-723 (1995).
36. Guertin, D.A., Trautmann, S. & McCollum, D. Cytokinesis in eukaryotes. *Microbiol Mol Biol Rev* **66**, 155-178 (2002).
37. Wolf, W.A., Chew, T.L. & Chisholm, R.L. Regulation of cytokinesis. *Cell Mol Life Sci* **55**, 108-120 (1999).
38. Satterwhite, L.L. & Pollard, T.D. Cytokinesis. *Curr Opin Cell Biol* **4**, 43-52 (1992).
39. Fishkind, D.J. & Wang, Y.L. New horizons for cytokinesis. *Curr Opin Cell Biol* **7**, 23-31 (1995).
40. Oegema, K. & Mitchison, T.J. Rappaport rules: cleavage furrow induction in animal cells. *Proc Natl Acad Sci U S A* **94**, 4817-4820 (1997).
41. Erozhina, I.L. [The proliferation and DNA synthesis during early stages of myocardial development]. *Tsitologiia* **10**, 162-172 (1968).
42. Erokhina, E.L. [Proliferation dynamics of cellular elements in the differentiating mouse myocardium]. *Tsitologiia* **10**, 1391-1409 (1968).
43. Soonpaa, M.H., Kim, K.K., Pajak, L., Franklin, M. & Field, L.J. Cardiomyocyte DNA synthesis and binucleation during murine development. *Am J Physiol* **271**, H2183-2189 (1996).
44. Li, F., Wang, X., Capasso, J.M. & Gerdes, A.M. Rapid transition of cardiac myocytes from hyperplasia to hypertrophy during postnatal development. *J Mol Cell Cardiol* **28**, 1737-1746 (1996).

45. Yoshizumi, M. et al. Disappearance of cyclin A correlates with permanent withdrawal of cardiomyocytes from the cell cycle in human and rat hearts. *J Clin Invest* **95**, 2275-2280 (1995).
46. Brockes, J.P. New approaches to amphibian limb regeneration. *Trends Genet* **10**, 169-173 (1994).
47. Kang, M.J. & Koh, G.Y. Differential and dramatic changes of cyclin-dependent kinase activities in cardiomyocytes during the neonatal period. *J Mol Cell Cardiol* **29**, 1767-1777 (1997).
48. Flink, I.L., Oana, S., Maitra, N., Bahl, J.J. & Morkin, E. Changes in E2F complexes containing retinoblastoma protein family members and increased cyclin-dependent kinase inhibitor activities during terminal differentiation of cardiomyocytes. *J Mol Cell Cardiol* **30**, 563-578 (1998).
49. Georgescu, S.P. et al. Downregulation of polo-like kinase correlates with loss of proliferative ability of cardiac myocytes. *J Mol Cell Cardiol* **29**, 929-937 (1997).
50. Burton, P.B., Yacoub, M.H. & Barton, P.J. Cyclin-dependent kinase inhibitor expression in human heart failure. A comparison with fetal development. *Eur Heart J* **20**, 604-611 (1999).
51. Li, J.M. & Brooks, G. Downregulation of cyclin-dependent kinase inhibitors p21 and p27 in pressure-overload hypertrophy. *Am J Physiol* **273**, H1358-1367 (1997).
52. Katzberg, A.A., Farmer, B.B. & Harris, R.A. The predominance of binucleation in isolated rat heart myocytes. *Am J Anat* **149**, 489-499 (1977).
53. Oparil, S., Bishop, S.P. & Clubb, F.J., Jr. Myocardial cell hypertrophy or hyperplasia. *Hypertension* **6**, III38-43 (1984).
54. Dorn, G.W., 2nd, Robbins, J. & Sugden, P.H. Phenotyping hypertrophy: eschew obfuscation. *Circ Res* **92**, 1171-1175 (2003).
55. Grabner, W. & Pfitzer, P. Number of nuclei in isolated myocardial cells of pigs. *Virchows Arch B Cell Pathol* **15**, 279-294 (1974).
56. Zak, R. Development and proliferative capacity of cardiac muscle cells. *Circ Res* **35**, suppl II:17-26 (1974).
57. Nag, A.C., Healy, C.J. & Cheng, M. DNA synthesis and mitosis in adult amphibian cardiac muscle cells in vitro. *Science* **205**, 1281-1282 (1979).
58. Jonker, S.S. et al. Myocyte enlargement, differentiation, and proliferation kinetics in the fetal sheep heart. *J Appl Physiol* **102**, 1130-1142 (2007).
59. Li, F., Wang, X., Bunger, P.C. & Gerdes, A.M. Formation of binucleated cardiac myocytes in rat heart: I. Role of actin-myosin contractile ring. *J Mol Cell Cardiol* **29**, 1541-1551 (1997).
60. Engel, F.B., Schebesta, M. & Keating, M.T. Anillin localization defect in cardiomyocyte binucleation. *J Mol Cell Cardiol* **41**, 601-612 (2006).
61. Storchova, Z. & Pellman, D. From polyploidy to aneuploidy, genome instability and cancer. *Nat Rev Mol Cell Biol* **5**, 45-54 (2004).
62. Ahuja, P., Sdek, P. & MacLellan, W.R. Cardiac myocyte cell cycle control in development, disease, and regeneration. *Physiol Rev* **87**, 521-544 (2007).
63. Liu, Z., Yue, S., Chen, X., Kubin, T. & Braun, T. Regulation of cardiomyocyte polyploidy and multinucleation by CyclinG1. *Circ Res* **106**, 1498-1506 (2010).
64. Budirahardja, Y. & Gonczy, P. Coupling the cell cycle to development. *Development* **136**, 2861-2872 (2009).
65. van Amerongen, M.J. & Engel, F.B. Features of cardiomyocyte proliferation and its potential for cardiac regeneration. *J Cell Mol Med* **12**, 2233-2244 (2008).
66. Poolman, R.A. & Brooks, G. Expressions and activities of cell cycle regulatory molecules during the transition from myocyte hyperplasia to hypertrophy. *J Mol Cell Cardiol* **30**, 2121-2135 (1998).

67. Tamamori, M. et al. Essential roles for G1 cyclin-dependent kinase activity in development of cardiomyocyte hypertrophy. *Am J Physiol* **275**, H2036-2040 (1998).
68. Zindy, F., Quelle, D.E., Roussel, M.F. & Sherr, C.J. Expression of the p16INK4a tumor suppressor versus other INK4 family members during mouse development and aging. *Oncogene* **15**, 203-211 (1997).
69. Wang, C. & Hu, S.M. Developmental regulation in the expression of rat heart glucose transporters. *Biochem Biophys Res Commun* **177**, 1095-1100 (1991).
70. Siedner, S. et al. Developmental changes in contractility and sarcomeric proteins from the early embryonic to the adult stage in the mouse heart. *J Physiol* **548**, 493-505 (2003).
71. Claycomb, W.C. Atrial-natriuretic-factor mRNA is developmentally regulated in heart ventricles and actively expressed in cultured ventricular cardiac muscle cells of rat and human. *Biochem J* **255**, 617-620 (1988).
72. Drenckhahn, J.D. et al. Compensatory growth of healthy cardiac cells in the presence of diseased cells restores tissue homeostasis during heart development. *Dev Cell* **15**, 521-533 (2008).
73. Meilhac, S.M. et al. A retrospective clonal analysis of the myocardium reveals two phases of clonal growth in the developing mouse heart. *Development* **130**, 3877-3889 (2003).
74. Herdrich, B.J. et al. Regenerative healing following foetal myocardial infarction. *Eur J Cardiothorac Surg* **38**, 691-698 (2010).
75. Porrello, E.R. et al. Transient regenerative potential of the neonatal mouse heart. *Science* **331**, 1078-1080 (2011).
76. Laflamme, M.A. & Murry, C.E. Heart regeneration. *Nature* **473**, 326-335 (2011).
77. Ieda, M. et al. Cardiac fibroblasts regulate myocardial proliferation through beta1 integrin signaling. *Dev Cell* **16**, 233-244 (2009).
78. Mahmoud, A.I. et al. Meis1 regulates postnatal cardiomyocyte cell cycle arrest. *Nature* **497**, 249-253 (2013).
79. Simsek, T. et al. The distinct metabolic profile of hematopoietic stem cells reflects their location in a hypoxic niche. *Cell Stem Cell* **7**, 380-390 (2010).
80. Spalding, K.L., Buchholz, B.A., Bergman, L.E., Druid, H. & Frisen, J. Forensics: age written in teeth by nuclear tests. *Nature* **437**, 333-334 (2005).
81. Libby, W.F., Berger, R., Mead, J.F., Alexander, G.V. & Ross, J.F. Replacement Rates for Human Tissue from Atmospheric Radiocarbon. *Science* **146**, 1170-1172 (1964).
82. Spalding, K.L. et al. Dynamics of fat cell turnover in humans. *Nature* **453**, 783-787 (2008).
83. Spalding, K.L., Bhardwaj, R.D., Buchholz, B.A., Druid, H. & Frisen, J. Retrospective birth dating of cells in humans. *Cell* **122**, 133-143 (2005).
84. Bergmann, O. et al. Evidence for cardiomyocyte renewal in humans. *Science* **324**, 98-102 (2009).
85. Senyo, S.E. et al. Mammalian heart renewal by pre-existing cardiomyocytes. *Nature* **493**, 433-436 (2013).
86. Kajstura, J. et al. Myocyte proliferation in end-stage cardiac failure in humans. *Proc Natl Acad Sci U S A* **95**, 8801-8805 (1998).
87. Engel, F.B., Hsieh, P.C., Lee, R.T. & Keating, M.T. FGF1/p38 MAP kinase inhibitor therapy induces cardiomyocyte mitosis, reduces scarring, and rescues function after myocardial infarction. *Proc Natl Acad Sci U S A* **103**, 15546-15551 (2006).
88. Pasumarthi, K.B., Nakajima, H., Nakajima, H.O., Soonpaa, M.H. & Field, L.J. Targeted expression of cyclin D2 results in cardiomyocyte DNA synthesis and infarct regression in transgenic mice. *Circ Res* **96**, 110-118 (2005).

89. Chaudhry, H.W. et al. Cyclin A2 mediates cardiomyocyte mitosis in the postmitotic myocardium. *J Biol Chem* **279**, 35858-35866 (2004).
90. Bicknell, K.A., Coxon, C.H. & Brooks, G. Forced expression of the cyclin B1-CDC2 complex induces proliferation in adult rat cardiomyocytes. *Biochem J* **382**, 411-416 (2004).
91. Hauck, L. et al. Protein kinase CK2 links extracellular growth factor signaling with the control of p27(Kip1) stability in the heart. *Nat Med* **14**, 315-324 (2008).
92. Perez-Roger, I., Kim, S.H., Griffiths, B., Sewing, A. & Land, H. Cyclins D1 and D2 mediate myc-induced proliferation via sequestration of p27(Kip1) and p21(Cip1). *EMBO J* **18**, 5310-5320 (1999).
93. Kirshenbaum, L.A. & Schneider, M.D. Adenovirus E1A represses cardiac gene transcription and reactivates DNA synthesis in ventricular myocytes, via alternative pocket protein- and p300-binding domains. *J Biol Chem* **270**, 7791-7794 (1995).
94. Brooks, G., Poolman, R.A., McGill, C.J. & Li, J.M. Expression and activities of cyclins and cyclin-dependent kinases in developing rat ventricular myocytes. *J Mol Cell Cardiol* **29**, 2261-2271 (1997).
95. Poolman, R.A., Li, J.M., Durand, B. & Brooks, G. Altered expression of cell cycle proteins and prolonged duration of cardiac myocyte hyperplasia in p27KIP1 knockout mice. *Circ Res* **85**, 117-127 (1999).
96. Jung, J., Kim, T.G., Lyons, G.E., Kim, H.R. & Lee, Y. Jumonji regulates cardiomyocyte proliferation via interaction with retinoblastoma protein. *J Biol Chem* **280**, 30916-30923 (2005).
97. Kajstura, J., Cheng, W., Reiss, K. & Anversa, P. The IGF-1-IGF-1 receptor system modulates myocyte proliferation but not myocyte cellular hypertrophy in vitro. *Exp Cell Res* **215**, 273-283 (1994).
98. Pasumarthi, K.B., Kardami, E. & Cattini, P.A. High and low molecular weight fibroblast growth factor-2 increase proliferation of neonatal rat cardiac myocytes but have differential effects on binucleation and nuclear morphology. Evidence for both paracrine and intracrine actions of fibroblast growth factor-2. *Circ Res* **78**, 126-136 (1996).
99. Novoyatleva, T. et al. TWEAK is a positive regulator of cardiomyocyte proliferation. *Cardiovasc Res* **85**, 681-690 (2010).
100. Eulalio, A. et al. Functional screening identifies miRNAs inducing cardiac regeneration. *Nature* **492**, 376-381 (2012).
101. Choi, W.Y. et al. In vivo monitoring of cardiomyocyte proliferation to identify chemical modifiers of heart regeneration. *Development* **140**, 660-666 (2013).
102. Bersell, K., Arab, S., Haring, B. & Kuhn, B. Neuregulin1/ErbB4 signaling induces cardiomyocyte proliferation and repair of heart injury. *Cell* **138**, 257-270 (2009).
103. Kajstura, J. et al. Cardiomyogenesis in the aging and failing human heart. *Circulation* **126**, 1869-1881 (2012).
104. Olivetti, G. et al. Aging, cardiac hypertrophy and ischemic cardiomyopathy do not affect the proportion of mononucleated and multinucleated myocytes in the human heart. *J Mol Cell Cardiol* **28**, 1463-1477 (1996).
105. Sakaue-Sawano, A. et al. Visualizing spatiotemporal dynamics of multicellular cell-cycle progression. *Cell* **132**, 487-498 (2008).
106. Nishitani, H., Lygerou, Z., Nishimoto, T. & Nurse, P. The Cdt1 protein is required to license DNA for replication in fission yeast. *Nature* **404**, 625-628 (2000).
107. Vodermaier, H.C. APC/C and SCF: controlling each other and the cell cycle. *Curr Biol* **14**, R787-796 (2004).
108. Wei, W. et al. Degradation of the SCF component Skp2 in cell-cycle phase G1 by the anaphase-promoting complex. *Nature* **428**, 194-198 (2004).

109. Benmaamar, R. & Pagano, M. Involvement of the SCF complex in the control of Cdh1 degradation in S-phase. *Cell Cycle* **4**, 1230-1232 (2005).
110. Inglese, J., Shamu, C.E. & Guy, R.K. Reporting data from high-throughput screening of small-molecule libraries. *Nat Chem Biol* **3**, 438-441 (2007).
111. Macarron, R. et al. Impact of high-throughput screening in biomedical research. *Nat Rev Drug Discov* **10**, 188-195 (2011).
112. Mably, J.D., Mohideen, M.A., Burns, C.G., Chen, J.N. & Fishman, M.C. heart of glass regulates the concentric growth of the heart in zebrafish. *Curr Biol* **13**, 2138-2147 (2003).
113. Birnboim, H.C. & Doly, J. A rapid alkaline extraction procedure for screening recombinant plasmid DNA. *Nucleic Acids Res* **7**, 1513-1523 (1979).
114. Lowry, O.H., Rosebrough, N.J., Farr, A.L. & Randall, R.J. Protein measurement with the Folin phenol reagent. *J Biol Chem* **193**, 265-275 (1951).
115. Laemmli, U.K. Cleavage of structural proteins during the assembly of the head of bacteriophage T4. *Nature* **227**, 680-685 (1970).
116. Engel, F.B. et al. p38 MAP kinase inhibition enables proliferation of adult mammalian cardiomyocytes. *Genes Dev* **19**, 1175-1187 (2005).
117. Engel, F.B. et al. A mammalian myocardial cell-free system to study cell cycle reentry in terminally differentiated cardiomyocytes. *Circ Res* **85**, 294-301 (1999).
118. Tseng, A.S., Engel, F.B. & Keating, M.T. The GSK-3 inhibitor BIO promotes proliferation in mammalian cardiomyocytes. *Chem Biol* **13**, 957-963 (2006).
119. Heallen, T. et al. Hippo pathway inhibits Wnt signaling to restrain cardiomyocyte proliferation and heart size. *Science* **332**, 458-461 (2011).
120. Liu, J. et al. Peroxisome proliferator-activated receptor beta/delta activation in adult hearts facilitates mitochondrial function and cardiac performance under pressure-overload condition. *Hypertension* **57**, 223-230 (2011).
121. Kim, T., Zhelyabovska, O., Liu, J. & Yang, Q. Generation of an inducible, cardiomyocyte-specific transgenic mouse model with PPAR beta/delta overexpression. *Methods Mol Biol* **952**, 57-65 (2013).
122. Sohal, D.S. et al. Temporally regulated and tissue-specific gene manipulations in the adult and embryonic heart using a tamoxifen-inducible Cre protein. *Circ Res* **89**, 20-25 (2001).
123. Chen, S. et al. A small molecule that directs differentiation of human ESCs into the pancreatic lineage. *Nat Chem Biol* **5**, 258-265 (2009).
124. Makhortova, N.R. et al. A screen for regulators of survival of motor neuron protein levels. *Nat Chem Biol* **7**, 544-552 (2011).
125. Mauritz, C. et al. Generation of functional murine cardiac myocytes from induced pluripotent stem cells. *Circulation* **118**, 507-517 (2008).
126. Wei, H., Juhasz, O., Li, J., Tarasova, Y.S. & Boheler, K.R. Embryonic stem cells and cardiomyocyte differentiation: phenotypic and molecular analyses. *J Cell Mol Med* **9**, 804-817 (2005).
127. Xiao, G. et al. Inducible activation of c-Myc in adult myocardium in vivo provokes cardiac myocyte hypertrophy and reactivation of DNA synthesis. *Circ Res* **89**, 1122-1129 (2001).
128. Jackson, T. et al. The c-myc proto-oncogene regulates cardiac development in transgenic mice. *Mol Cell Biol* **10**, 3709-3716 (1990).
129. Ng, S.Y., Wong, C.K. & Tsang, S.Y. Differential gene expressions in atrial and ventricular myocytes: insights into the road of applying embryonic stem cell-derived cardiomyocytes for future therapies. *Am J Physiol Cell Physiol* **299**, C1234-1249 (2010).
130. Rumyantsev, P.P. Interrelations of the proliferation and differentiation processes during cardiact myogenesis and regeneration. *Int Rev Cytol* **51**, 186-273 (1977).

131. Shi, Y., Hon, M. & Evans, R.M. The peroxisome proliferator-activated receptor delta, an integrator of transcriptional repression and nuclear receptor signaling. *Proc Natl Acad Sci U S A* **99**, 2613-2618 (2002).
132. Bishop-Bailey, D. PPARs and angiogenesis. *Biochem Soc Trans* **39**, 1601-1605 (2011).
133. Lecarpentier, Y., Claes, V. & Hebert, J.L. PPARs, Cardiovascular Metabolism, and Function: Near- or Far-from-Equilibrium Pathways. *PPAR Res* **2010** (2010).
134. Barbieri, S.S. et al. Cyclooxygenase-2-derived prostacyclin regulates arterial thrombus formation by suppressing tissue factor in a sirtuin-1-dependent-manner. *Circulation* **126**, 1373-1384 (2012).
135. Han, J.K. et al. Peroxisome proliferator-activated receptor-delta agonist enhances vasculogenesis by regulating endothelial progenitor cells through genomic and nongenomic activations of the phosphatidylinositol 3-kinase/Akt pathway. *Circulation* **118**, 1021-1033 (2008).
136. Wang, P. et al. Peroxisome proliferator-activated receptor {delta} is an essential transcriptional regulator for mitochondrial protection and biogenesis in adult heart. *Circ Res* **106**, 911-919 (2010).
137. Cheng, L. et al. Cardiomyocyte-restricted peroxisome proliferator-activated receptor-delta deletion perturbs myocardial fatty acid oxidation and leads to cardiomyopathy. *Nat Med* **10**, 1245-1250 (2004).
138. Burkart, E.M. et al. Nuclear receptors PPARbeta/delta and PPARalpha direct distinct metabolic regulatory programs in the mouse heart. *J Clin Invest* **117**, 3930-3939 (2007).
139. Bishop-Bailey, D. PPARs and angiogenesis. *Biochem Soc Trans* **39**, 1601-1605 (2011).
140. Peters, J.M. & Gonzalez, F.J. Sorting out the functional role(s) of peroxisome proliferator-activated receptor-beta/delta (PPARbeta/delta) in cell proliferation and cancer. *Biochim Biophys Acta* **1796**, 230-241 (2009).
141. Pollock, C.B. et al. Induction of metastatic gastric cancer by peroxisome proliferator-activated receptordelta activation. *PPAR Res* **2010**, 571783 (2010).
142. Han, C., Lim, K., Xu, L., Li, G. & Wu, T. Regulation of Wnt/beta-catenin pathway by cPLA2alpha and PPARdelta. *J Cell Biochem* **105**, 534-545 (2008).
143. Pollock, C.B. et al. PPARdelta activation acts cooperatively with 3-phosphoinositide-dependent protein kinase-1 to enhance mammary tumorigenesis. *PLoS One* **6**, e16215 (2011).
144. Scholtysek, C. et al. PPARbeta/delta governs Wnt signaling and bone turnover. *Nat Med* (2013).
145. Ryckebusch, L. et al. Retinoic acid deficiency alters second heart field formation. *Proc Natl Acad Sci U S A* **105**, 2913-2918 (2008).
146. Kikuchi, K. et al. Retinoic acid production by endocardium and epicardium is an injury response essential for zebrafish heart regeneration. *Dev Cell* **20**, 397-404 (2011).
147. Schug, T.T., Berry, D.C., Shaw, N.S., Travis, S.N. & Noy, N. Opposing effects of retinoic acid on cell growth result from alternate activation of two different nuclear receptors. *Cell* **129**, 723-733 (2007).
148. Narkar, V.A. et al. AMPK and PPARdelta agonists are exercise mimetics. *Cell* **134**, 405-415 (2008).
149. Taegtmeyer, H., Sen, S. & Vela, D. Return to the fetal gene program: a suggested metabolic link to gene expression in the heart. *Ann N Y Acad Sci* **1188**, 191-198 (2010).
150. Sengupta, A., Kalinichenko, V.V. & Yutzey, K.E. FoxO1 and FoxM1 transcription factors have antagonistic functions in neonatal cardiomyocyte cell-cycle withdrawal and IGF1 gene regulation. *Circ Res* **112**, 267-277 (2013).

Appendix

Screening results

No.	compounds	time [h]	12	24	36	48	60	72	84	96
1	**DMSO**		**0**	**0**	**1**	**1**	**0**	**1**	**0**	**0**
2	25-Hydroxyvitamin D3	10 nm	1	1	1	1	1	0	0	0
		250 nm	1	1	1	1	0	1	0	0
		30 µM	1	1	1	1	0	0	0	0
3	**Retinoic acid, all trans**	**10 nm**	**1**	**2**	**2**	**2**	**2**	**2**	**1**	**1**
		250 nm	1	2	1	1	1	1	1	1
		30 µM	1	1	1	1	1	1	1	1
4	9-cis Retinoic acid	10 nm	1	2	2	1	1	1	0	0
		250 nm	1	1	1	1	1	1	1	1
		30 µM	1	1	1	1	0	0	0	0
5	13-cis Retinoic acid	10 nm	1	1	2	2	1	1	1	1
		250 nm	1	1	1	1	1	0	0	0
		30 µM	1	1	1	1	0	1	0	0
6	4-Hydroxyphenylretinamide	10 nm	1	1	1	1	1	1	0	0
		250 nm	0	1	1	1	1	1	0	0
		30 µM	1	1	1	1	0	0	0	0
7	AM-580	10 nm	1	1	1	1	1	1	1	1
		250 nm	1	1	1	0	1	0	0	0
		30 µM	1	1	1	1	0	0	0	0
8	**TTNPB**	**10 nm**	**2**	**2**	**2**	**3**	**2**	**1**	**1**	**1**
		250 nm	1	2	1	1	1	1	1	1
		30 µM	0	1	1	0	0	0	0	0
9	Methoprene acid	10 nm	1	1	1	1	1	1	1	1
		250 nm	1	1	1	1	0	1	1	1
		30 µM	1	1	1	1	0	0	0	0
10	WY-14643	10 nm	0	1	1	1	1	0	1	1
		250 nm	1	1	0	1	0	1	1	1
		30 µM	1	1	1	1	1	1	1	1
11	Ciglitazone	10 nm	1	0	1	0	1	1	0	0
		250 nm	1	1	1	1	0	0	0	0
		30 µM	0	1	1	0	0	0	0	0
12	Tetradecylthioacetic acid	10 nm	1	1	1	1	1	0	0	0
		250 nm	1	1	1	1	0	1	0	0
		30 µM	1	1	0	1	0	0	0	0
13	5,8,11,14-Eicosatetraynoic acid	10 nm	0	1	1	1	0	1	1	1
		250 nm	1	1	1	1	1	0	0	0
		30 µM	1	1	1	0	0	0	0	0
14	6-Formylindolo [3,2-B] carbazole	10 nm	1	1	1	1	1	0	0	0
		250 nm	1	1	1	1	0	0	0	0
		30 µM	1	1	1	0	0	0	0	0
15	Diindolylmethane	10 nm	1	1	1	0	0	0	0	0
		250 nm	1	1	0	0	0	0	0	0

		30 µM	0	0	0	0	0	0	0	0
16	Acetyl-S-farnesyl-L-cysteine	10 nm	1	1	1	1	1	1	1	1
		250 nm	1	1	1	1	1	0	0	0
		30 µM	1	1	0	0	0	1	0	0
17	S-Farnesyl-L-cysteine	10 nm	1	1	1	1	1	1	1	1
	methyl ester	250 nm	1	1	1	1	1	1	1	1
		30 µM	1	0	0	0	0	0	0	0
18	N-Acetyl-S-geranygeranyl-	10 nm	1	1	1	1	1	1	1	1
	L-cysteine	250 nm	1	1	1	1	1	1	1	1
		30 µM	1	1	1	1	1	1	1	1
19	AGC (Acetyl-geranyl-cysteine)	10 nm	1	1	1	1	0	1	0	0
		250 nm	1	1	1	0	0	0	0	0
		30 µM	0	1	1	1	0	0	0	0
20	Farnesylthioacetic acid	10 nm	1	1	1	1	0	1	0	0
		250 nm	1	1	1	1	0	1	0	0
		30 µM	1	0	0	0	0	0	0	0
21	Bezafibrate	10 nm	1	1	1	1	1	1	0	0
		250 nm	1	1	1	1	0	1	0	0
		30 µM	1	1	1	1	0	0	1	1
22	LY 171883	10 nm	1	1	1	1	1	0	0	0
		250 nm	1	1	1	1	1	0	0	0
		30 µM	1	1	1	1	0	0	0	0
23	15-Deoxy-D12,14-	10 nm	1	1	0	1	1	0	1	1
	prostaglandin J2	250 nm	1	0	1	1	0	0	0	0
		30 µM	1	1	1	1	1	0	0	0
24	Troglitazone	10 nm	1	1	1	1	1	1	1	1
		250 nm	1	1	1	1	0	0	0	0
		30 µM	0	1	0	0	0	0	0	0
25	CITCO	10 nm	1	1	1	1	1	1	1	1
		250 nm	1	1	1	0	0	0	0	0
		30 µM	1	1	0	0	0	0	0	0
26	Paxilline	10 nm	1	1	1	1	1	1	1	1
		250 nm	1	1	1	1	1	0	0	0
		30 µM	0	1	0	0	0	0	0	0
27	24(S)-Hydroxycholesterol	10 nm	1	1	0	1	0	1	0	0
		250 nm	1	1	1	1	0	0	0	0
		30 µM	0	1	0	0	0	0	0	0
28	24(S),25-Epoxycholesterol	10 nm	0	1	1	0	0	0	1	1
		250 nm	1	1	1	0	0	0	0	0
		30 µM	1	1	0	0	0	0	0	0
29	Pregnenolone-16(alpha)-	10 nm	1	1	1	0	1	0	0	0
	carbonitrile	250 nm	1	1	1	0	0	0	0	0
		30 µM	1	1	0	0	0	0	0	0
30	**Carbacyclin**	10 nm	1	2	2	2	2	1	1	1

	250 nm	**4**	**8**	**9**	**9**	**8**	**6**	**5**	**5**
	30 µM	1	1	1	1	1	1	1	1
31 Clofibric acid	10 nm	0	1	1	1	0	1	0	0
	250 nm	1	1	1	1	1	0	0	0
	30 µM	0	1	1	1	0	1	0	0
32 BADGE	10 nm	1	1	0	1	1	0	0	0
	250 nm	1	1	1	1	0	1	0	0
	30 µM	1	1	0	1	0	0	0	0
33 GW 9662	10 nm	1	1	2	1	1	1	1	1
	250 nm	1	1	0	0	0	0	0	0
	30 µM	1	0	0	0	0	0	0	0
34 Gemfibrozil	10 nm	0	1	1	1	1	0	1	1
	250 nm	1	1	1	1	1	0	0	0
	30 µM	1	0	0	0	0	1	0	0
35 GW 7647	10 nm	1	1	1	1	1	1	1	1
	250 nm	1	1	2	1	1	1	1	1
	30 µM	1	1	1	1	0	0	0	0
36 3,5-Diiodo-L-thyronine	10 nm	1	1	1	1	0	1	0	0
	250 nm	1	1	1	1	1	0	0	0
	30 µM	1	1	1	0	0	0	0	0
37 3,5-Diiodo-L-tyrosine	10 nm	0	1	1	1	1	1	0	0
	250 nm	1	1	1	1	0	0	1	1
	30 µM	1	1	1	0	0	0	0	0
38 all-trans-Retinol	10 nm	1	1	1	1	0	1	1	1
	250 nm	1	1	1	1	1	1	1	1
	30 µM	1	1	0	0	0	0	0	0
39 13-cis-Retinol	10 nm	1	1	1	1	1	1	1	1
	250 nm	1	1	1	1	0	0	0	0
	30 µM	1	1	0	0	0	0	0	0
40 Retinyl acetate	10 nm	1	1	1	1	1	1	1	1
	250 nm	1	2	2	1	1	0	0	0
	30 µM	1	0	0	0	0	0	0	0
41 3,5-Diiodo-4-hydroxy-	10 nm	1	1	1	1	1	1	0	0
phenylpropionic acid	250 nm	1	1	1	1	0	0	0	0
	30 µM	1	1	0	0	0	0	0	0
42 Cholic acid	10 nm	1	1	1	1	0	1	0	0
	250 nm	1	1	1	1	0	0	0	0
	30 µM	1	1	0	0	0	0	0	0
43 Deoxycholic acid	10 nm	0	1	1	1	1	1	1	1
	250 nm	1	1	1	1	1	0	1	1
	30 µM	1	0	1	1	0	0	0	0
44 Chenodeoxycholic acid	10 nm	1	1	1	1	0	0	0	0
	250 nm	0	0	0	0	0	0	0	0
	30 µM	0	0	0	0	0	0	0	0

45	Glycocholic acid	10 nm	1	1	1	0	0	0	1	1
		250 nm	1	0	0	0	0	0	0	0
		30 µM	0	0	0	0	0	0	0	0
46	Glycodeoxycholic acid	10 nm	1	0	0	0	0	0	0	0
		250 nm	0	0	0	0	0	0	0	0
		30 µM	1	1	1	1	1	1	1	1
47	Taurocholic acid	10 nm	1	1	1	1	0	0	0	0
		250 nm	1	0	0	0	0	0	0	0
		30 µM	0	0	0	0	0	0	0	0
48	Taurodeoxycholic acid	10 nm	1	1	1	1	1	0	0	0
		250 nm	1	1	1	1	0	0	0	0
		30 µM	1	1	0	0	0	0	0	0
49	Rifampicin	10 nm	1	1	1	1	1	1	0	0
		250 nm	1	1	1	1	1	1	0	0
		30 µM	1	1	1	1	1	0	0	0
50	Dexamethasone	10 nm	1	1	0	0	0	0	0	0
		250 nm	0	0	0	0	0	0	0	0
		30 µM	0	0	0	0	0	0	0	0
51	Lithocholic acid	10 nm	1	1	1	0	1	1	0	0
		250 nm	1	1	1	1	1	0	0	0
		30 µM	1	1	0	0	0	0	0	0
52	5b-Pregnan-3,20-dione	10 nm	1	1	1	1	1	0	1	1
		250 nm	1	1	2	1	1	0	0	0
		30 µM	1	0	0	0	0	0	0	0
53	Hyperforin	10 nm	1	1	1	1	1	0	0	0
		250 nm	1	1	1	0	0	0	0	0
		30 µM	1	0	0	0	0	0	0	0
54	Farnesol	10 nm	1	1	1	1	1	1	0	0
		250 nm	1	1	2	1	1	0	1	1
		30 µM	1	1	1	0	0	0	0	0
55	3a, 5a-Androstenol	10 nm	1	1	1	1	0	1	1	1
		250 nm	1	1	1	1	0	0	0	0
		30 µM	1	1	0	0	0	0	0	0
56	TCPOBOP	10 nm	1	1	1	1	1	0	0	0
		250 nm	1	1	1	1	0	0	0	0
		30 µM	1	0	0	0	0	0	0	0
57	N-Oleoylethanolamide	10 nm	1	1	1	1	1	1	0	0
		250 nm	1	1	1	1	0	0	0	0
		30 µM	1	0	0	0	0	0	0	0
58	GW4064	10 nm	1	1	1	1	1	0	0	0
		250 nm	1	1	1	1	1	0	0	0
		30 µM	1	1	1	0	0	0	0	0
59	Geranylgeraniol	10 nm	1	1	1	1	1	1	0	0
		250 nm	1	1	1	1	1	0	0	0

		30 µM	1	0	0	0	0	0	0	0
60	6a-Fluorotestosterone	10 nm	1	1	1	1	1	0	0	0
		250 nm	1	1	1	0	0	0	0	0
		30 µM	1	0	0	0	0	0	0	0
61	Tamoxifen	10 nm	1	1	1	1	1	1	0	0
		250 nm	1	1	1	1	1	0	0	0
		30 µM	0	0	0	0	0	0	0	0
62	Mifepristone	10 nm	1	1	1	1	0	0	0	0
		250 nm	1	1	1	0	0	0	0	0
		30 µM	0	0	0	0	0	0	0	0
63	Estrone	10 nm	1	1	1	1	1	1	0	0
		250 nm	1	1	1	0	0	0	0	0
		30 µM	0	0	0	0	0	0	0	0
64	13(S)-Hydroxy-9Z,	10 nm	1	1	1	1	1	0	0	0
	11E-octadecadienoic acid	250 nm	1	1	1	0	0	0	0	0
		30 µM	0	0	0	0	0	0	0	0
65	Cortisone	10 nm	1	1	1	1	1	0	0	0
		250 nm	1	0	1	0	0	0	0	0
		30 µM	0	0	0	0	0	0	0	0
66	Progesterone	10 nm	1	1	1	1	1	0	0	0
		250 nm	1	1	1	0	0	0	0	0
		30 µM	1	1	0	0	0	0	0	0
67	17b-Estradiol	10 nm	1	1	1	1	1	1	0	0
		250 nm	0	1	1	1	1	0	0	0
		30 µM	1	0	0	0	0	0	0	0
68	Pregnenolone	10 nm	0	1	1	1	1	0	0	0
		250 nm	1	1	1	1	0	0	0	0
		30 µM	1	0	0	0	0	0	0	0
69	Androstenedione	10 nm	1	1	1	1	1	0	0	0
		250 nm	1	1	1	1	0	0	0	0
		30 µM	1	0	0	0	0	0	0	0
70	1a,25-Dihydroxyvitamin D3	10 nm	0	1	1	1	1	1	1	0
		250 nm	1	1	1	1	0	0	0	0
		30 µM	1	0	0	0	0	0	0	0
71	Docosa-4Z,7Z,10Z,13Z,	10 nm	1	1	1	1	1	0	0	1
	16Z,19Z-hexaenoic acid	250 nm	1	1	1	1	0	0	0	0
		30 µM	1	0	0	0	0	0	0	0
72	3-Methylcholanthrene	10 nm	1	1	1	1	1	1	1	0
		250 nm	1	1	1	1	0	0	0	0
		30 µM	0	0	0	0	0	0	0	0
73	Acitretin	10 nm	1	1	1	1	1	0	0	1
		250 nm	1	1	1	1	0	0	0	0
		30 µM	1	0	0	0	0	0	0	0
74	Pioglitazone	10 nm	1	1	1	1	1	0	0	0

	250 nm	1	1	1	1	1	0	0	0
	30 µM	1	0	0	0	0	0	0	0
75 **4-Hydroxyretinoic acid**	**10 nm**	**2**	**3**	**3**	**2**	**2**	**1**	**0**	**0**
	250 nm	1	1	1	1	1	1	1	0
	30 µM	1	1	1	0	0	0	0	0
76 3-amino benzamide	10 nm	1	1	0	1	1	1	1	0
	250 nm	1	0	0	1	1	1	1	1
	30 µM	1	0	1	0	0	0	0	0
77 Phthalazinone pyrazole	10 nm	1	1	1	1	1	1	1	1
	250 nm	1	0	1	0	0	0	0	1
	30 µM	1	1	1	1	0	0	0	0
78 AGK2	10 nm	1	1	1	0	1	1	0	1
	250 nm	1	1	1	1	1	1	1	0
	30 µM	1	1	1	0	0	0	0	0
79 Mirin	10 nm	1	1	1	1	1	0	0	0
	250 nm	1	1	1	1	0	0	1	1
	30 µM	1	1	1	1	1	0	0	0
80 chidamide	10 nm	1	1	1	1	1	1	0	0
	250 nm	1	1	1	1	1	1	1	1
	30 µM	1	1	1	1	0	0	0	0
81 SAHA	10 nm	1	1	1	1	1	1	1	0
	250 nm	1	1	1	1	0	0	1	1
	30 µM	1	1	0	1	0	0	0	0
82 F-Amidine	10 nm	1	1	1	1	1	0	1	1
	250 nm	1	1	1	1	0	1	0	1
	30 µM	1	1	0	0	0	0	0	0
83 4-iodo-SAHA	10 nm	1	1	1	1	1	0	1	1
	250 nm	1	1	1	1	1	0	0	0
	30 µM	1	1	0	0	0	0	0	0
84 UNC0321	10 nm	1	1	1	1	0	0	0	1
	250 nm	1	1	0	0	1	0	0	0
	30 µM	1	0	0	0	0	0	0	0
85 Isoliquiritigenin	10 nm	1	1	1	1	0	1	1	0
	250 nm	1	1	1	1	1	0	0	0
	30 µM	1	0	0	0	0	0	0	0
86 CAY10603	10 nm	1	0	1	1	0	0	1	1
	250 nm	1	1	1	0	0	0	0	0
	30 µM	1	1	1	0	0	0	0	0
87 Pimelic diphenylamide 106	10 nm	1	1	1	1	0	1	0	1
	250 nm	1	1	1	1	1	0	0	0
	30 µM	1	1	1	0	0	0	0	0
88 3-deazaneplanocin-A	10 nm	1	1	1	1	1	0	1	0
	250 nm	1	1	1	1	0	0	0	0
	30 µM	1	1	0	0	0	0	0	0

89	2,4-OPD	10 nm	1	1	1	1	1	0	0	1
		250 nm	1	1	1	1	1	1	1	0
		30 µM	1	0	1	1	0	0	0	0
90	2-PCPA (hydrochloride)	10 nm	1	1	1	1	1	1	1	0
		250 nm	1	1	1	1	0	1	0	1
		30 µM	1	1	0	0	0	0	0	0
91	Tubastatin A (trifluroacetate salt)	10 nm	1	1	1	1	1	0	0	1
		250 nm	1	1	0	0	0	0	0	0
		30 µM	1	0	1	0	0	0	0	0
92	**Nicotinamide**	10 nm	1	1	1	1	1	1	1	0
		250 nm	**1**	**2**	**2**	**2**	**2**	**2**	**1**	**0**
		30 µM	1	1	1	0	1	0	0	0
93	Zebularine	10 nm	1	1	1	1	0	1	0	1
		250 nm	1	1	1	1	0	1	1	1
		30 µM	1	1	0	0	0	0	0	0
94	(S)-HDAC-42	10 nm	1	1	1	1	1	1	1	0
		250 nm	1	1	1	1	1	1	1	1
		30 µM	1	1	1	1	1	1	1	0
95	Trans-resveratrol	10 nm	1	1	1	1	1	0	0	1
		250 nm	1	1	1	1	1	0	1	1
		30 µM	1	1	1	0	0	0	0	1
96	DMOG	10 nm	1	1	1	1	0	1	1	0
		250 nm	1	1	1	1	1	1	0	1
		30 µM	1	1	1	1	1	0	1	0
97	Cl-Amidine	10 nm	1	1	1	1	1	1	0	1
		250 nm	1	1	1	1	0	0	1	0
		30 µM	1	1	1	0	0	0	0	1
98	Garcinol	10 nm	1	1	1	1	0	1	0	0
		250 nm	1	1	1	1	1	1	1	1
		30 µM	1	1	1	0	0	0	0	0
99	BIX01284 (hydrocholride hydrate)	10 nm	1	1	1	1	1	1	0	0
		250 nm	1	1	1	1	1	0	0	1
		30 µM	1	1	1	1	0	0	0	0
100	Valproic acid (sodium salt)	10 nm	1	1	1	1	1	0	1	0
		250 nm	1	1	1	1	1	1	1	0
		30 µM	1	1	1	1	1	0	1	0
101	splitomicin	10 nm	1	1	1	1	1	0	1	1
		250 nm	1	1	1	1	1	1	0	1
		30 µM	1	1	1	1	0	1	0	1
102	MS-275	10 nm	1	1	1	1	1	1	0	1
		250 nm	1	1	1	1	0	0	1	0
		30 µM	1	1	1	0	1	0	0	0
103	trichostatin A	10 nm	0	1	1	1	1	1	1	0
		250 nm	1	1	1	1	0	0	0	1

	30 µM	1	0	1	0	0	0	0	0
104 Ellagic acid	10 nm	1	1	1	1	0	1	0	1
	250 nm	1	1	1	1	0	0	0	0
	30 µM	1	1	1	1	1	0	0	0
105 Suramin (sodium salt)	10 nm	1	1	1	0	1	1	1	0
	250 nm	1	1	1	1	1	0	0	0
	30 µM	1	1	1	1	0	0	0	0
106 Tenovin-1	10 nm	1	1	1	1	1	0	0	1
	250 nm	1	1	1	1	0	1	0	0
	30 µM	1	1	1	0	0	0	0	0
107 CBHA	10 nm	1	1	1	1	1	0	1	0
	250 nm	1	1	1	1	1	0	0	0
	30 µM	1	1	1	1	0	0	0	0
108 HNHA	10 nm	1	1	1	1	1	1	1	1
	250 nm	1	1	1	1	1	1	1	0
	30 µM	1	1	1	1	1	1	1	0
109 (-)- Neplanocin A	10 nm	1	1	1	1	1	0	1	1
	250 nm	1	1	1	1	1	0	0	1
	30 µM	1	1	1	1	0	0	0	1
110 Sciptaid	10 nm	1	1	1	1	1	1	0	1
	250 nm	1	1	1	1	0	0	1	0
	30 µM	1	1	1	1	0	0	0	0
111 JGB1741	10 nm	1	1	1	1	0	1	1	0
	250 nm	1	1	1	1	1	0	0	1
	30 µM	1	1	1	1	1	1	0	0
112 Tinovin-6	10 nm	0	1	1	1	1	1	1	1
	250 nm	1	1	1	1	1	1	1	0
	30 µM	1	1	1	1	0	0	0	0
113 M-344	10 nm	1	1	1	1	0	1	0	1
	250 nm	1	1	1	1	0	1	0	1
	30 µM	1	1	1	0	0	0	0	0
114 RG-108	10 nm	1	1	1	1	1	1	0	0
	250 nm	**1**	**2**	**2**	**3**	**3**	**2**	**1**	**0**
	30 µM	1	1	1	1	1	1	1	0
115 CAY10433	10 nm	1	1	2	1	1	1	1	0
	250 nm	**2**	**2**	**3**	**3**	**3**	**2**	**1**	**1**
	30 µM	1	1	1	1	1	1	0	1
116 Sinefungin	10 nm	1	1	1	1	1	0	1	1
	250 nm	**1**	**2**	**2**	**2**	**2**	**1**	**1**	**1**
	30 µM	1	1	1	1	0	1	0	0
117 Suberohydroxamic acid	10 nm	1	1	1	1	1	0	1	1
	250 nm	1	1	1	1	0	0	0	1
	30 µM	1	0	0	0	0	0	0	0
118 I-BET	10 nm	1	1	1	1	1	1	0	1

	250 nm	0	1	1	1	1	0	0	0
	30 µM	1	1	1	1	0	0	0	0
119 Sodium butyrate	10 nm	1	1	1	1	1	0	0	0
	250 nm	1	1	1	1	0	0	0	0
	30 µM	1	1	1	0	0	0	0	0
120 Oxamflatin	10 nm	1	1	1	1	1	0	0	0
	250 nm	1	0	0	0	0	0	0	0
	30 µM	0	0	0	0	0	0	0	0
121 2,3,5-triacetyle-5-azacytidine	10 nm	1	1	1	1	0	1	0	0
	250 nm	1	1	1	1	1	0	0	0
	30 µM	1	1	1	0	0	0	0	0
122 piceatannol	10 nm	1	1	1	1	1	1	0	0
	250 nm	1	1	1	1	1	0	0	0
	30 µM	1	1	1	0	0	0	0	0
123 S-adenosylhomocysteine	10 nm	1	1	1	1	1	0	0	0
	250 nm	1	1	1	1	0	0	0	0
	30 µM	1	1	1	0	0	0	0	0
124 UNC0638	10 nm	1	1	1	1	1	0	1	0
	250 nm	0	1	1	1	0	1	0	0
	30 µM	1	1	1	1	0	0	0	0
125 Anacardic acid	10 nm	1	1	1	1	0	1	0	1
	250 nm	0	1	1	1	1	0	0	0
	30 µM	1	1	1	0	0	0	0	0
126 Salermide	10 nm	1	1	1	1	1	0	1	0
	250 nm	1	1	0	1	0	1	0	0
	30 µM	0	1	1	0	0	0	0	0
127 UNC0224	10 nm	1	1	1	0	0	1	0	1
	250 nm	1	1	1	0	0	0	0	0
	30 µM	1	1	0	0	0	1	0	0
128 EX-527	10 nm	1	1	1	1	1	1	1	0
	250 nm	1	1	1	1	0	1	1	0
	30 µM	1	1	0	1	1	1	1	0
129 CCG-100402	10 nm	1	1	1	1	1	0	0	1
	250 nm	1	1	1	1	0	0	1	1
	30 µM	1	1	1	0	0	0	0	1
130 10% FCS		**2**	**3**	**4**	**5**	**6**	**6**	**4**	**2**
131 FGF1+ p38 inhibitor		**3**	**8**	**9**	**10**	**10**	**9**	**7**	**3**

Acknowledgements

First and foremost, I would like to thank my supervisor, Prof. Dr. Felix B. Engel, for providing me with an opportunity to work in his lab and learn under his supervision. I am extremely grateful for your guidance, encouragement, contribution, positive attitude, and critical reading and helpful suggestions for this thesis and manuscript.

I am thankful to many people who gave me immense support during my research and even more to complete my Ph.D. thesis. I would like to show my gratitude towards Prof. Dr. Dr. Thomas Braun for giving me the opportunity to perform my thesis work at the Max Planck Institute for Heart Lung Research in Dr. Engel's Laboratory. It is my pleasure to thank Prof. Dr. Heinrich Sauer, Justus-Liebig-University, Giessen, Germany, for being my university supervisor and for his creative suggestions and constructive criticism during my semester PhD program meetings.

I would like also to thank my colleagues in Dr. Engel's laboratory for their help and for creating a good atmosphere in the group. They became good friends during my Ph.D. study: Tatyana Novoyatleva, Chinmoy Patra, David Zebrowski, Ingrid Hauck-Schmalenberger, Filomena Ricciardi, Marina Leone, Amana Sajjad and Harsha vardhan Renikunta.

I would like to thank all the people at the International Giessen Graduate Centre for the Life Sciences (GGL) organizing committee for providing a structured PhD program including regular workshops covering different aspects.

Finally, I would like to thank my parents Suresh Magadum and Kalpana Magadum, my grandparents Bharamu Magadum and Akkatai Magadum and my wife Manpreetkaur and her family. They have always stood behind me and have inspired me to pursue my studies.

This work was suppoby a grant from the Protecting the Heart from Ischemia (PROMISE), Alexander von Humboldt Foundation (Sofja Kovalevskaja Award to F. B. E.) and the Excellence Cluster Cardio-Pulmonary Systems (DFG).

Der Lebenslauf wurde aus der elektronischen Version der Arbeit entfernt.
The curriculum vitae was removed from the electronic version of the paper.

PUBLICATIONS:

Publications related to this thesis:

Peer-reviewed publications:

1. **Ajit Magadum,** Teayoun Kim, Qinglin Yang, and Felix B. Engel, “Small molecule screen identifies carbacyclin as an inducer of mammalian cardiomyocyte proliferation” (**under review**).

Published work unrelated to this thesis:
Peer-reviewed publications:

1. Hideki Uosaki, **Ajit Magadum**, Kinya Seo, Hiroyuki Fukushima, Ayako Takeuchi, Yasuaki Nakagawa, Kara White Moyes, Genta Narazaki, Koichiro Kuwahara, Michael Laflamme, Satoshi Matsuoka, Norio Nakatsuji, Kazuwa Nakao, Shinya Yamanaka, Chulan Kwon, David A Kass, Felix B Engel, Jun K. Yamashita, "Identification of Chemicals Inducing Cardiomyocyte Proliferation in Developmental Stage-Specific Manner with Pluripotent Stem Cells" (**under review**).

2. **Ajit Magadum**, Harsha vardhan Renikunta, Felix B. Engel "A functional chemical screen identified regulators of stem cell derived cardiomyocyte proliferation" (**manuscript under preparation**).

3. S. K. Soni, **A. Magdum**, J. M. Khire "Purification and characterization of two distinct acidic phytases with broad pH stability from *Aspergillus niger* NCIM 563" ***World J Microbiol Biotechnol***. 2010 Nov;26(11):2009-2018. Epub 2010 Mar 27.

CONFERENCES

Oral presentation:

1. **Ajit Magadum,** Felix B. Engel (2011)." Cardiac repair and cardiomyocyte proliferation". **Keystone symposia on nuclear receptors and friends, Austria.**

2. **Ajit Magadum,** Felix B. Engel (2011)." Cardiac repair and cardiomyocyte proliferation". **PROMISE retreat in Rauischholzhausen, Germany. 1st April 2011.**

3. **Ajit Magadum,** Felix B. Engel (2010). "Cardiac repair and cardiomyocyte proliferation". **1 st GGL conference, Giessen, Germany.**

Poster presentation:

1. **Ajit Magadum,** Teayoun Kim, Qinglin Yang, and Felix B. Engel (2013)."Small molecule screen identifies new inducers of mammalian cardiomyocyte proliferation". **Keystone symposia on nuclear receptors and friends, Austria.**

2. **Ajit Magadum,** Felix B. Engel (2013). "Small molecule screen identifies new inducers of mammalian cardiomyocyte proliferation". **Cardiovascular network retreat, Germany.**

3. **Ajit Magadum,** Felix B. Engel (2012) “Cardiac repair and cardiomyocyte proliferation”. **3rd PROMISE annual meeting, Barcelona, Spain.**

4. **Ajit Magadum,** Felix B. Engel (2012). “Small molecule screen identifies new inducers of mammalian cardiomyocyte proliferation”. **Cardiovascular network retreat, Germany.**

5. **Ajit Magadum,** Felix B. Engel (2010) “Cardiac Repair through Repopulation of the Heart by Inducing Cardiomyocyte Proliferation ”. **The 2nd GGL conference, Giessen, Germany 2010.**